UNIVERSITY OF CALIFORNIA, SAN DIEGO

Engineering Protein Kinase A to Identify Novel PKA Substrates

A dissertation submitted in partial
satisfaction of the requirements for the
degree Doctor of Philosophy

in

Chemistry

by

Sharmin May Schauble

Committee in charge:

Professor Susan S. Taylor, Chair
Professor Gourisankar Ghosh
Professor Simpson Joseph
Professor Alexandra Newton
Professor Emmanuel Theodorakis

2006

The dissertation of Sharmin May Schauble is approved, and it is acceptable in quality and form for publication on microfilm:

_____

_____

_____

_____

_____

_____

Chair

DEDICATION

To my son, Caleb, and to my parents.

TABLE OF CONTENTS

ABBREVIATIONS

2-D. Two-dimensional.

AKAP. A-kinase anchoring protein

ATP. adenosine triphosphate

BLAST. Basic Local Alignment Search Tool.

cAMP. adenosine 3',5'-cyclic monophosphate.

CHCH. Coiled coil-helix coiled coil-helix domain.

ChChd3. CHCH domain-containing protein 3.

C-subunit. The Catalytic Subunit of PKA.

C-terminus. Carboxy-terminus

D-AKAP1. Dual A-Kinase anchoring protein-1.

D-AKAP2. Dual A-kinase anchoring protein-2.

DNA. Deoxyribonucleic Acid.

DTT. Dithiothreitol.

DUF737. Domain of unknown function number 737.

ECL. Emission spectrum of luminal.

E. coli. *Escherichia coli*

EDTA. Ethylenediaminetetraacetic acid.

EGTA. Ethylene glycol-bis(2-aminoethylether)-N,N,N',N'-tetraacetic acid

GRASP. Graphical Representation and Analysis of Structural Properties

GST. Glutathione S-transferase.

Hck. Hematopoietic cell kinase

HCl. Hydrochloric acid

IM. Inner mitochondrial membrane.

IMS. Inner mitochondrial space.

IP20. Residues 5-24 of PKI.

IPG. Immobilized pH gradient.

***k*cat**. Substrate turnover rate.

kDa. Kilodaltons.

Km. Substrate concentration at half maximum rate.

MALDI. Matrix-Assisted Laser Desorption/Ionization

MES. 2-(N-morpholino) ethanesulfonic acid

$MgCl_2$. Magnesium chloride.

MOPS. 3-(N-morpholino) propanesulfonic acid.

mRNA. Messenger ribonucleic acid.

NaCl. Sodium chloride

NADH. Nicotinamide Adenine Dinucleotide

$NaHPO_4$. Sodium phosphate.

NCMIR. National Center for Microscopy and Imaging Research.

N-terminus. Amino-terminus.

OM. Outer mitochondrial membrane.

PBS. Phosphate buffered solution.

PDB. Protein data bank.

PDK1. Phosphoinositide dependent kinase-1.

pI. Isoelectric point.

PKA. Protein Kinase A or cyclic-AMP Dependent Protein Kinase

PKI. Protein kinase A inhibitor.

PVDF. Polyvinylidene fluoride.

R-subunit. The Regulatory Subunit of PKA.

SDS-PAGE. Sodium dodecyl sulfate polyacrylamine gel electrophoresis.

TBST. Tris-Buffered Saline Tween-20

TOF. Time of flight.

TOM. Translocase of the outer mitochondrial membrane.

Tris. Tris Hydroxymethylaminoethane.

UBHD. University of Houston Brownian Dynamics program.

WT. Wild type.

LIST OF FIGURES

LIST OF TABLES

ACKNOWLEDGMENTS

I would like to thank Susan Taylor for believing in me and giving me the support I really needed to finish this. I would also like to thank Mary Ellen Perry for doing all the little things that I had trouble getting done. I appreciate my committee members for their suggestions.

Thanks to C.C. King who instructed me on how to run a 2-D gel. Dr. King also assisted in the preparation of the samples for mass spectrometry, ran the MALDI-TOF, and taught me how to analyze the peaks. Thanks to Kavita Shah for guidance on the project, for supplying me with radioactive and unlabeled analogs, and assisting with the preparation of this dissertation.

Thank you to all of the current and previous Taylor lab members who have helped with my project. Thanks to Juniper Pennypacker for the Src and ChChd3 constructs; Manjula Darshi for the cell images and discussions about the myristylation project; Dave Barraclough for the mitochondrial fractionation; Mira Sastri for advice and the Northern blot; Frank Ma for guidance in molecular biology and cell imaging; Michael Moore who guided me with the ^{32}P assays and helped me get started in the lab; Ganesh Anand for help on the MALDI. Thanks to Elzbieta Radzio-Andhelm for assistance with the figures.

I would also like to thank the Taylor lab members who I will always remember fondly and have a special place in my heart: Mira, Dave, Mike Moore, Peter Carmichael, Ganesh Anand, Ken Humphries, Celina Juliano, Alison Getz, Marsha Crochiere, Nina Haste, Pearl Akamine, Kerri Zawadzki and many others. Working with

these wonderful, funny people has kept me going when times were difficult. They made it all worthwhile.

Finally, I would like to thank my family. My mom who wouldn't let me quit, and my significant other, Simon Brown, who supported me in everyday life, and my son Caleb.

VITA

1997 B.S., Biochemistry, University of Nebraska – Lincoln. Lincoln, Nebraska.

2000 M.S, Chemistry, University of California, San Diego. La Jolla, California.

2006 Ph.D., Chemistry, University of California, San Diego. La Jolla, California.

ABSTRACT OF THE DISSERTATION

Engineering Protein Kinase A to Identify Novel

PKA Substrates

by

Sharmin May Schauble

Doctor of Philosophy in Chemistry

University of California, San Diego, 2006

Professor Susan S. Taylor, Chair

Protein kinases regulate numerous activities in eukaryotic cells by phosphorylation of substrates. Cyclic-AMP-dependent protein kinase (PKA) is one of the most important and well studied of these protein kinases. In its inactive form, this kinase exists as a tetrameric protein with a regulatory (R) subunit dimer bound to two catalytic (C) subunits. PKA is activated when the second-messenger cAMP binds cooperatively to the regulatory subunits of PKA.

Due to the numerous kinases in the cell, many with overlapping substrates, it is difficult to find novel substrates. Our lab is particularly interested in PKA substrates at the mitochondria because of the discovery of two Dual A-Kinase Anchoring Proteins (AKAPs). The goal of this dissertation is to engineer the PKA catalytic subunit to

accept bulky N^6-substituted ATP analogs, using a chemical genetics approach initially pioneered with v-Src (Shah, Liu et al. 1997), and to identify novel substrates at the mitochondria. Methionine 120 was mutated to alanine in the ATP binding pocket of the catalytic subunit. The mutant C-subunit had to be expressed with PDK1 in order to be soluble and phosphorylated. The mutant preferred N^6(benzyl)-ATP and N^6(phenethyl)-ATP over other analogs, according to results obtained through qualitative and kinetic analyses.

Mitochondria isolated from mouse brain were used in an *in vitro* assay with recombinant M120G C-subunit and radiolabeled N^6(benzyl)-ATP in order to find novel direct substrates. Two-dimensional gel electrophoresis was used to separate proteins. From one of the phosphorylated spots, ChChd3 was identified using mass spectrometry and subsequently characterized.

ChChd3 has three motifs/domains of interest: a myristylation motif, where a highly conserved PKA phosphorylation site is located; a DUF737 domain, which has an unknown function; and a CHCH domain, which is characterized by a Cys-X_9-Cys motif. The myristylation motif is not sufficient to target the protein to the mitochondria, however, the CHCH domain is necessary for mitochondrial localization. We propose that ChChd3 uses a mitochondrial import mechanism involving Mia40 and Erv1 where the protein is disulfide-bonded and folded once in the inner mitochondrial space. PKA phosphorylation on the N-terminus of ChChd3 may regulate targeting of the protein to membranes.

CHAPTER I

Introduction

Protein kinases represent one of the largest gene families in eukaryotic cells. The kinome shown in Figure 1.1 includes over 500 protein kinases and accounts for approximately two percent of the human genome (Manning, Whyte et al. 2002). In plants protein Ser/Thr kinases account for nearly four percent of the genome (Champion, Kreiss et al. 2004). Protein kinases regulate numerous activities in eukaryotic cells by phosphorylation of protein substrates. Cyclic-AMP-dependent protein kinase (PKA) is one of the most important and well studied of these protein kinases. It is also one of the simplest members of the protein kinase superfamily. It is ubiquitous in every mammalian cell and regulates numerous processes including differentiation, memory, growth, and metabolism. Depending on the cell type, the substrates of PKA vary as does the mechanism for activation. In the brain, for example, PKA is highly involved in memory (Kandel and Squire 2000), while in the heart it is involved in excitation-contraction coupling (Wehrens, Lehnart et al. 2006). PKA is also linked to many cancers such as breast cancer (Stratakis, Cho-Chung 2002).

As seen in Figure 1.2, PKA exists in its inactive form as a tetrameric protein with a regulatory (R) subunit dimer bound to two catalytic (C) subunits. Each R subunit has two cAMP binding domains at the C-terminus. PKA is activated when the second-messenger, cAMP, binds cooperatively to the regulatory subunits of PKA, causing a conformational change in the R subunits that unleashes the catalytic subunits (for review see Taylor, Buechler et al. 1990). After release, the free C subunits mediate signals and regulate proteins by transferring the gamma-phosphate of ATP to a serine or threonine on the substrate protein.

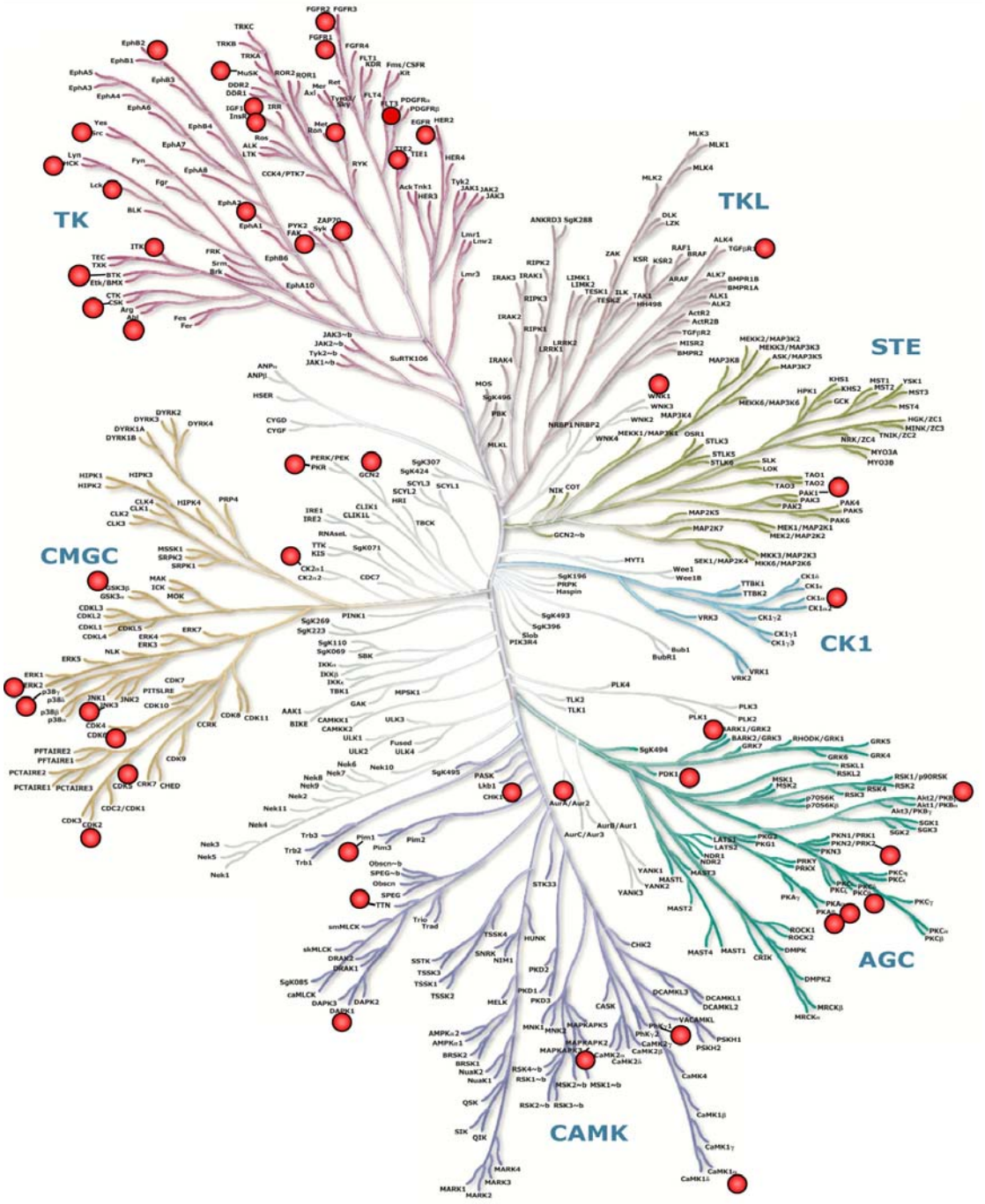

Figure 1.1: The human kinome. This kinome predicts all of the protein kinases encoded for by the human genome. PKA is in the PKA, PKG, PKC (AGC) group. The figure was taken from Manning, et al. (2002). The red balls indicate kinases where a crystal structure is available.

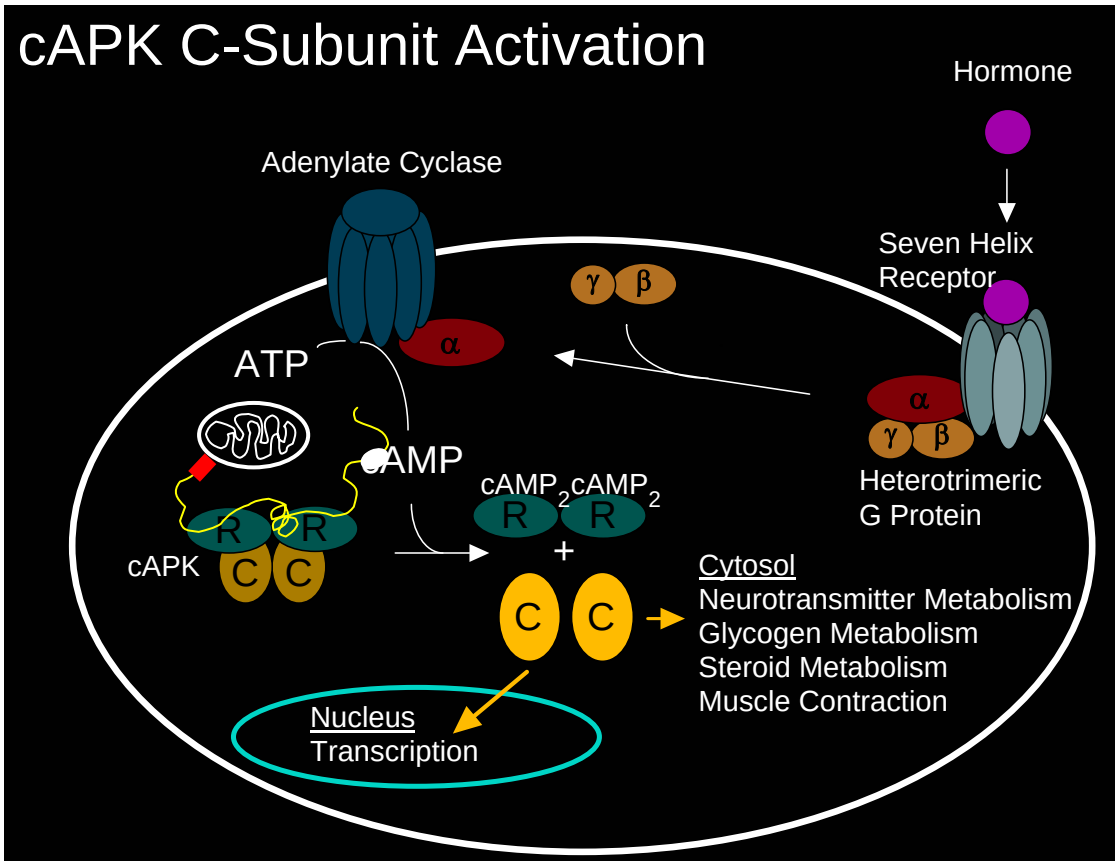

Figure 1.2: Activation of PKA by cAMP. In addition to the regulatory and catalytic subunits, PKA is often localized to specific sites by A-Kinase Anchoring Proteins (AKAPs).

Specificity for PKA is achieved not only through the regulation of catalytic activity but also through localization via A-kinase anchoring proteins (AKAPs) (for review see Wong and Scott 2004). As seen in Figure 1.3, the AKAPs create local environments within the cell where PKA is localized close to its substrates. Often these substrates are tissue-specific. It is difficult to find novel substrates or substrates that are the direct targets of any protein kinase as opposed to indirect substrates, such as a protein in a phosphorylation cascade downstream of the actual PKA substrate. Additionally, there are numerous other kinases within the cell, each with different and even overlapping substrates that further complicate the picture. At this point, it is important to define each kinase very specifically in terms of its substrates but also in terms of its special localization which includes other significant players such as the scaffold proteins.

The catalytic subunit of PKA is one of the best understood kinases. It was the first kinase to have its protein structure determined (Knighton, Zheng et al. 1991). The catalytic subunit consists of a large lobe and a small lobe with the binding of ATP in between the lobes (see Figure 1.4). This basic structure of PKA is shared by all kinases. The structure of this single subunit shows very well the conserved fold of the kinase as well as the specific conserved residues. The small lobe is mostly made up of β-strands, while the large lobe is mostly α-helical. The adenine ring docks to a deep hydrophobic pocket that lies in the cleft between the two lobes.

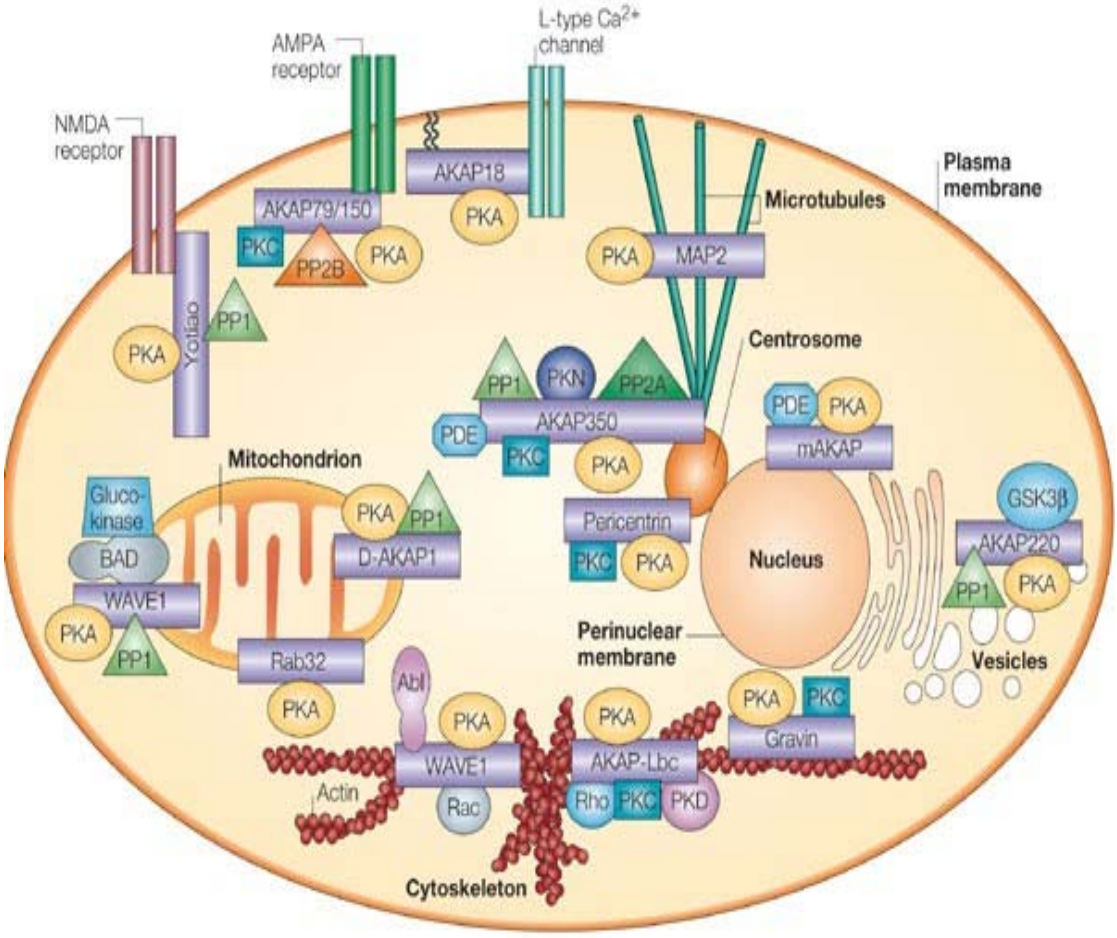

Figure 1.3: Localization of PKA is achieved through A-kinase anchoring proteins. Localization of PKA creates micro-domains in which PKA can selectively phosphorylate substrates and is another level of regulation of the kinase. This figure is taken from Wong and Scott (2004).

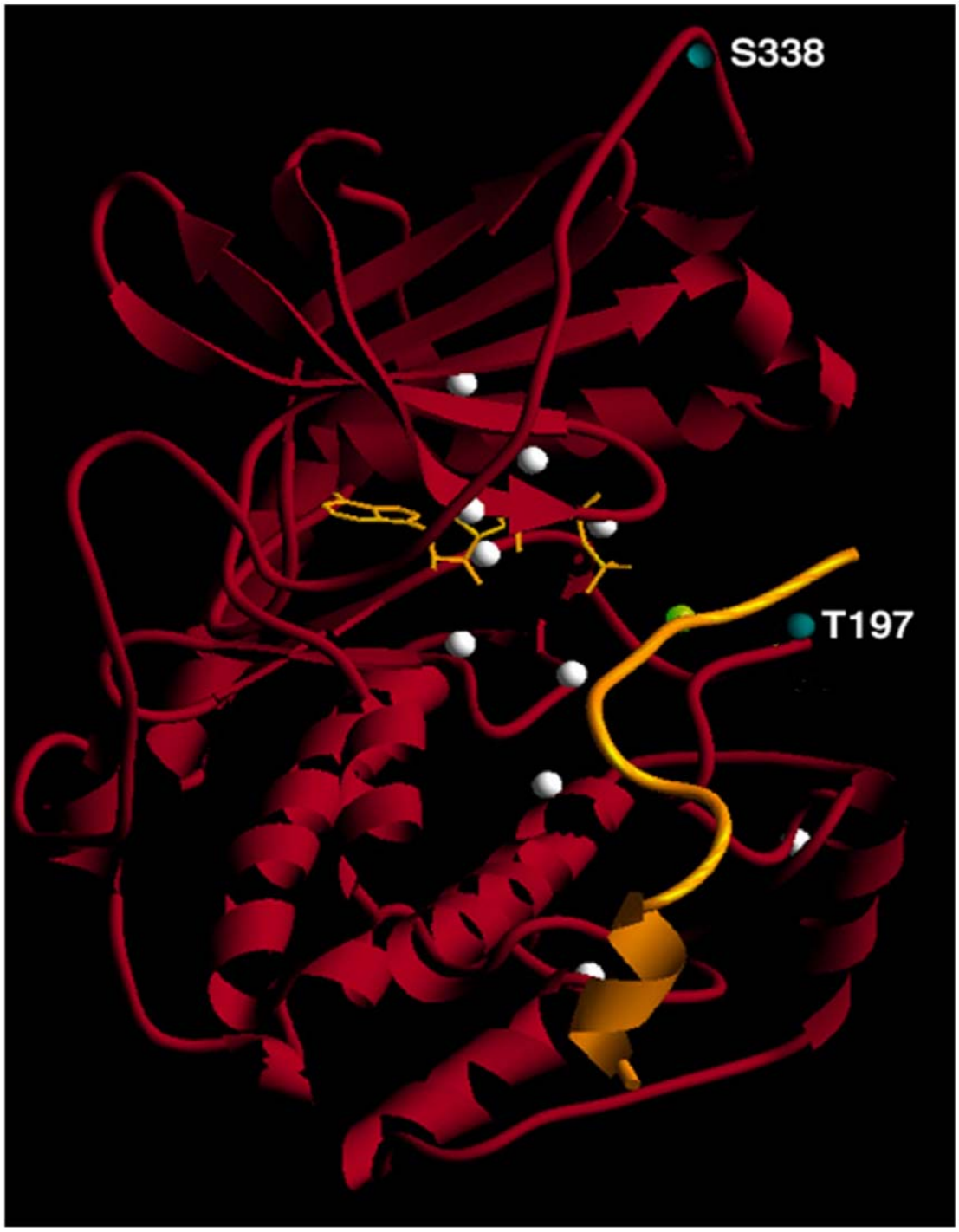

Figure 1.4: Structure of the catalytic subunit of PKA. Represents the ternary complex of the catalytic subunit bound to ATP and IP20 (yellow) (Zheng et al. 1993). White dots represent the conserved residues among kinases. The blue dots mark the phosphorylation sites. The Protein Data Bank code is 1ATP.

Several phosphorylation sites are known for the catalytic subunit. When the catalytic subunit is expressed in *E. coli*, it is autophosphorylated on Ser10, Ser138, Thr197, and Ser 338. The Thr197 site in the activation loop is important for activation of the kinase and also improves recognition of substrates (Adams, McGlone et al. 1995). The mammalian C-subunit can autophosphorylate on Ser10 (Toner-Webb, van Patten et al. 1992); however, Thr197 and Ser 338 are the only sites found when the endogenous catalytic subunit is purified from mammalian tissues (Shoji, Titani et al. 1979). These sites can be seen in Figure 1.4.

The catalytic subunit recognizes and phosphorylates the primary consensus sequence R-R-X-S/T-Y in many of its substrates (Figure 1.5) (Kemp, Graves et al. 1977). The Y in the sequence is a large hydrophobic residue and the X is variable (Zetterqvist, Ragnarsson et al. 1990). Another, less likely, consensus sequence is R-X-X-R-X-X-S/T-Y. The hydrophobic residue, at the P+1 site along with three basic residues at the P-6, P-3, and P-2 sites before the phosphorylation (P) site, are important elements for recognition (Järv and Ragnarsson, 1991). A commonly used ideal peptide substrate for PKA is Kemptide, with the sequence L-R-R-A-S-L-G (Kemp 1979).

The regulatory subunits bind to the catalytic subunits and inactivate the kinase. There are four different types of regulatory subunits: RIα, RIβ, RIIα, and RIIβ. These isoforms are not functionally redundant and also contribute to PKA specificity. All of the R subunits share a basic domain organization that consists of a dimerization/docking (DD) domain, an inhibitor site, and two cAMP-binding domains (see Figure 1.6). The DD domain is important for R dimerization and for localization through binding to A-kinase anchoring proteins. The inhibitor site binds to the active site cleft of the catalytic

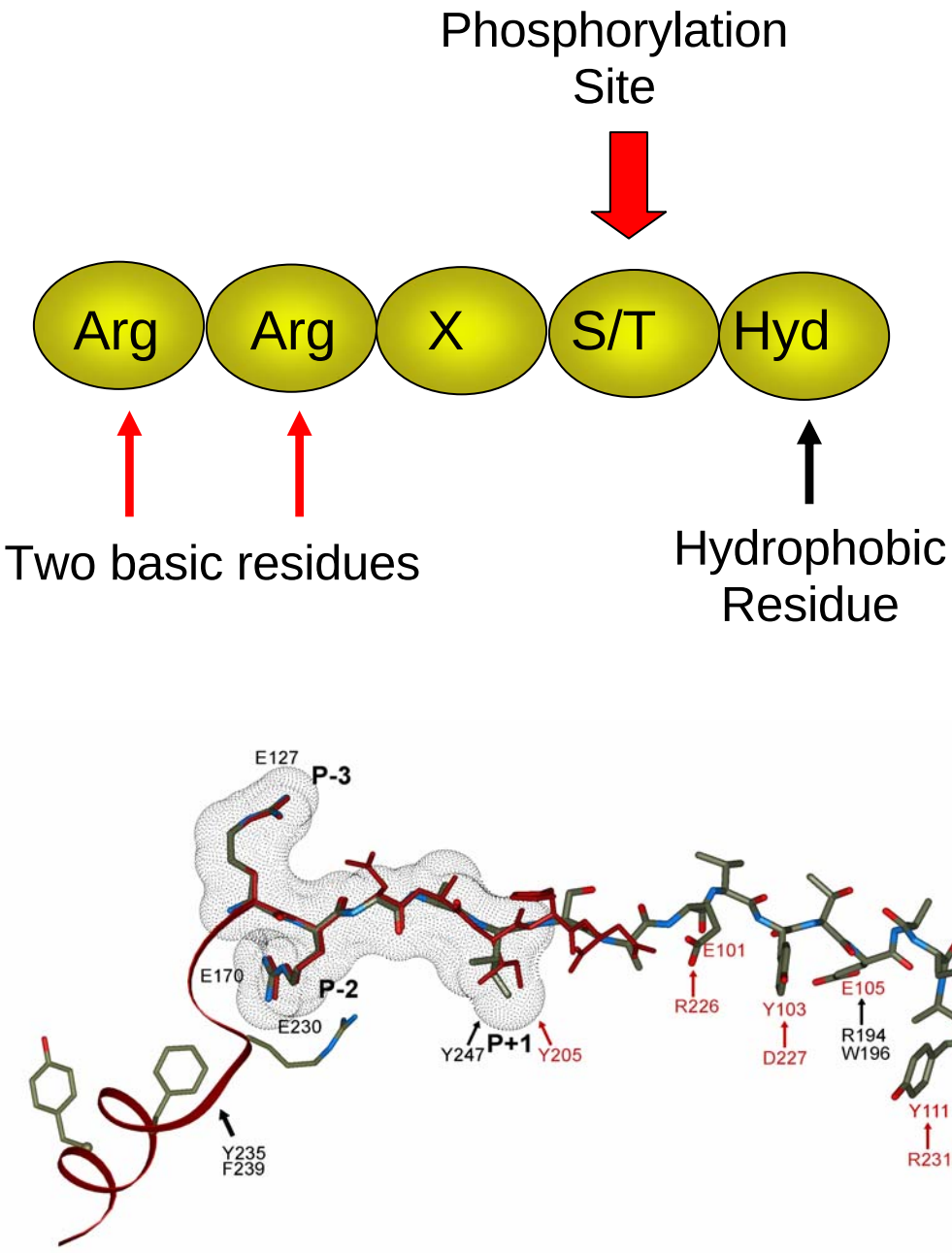

Figure 1.5: The peptide recognition site for PKA and the pseudosubstrate site in RIα and PKI. The minimal consensus site peptide for PKA is shown at the top. Below is the P-3 to P+1 consensus site segment bound to the catalytic subunit. The sequence for PKI is RRNAI while the RIα inhibition site is RRGAI. Both are pseudo substrates.

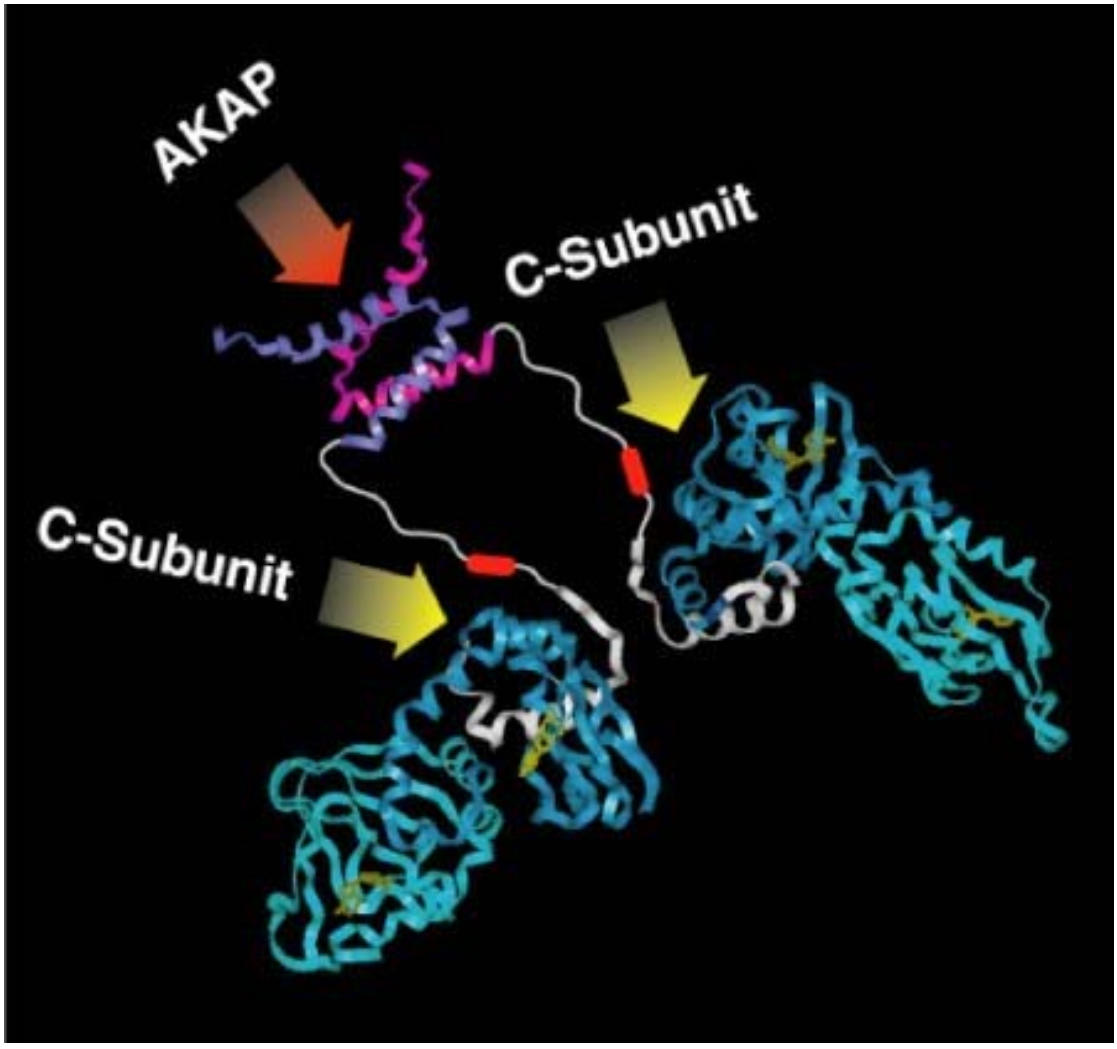

Figure 1.6: The RIα regulatory subunit. Arrows show where the C-Subunit and AKAPs bind to the dimerized regulatory subunits. The dimerization domain (DD) is shown in pink and purple. The cAMP binding domains A and B are shown in blue. Highlighted in red is the inhibitor site that binds to the catalytic subunit active site.

subunit. Each R protein contains two cAMP binding domains (A and B) that differ in their affinity for cAMP. The structures of RIα and RIIβ have been solved (Su, Dostman, et al. 1995; Diller, Madhusudan et al. 2001). Recently we have solved structures of regulatory subunits bound to the catalytic subunit (Kim, Xuong, et al. 2005). In addition to showing the mechanism of inhibition, these structures also confirm that the inhibitor site that resembles a PKA substrate does indeed bind to the active site cleft (see Figure 1.5). RII is actually phosphorylated by PKA at the P site whereas RI is not; instead RI contains a pseudosubstrate site similar to that of PKI (see following section on PKI).

The protein inhibitor of PKA, PKI, is also important for regulation and localization. PKI has three distinct forms, PKIα, PKIβ, and PKIγ (for review see Dalton and Dewey 2005). PKIα is the original form purified from rabbit skeletal muscle; it also the most abundant form expressed in the brain. PKI is involved in the regulation of synaptic activity (De Lecea et al., 1998) and the regulation of active C-subunit in the nucleus. PKI has a nuclear export signal (NES) near the C-terminus (Wen, Meinkoth et al. 1995) that is important for exporting the catalytic subunit out of the nucleus, where PKA mediates gene expression, and into the cytoplasm. PKIα binds very tightly to the catalytic subunit (K_i = 0.22 nM), and also is highly specific for PKA. PKIα consists of 75 amino acids. The structure has two ordered helical regions, but the rest is disordered and allows the protein to assume several different shapes (McPherson, Whitehouse et al., 1979; Whitehouse and Walsh, 1982; Thomas, Van Patten et al., 1991; Hauer, Taylor et al., 1999). The two functional domains, which overlap with the two helical regions, are the nuclear export signal in the middle of the protein and a kinase inhibitory domain

near the N-terminus. Within the kinase inhibitory domain is a pseudosubstrate site that has a consensus sequence similar to that of a substrate, except that the phosphorylatable Ser/Thr is replaced by an Ala (A21). The amino terminal region of PKI (residues 5-24) is referred to as IP20, and this peptide is sufficient to inhibit the catalytic subunit. IP20 is shown crystallized with the C-subunit in Figure 1.4.

The regulatory subunits also localize the catalytic subunits through an interaction of their DD domains with AKAPs. AKAPs are found all over the cell, from the plasma membrane to mitochondria. Initially, the AKAPs were thought to interact exclusively with RII holoenzyme complexes. Our lab, however, identified two dual-specific AKAPs, D-AKAP1 and D-AKAP2, which interact with both RI and RII (Huang, Durick et al. 1997; Huang, Durick et al. 1997). Both D-AKAPs have several splice variants, with some showing endoplasmic reticulum localization and others showing mitochondrial localization (Huang, Ma et al. 1999; Wang, Sunahara et al. 2001)). Of particular interest is D-AKAP1 which has a well-defined mitochondrial localization motif at its N-terminus. As summarized in Figure 1.7, many other proteins have been shown to interact with D-AKAP1. Overlapping with the mitochondrial targeting motif is a tubulin binding site (Cardone, de Cristofaro et al. 2002). The protein tyrosine phosphatase D1 (PTPD1) binds to D-AKAP1c near the N-terminus and is important for regulating Src (Cardone, Carlucci et al. 2004). A Ser/Thr protein phosphatase (PP1) also interacts with D-AKAP1c (Steen, Martins et al. 2000). The AKB domain stands for the A-kinase binding domain and is where the dimerization/docking domain of the R-subunits docks. Near the C-terminus is the KH domain which binds 3' mRNA

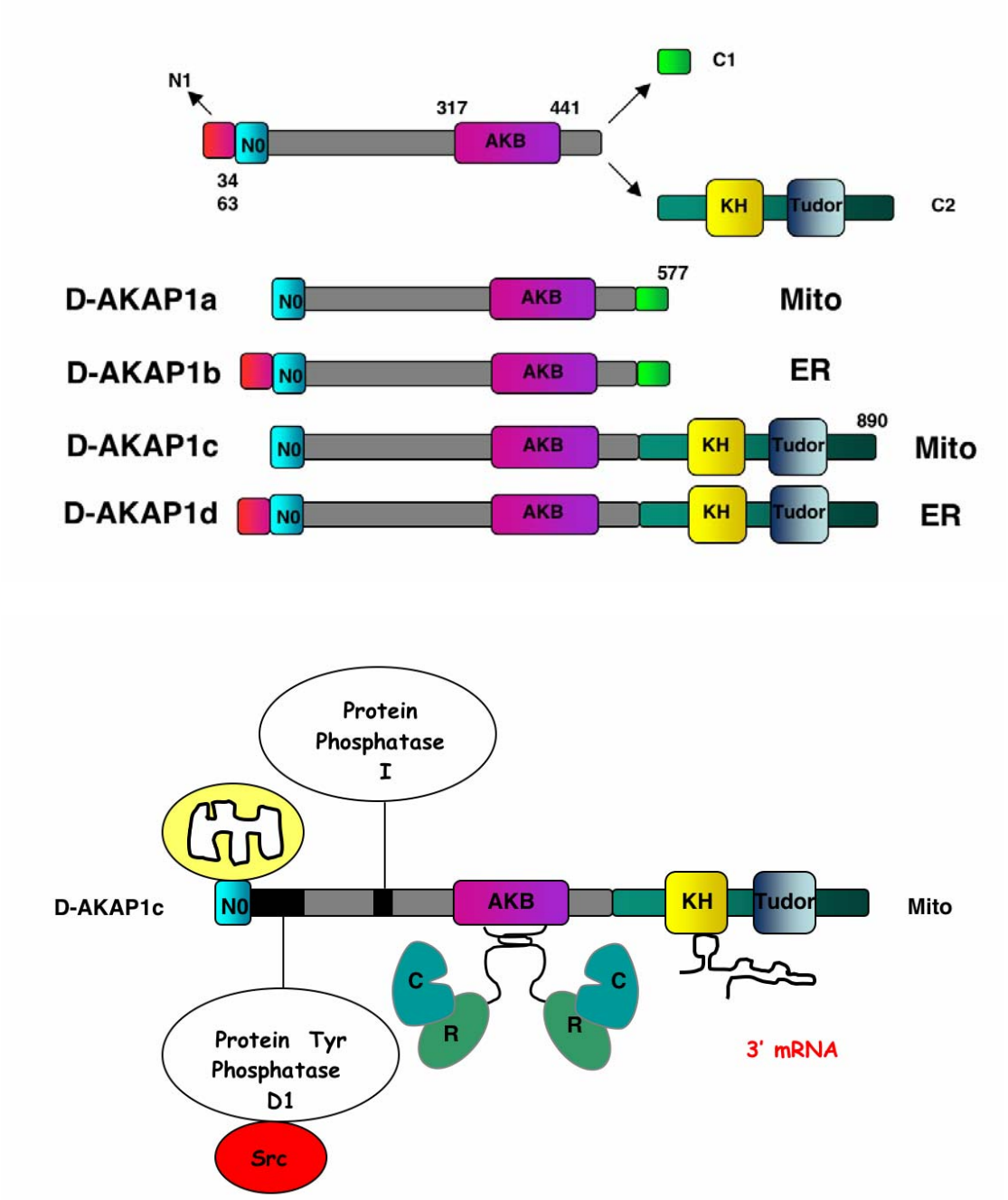

Figure 1.7: Splice variants of D-AKAP1 and the reported interacting partners of D-AKAP1c. The top figure details the splice variants and the localization of each. The mitochondrial localization signal is red, the ER localization signal = N0, A-kinase binding domain = AKB, mRNA binding domain = KH, Tudor binding domain = Tudor. The bottom figure shows the reported proteins that bind to D-AKAP1. The bottom figure was taken from Cardone, et al. (2004).

(Trendelenburg, Hummel et al. 1996; Ranganathan, Phan et al. 2002; Ginsberg, Feliciello et al. 2003).

Due to the discovery of D-AKAP1 and 2, we especially want to know what is PKA's role at the mitochondria? Several PKA substrates at the mitochondria have been reported. The 18kDa AQDQ subunit of the NADH:ubiquinone oxidoreductase complex I (NDUFS4), and possibly subunits of other complexes in the inner mitochondrial membrane and matrix, was reported to be phosphorylated by PKA (Papa, Sardanelli et al. 1996)). Another article disputes this, and reports instead that the 18kDa protein is the ESSS subunit from complex I and additionally found a 10kDa complex I protein phosphorylated, MWFE (NDUFA1) (Chen, Fearnley et al. 2004). BAD, a protein that induces apoptosis when active at the mitochondria, is phosphorylated by mitochondrial localized PKA on Ser112 and consequently inactivated because it binds to 14-3-3 protein which displaces it from the mitochondria (Harada, Becknell et al. 1999; Lizcano, Morrice et al. 2000). PKA regulates the activity of carnitine palmitoyl transferase through its phosphorylation of the lipogenesis enzyme acetyl CoA carboxylase (Winder, Wilson et al. 1997; and Kim, Lopez-Casillas et al. 1989). The protein AAT-1 in the mitochondria of spermatozoa and HeLa cells was demonstrated to be phosphorylated by PKA and associated with AMY-1 (a c-Myc binding protein), RII, and the mitochondrial localized S-AKAP84/AKAP149 (also known as D-AKAP1) (Yukitake, Furusawa 2002). In addition to direct substrates found, PKA is implicated in a number of pathways in the mitochondria. A recent report states that increased cAMP levels causes the tyrosine phosphorylation and subsequent inhibition of subunit 1 of cytochrome c oxidase (COX) (Yang, Iacona et al. 1998; Lee, Salomon et al. 2005). These findings of

putative PKA substrates in the mitochondria, coupled with D-AKAP1 localization to the mitochondria, suggest that PKA may be involved in electron transport, mitochondrial respiration, and/or apoptosis. Recently, an Italian group linked the interaction of D-AKAP1 (AKAP121), PTPD1, Src, and cAMP levels to oxidative metabolism (Livigni, Scorziello et al. 2006). On this basis, we chose to search specifically for direct substrates of PKA in the mitochondria.

Although PKA has been widely studied, the direct substrates of PKA are difficult to distinguish from indirect substrates that are phosphorylated as a result of the activation of PKA. A possible way to determine whether identified substrates are modified by the kinase directly or indirectly via an intermediary kinase is to engineer the ATP binding pocket of the kinase in question to accept a bulky ATP analog that cannot be used by the wild type kinases. Kevan Shokat and his collaborators accomplished this engineering initially in v-Src, a tyrosine kinase isolated from Rous Sarcoma Virus (Shah, Liu et al. 1997), and have subsequently used this strategy for other protein kinases (Dephoure, Howson et al. 2005). This strategy is summarized in Figure 1.8. They found that a single mutation conferred specificity for ATP analogs that have a large substituent on the nitrogen at position 6 (N^6) on the purine ring of ATP (Liu, Shah, et al. 1998). In an earlier paper, they mutated two residues that were found within five Å of the N^6 position on ATP based on the structures of PKA and CDK2 (cyclin-dependent kinase 2) since the crystal structure of v-Src was not available at the time (Shah, Liu et al. 1997). In v-Src, these residues are Val323 and Ile338, while the corresponding residues in PKA are Val104 and Met120. Although the Val323 mutation was found to be not important for conferring specificity in v-Src, mutation of

Ile338 to Ala did alter the specificity of v-Src and allowed the enzyme to use a bulky analog of ATP. Once the crystal structure of hematopoietic cell kinase (Hck), a Src family tyrosine kinase was available, Shokat's group employed molecular modeling programs to explore more fully the binding pocket of Hck to find the best analog for the single mutation (Liu, Shah, et al. 1998). They found that this single mutation opened up another pocket that was otherwise inaccessible and thus termed this residue the "gatekeeper." The best analog, based on the modeling, was found to be N^6(phenethyl)-ATP. Experimentally, N^6(phenethyl)-ATP was preferred by the mutant but was a poor substrate for wild type v-Src. Their method of engineering the ATP-binding pocket was referred to as "chemical genetics" (Bishop, Buzko et al. 2000).

The Shokat technique has been applied to find direct substrates of v-Src (Shah and Shokat 2002) and most recently Yersinia PKA (YpkA) (Juris, Shah et al. 2006). In YpkA, the corresponding residue to Src's Ile338 is Met211. This residue was mutated to both Gly and Ala and conferred specificity for N^6(phenethyl)-ATP. Using cytosolic proteins isolated from J774 macrophages and bovine brain cells, otubain 1, a protein believed to be involved in immune cell anergy, was identified as a substrate for YpkA from *in vitro* assays. The chemical genetics approach has also been used to inhibit analog-sensitive mutants of Cla4p, a protein involved in bud formation in budding yeast (Weiss, Bishop et al. 2000); and Cdc28 (a cyclin-dependent kinase), which is involved in the cell cycle (Benjamin, Zhang et al. 2003).

Our goals for this project were several fold. Initially I engineered a mutant form of the PKA catalytic subunit that accepts a bulky analog of ATP. The modeling of this

mutant, the engineering of the mutant and the expression of the mutant protein in *E. coli* are described in Chapter 2. I then used this protein to identify specific PKA substrates in the mitochondria using mitochondrial-enriched tissue fractions followed by 2-D gel electrophoresis. This led to the identification of a novel protein, ChChd3. The identification of ChChd3 and its subsequent expression in *E. coli* is included in Chapter 3. In Chapter 4 I discuss the domain organization of ChChd3 and then demonstrate by immunofluorescence, tissue fraction, and subcellular fractionation of mitochondria that ChChd3 is a mitochondrial protein localized primarily to the inner mitochondrial membrane.

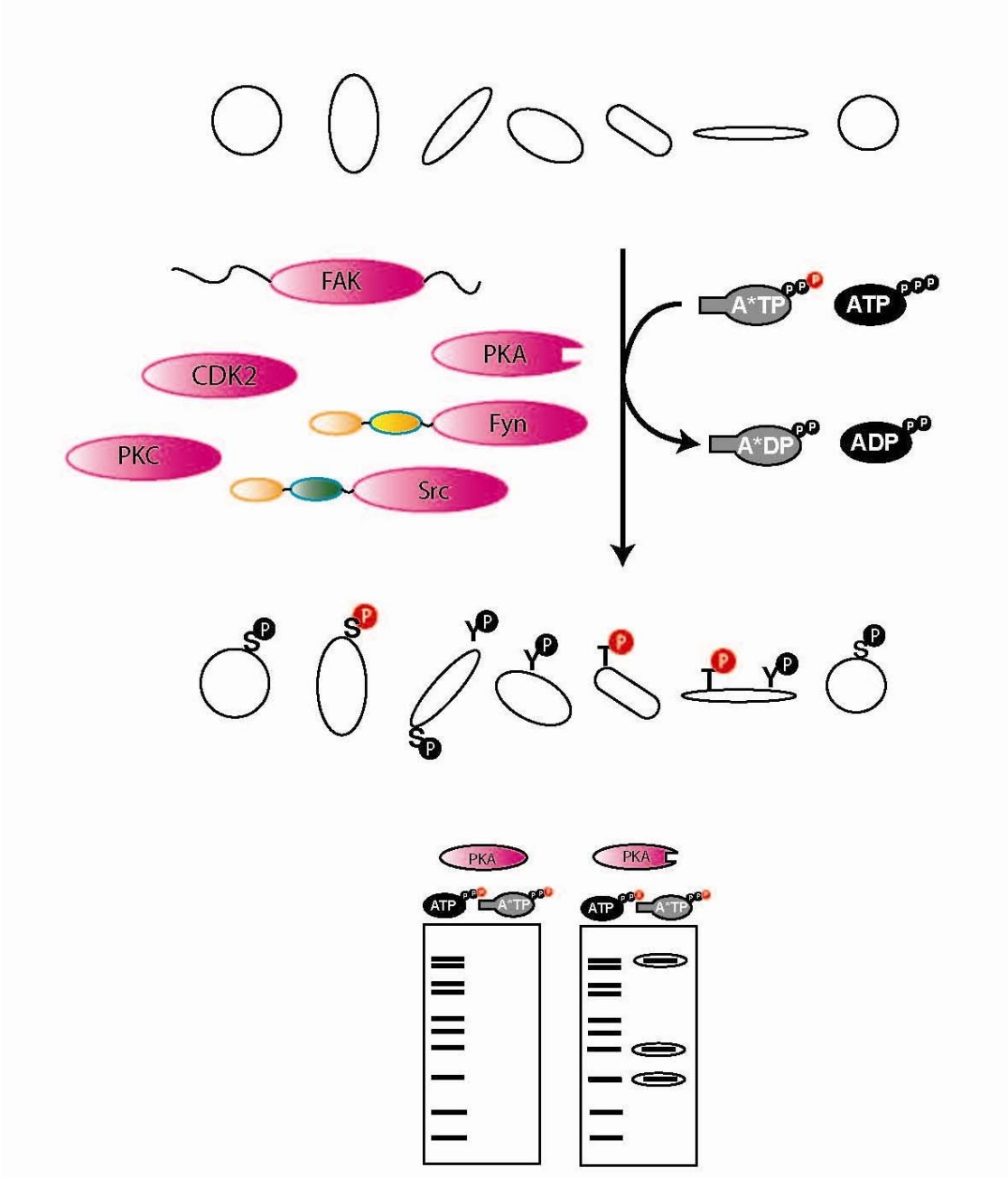

Figure 1.8: Chemical genetic approach to identify the direct substrates of PKA. The PKA is shown with a cut-out to indicate a mutation in the ATP-binding pocket. The A*TP is the ATP analog with a bulky substitution on the adenosine ring; the red ball is the [γ-^{32}P] labeled phosphate. The ovals represent possible substrates that could be phosphorylated by the mutant kinase. At the bottom is a representative autoradiograph of the phosphorylated substrates by the mutant kinase, that are not phosphorylated by the wild type kinase in the presence of the ATP analog. Kindly provided by K. Shah, Purdue University.

CHAPTER II

Engineering the Catalytic Subunit of PKA to Accept Bulky Analogs of ATP

One method developed to find the direct protein kinase substrates, involves engineering the kinase to allow it to accept a modified ATP molecule. Based on previous analysis, a single mutation in the kinase is sufficient to confer specificity for N6-substituted ATP analogs (Liu, Shah et al. 1998). This mutation opens up a larger pocket in the ATP-binding pocket of a kinase allowing for a bulky N6-substituted ATP analog, such as N6(benzyl)ATP, to serve as a substrate (Liu, Shah et al. 1998). Using [32P]-labeled □-phosphate ATP-analogs, one can then detect the substrates that have been phosphorylated. This approach was used here on the catalytic subunit of PKA.

Using the same techniques of molecular modeling, the ATP binding pockets of the wild type PKA catalytic subunit and mutant PKA catalytic subunit were explored. In the first part of this chapter I describe the *in situ* modeling of the ATP binding pocket of the catalytic subunit. In the second part I engineered a mutant form of PKA that will accept bulky analogs of ATP. In the final section I describe the expression of the mutant in *E. coli* and characterize its biochemical properties.

Section 2.1: Computer Modeling of the ATP-Binding Pocket with ATP Analogs

The complementary residues that were mutated in v-Src, Valine 323 and Isoleucine 338, are Valine 104 and Methionine 120 in the ATP binding site of PKA. Methionine 120 (Met120) sits in the hinge region between the characteristic kinase lobes. The adenine ring of ATP lies in a deep hydrophobic pocket at the base of the cleft between the two lobes. The adenine pocket is formed by residues coming from three parts of the molecule. Residues 120-127 in PKA (residues 338-345 in v-Src)

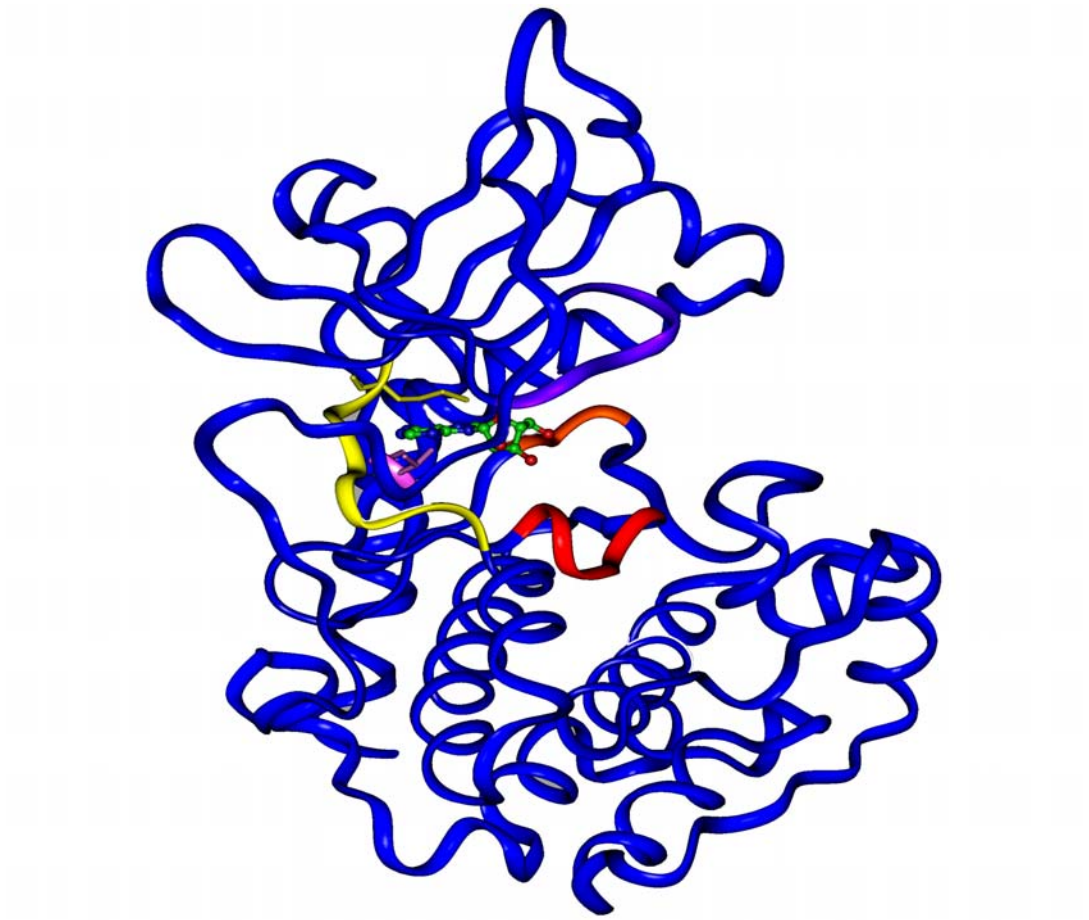

Figure 2.1: Ribbon model of protein kinase A. An adenosine molecule is shown bound to the ATP binding pocket and is colored mostly green with oxygen and nitrogen atoms colored red and blue, respectively. The linker strand (residues 120-127) is yellow with the side chain of M120 shown above the adenosine. Valine 104 is pink and lies beneath the adenosine. The Mg^{+2} positioning loop (residues 184-186) is orange and the catalytic loop (residues 166-171) is red. This picture was created using the 1BKX structure of PKA (Narayana, Cox et al. 1997) in the molecular modeling program InsightII.

comprise the linker region that joins the small and large lobes. Residues from beta strand 4 (specifically Val104 in PKA and Val323 in v-Src) also contribute to the hydrophobic pocket. Leu173 from beta strand 7 from the large lobe also contributes to this pocket.

The crystal structure of the binary complex of adenosine and the C-subunit (Protein Data Bank Code: 1BKX), depicted in Figure 2.1 was an appropriate choice for the modeling of the ATP binding pocket, because it does not have any additional molecules or proteins bound. It is the simplest structure for this study. In analyzing the binding pocket, one can see what needs to be accomplished; a long, flexible substituent must be added onto the N^6 position of ATP in order to move into the area that will open up as a result of shortening the Met120 side chain to Gly or Ala (see Figure 2.2). The Val104 mutation to Ala or Gly may not significantly increase the volume to accept an analog that will not bind to wild type PKA.

Mutations can easily be introduced *in silico* into the protein by simply deleting carbons in the side chains using InsightII (Molecular Simulations, Inc; San Diego, CA) and adding hydrogens where necessary using the "MolBuilder" feature. Two mutants were created, M120G and M120A. Val104 was not mutated based on our modeling and on the conclusions made earlier in the Src study. The adenosine analogs were created by adding groups onto the N^6 with the "Builder" module in Insight. Seven different analogs pictured in Figure 2.3 were made: methoxy (1), ethoxy (2), benzyl (5), benzyloxy (6), cyclopentyloxy (9), cyclohexyl (11), and phenethyl (not shown (13)). The phenethyl substituent has an additional CH_2 between the nitrogen and benzene ring of the benzyl (5) structure.

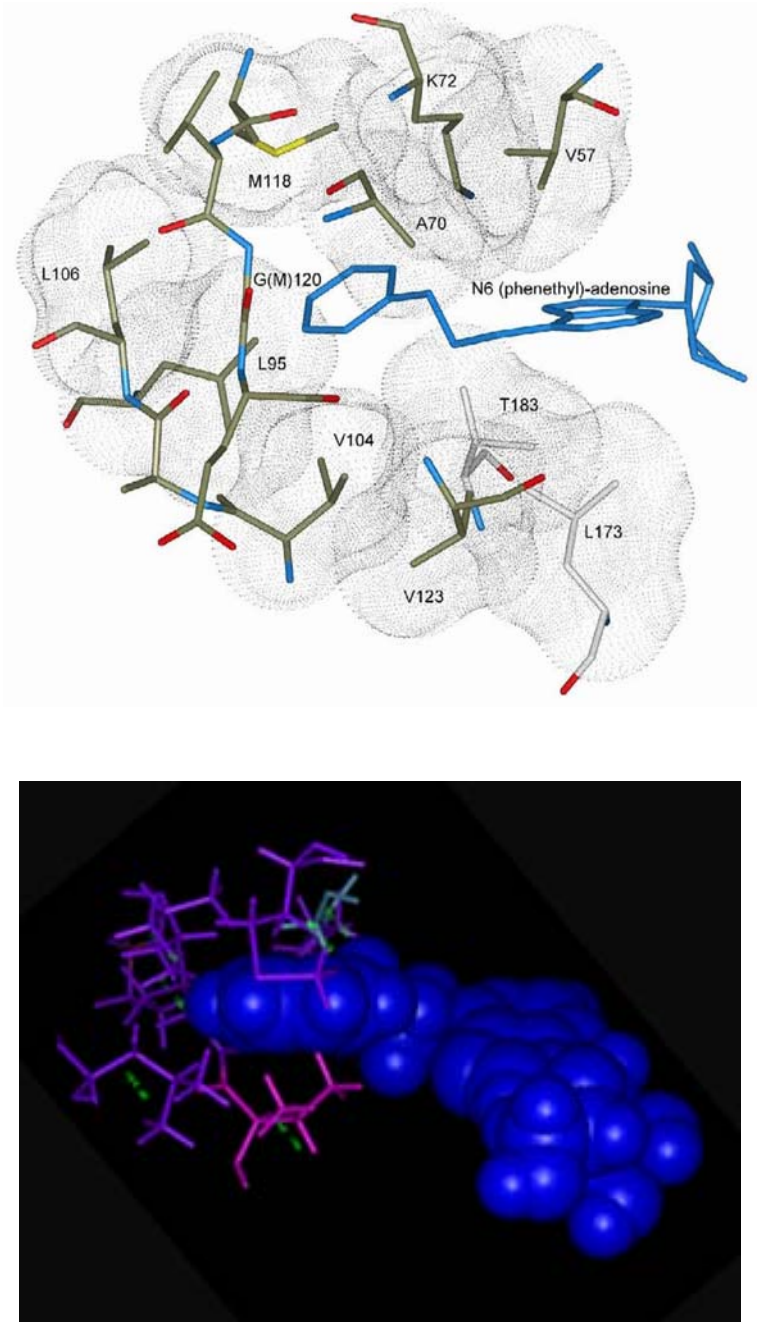

Figure 2.2: Computer models of N^6(phenethyl)-adenosine surrounded by residues close to the hydrophobic ring. Top, N^6(phenethyl)–adensosine surrounded by residues within 4 Å of the benzene ring. Bottom, space filling CPK (Corey, Pauling, Kolton) model of benzyl-ring surrounded by residues 95, 104-106, & 118-121. Val104 is pink, Met120Gly is light blue and the other residues are all purple. These residues appear to accommodate the benzene ring on the phenethyl group of the analog very well. This figure was generated using InsightII.

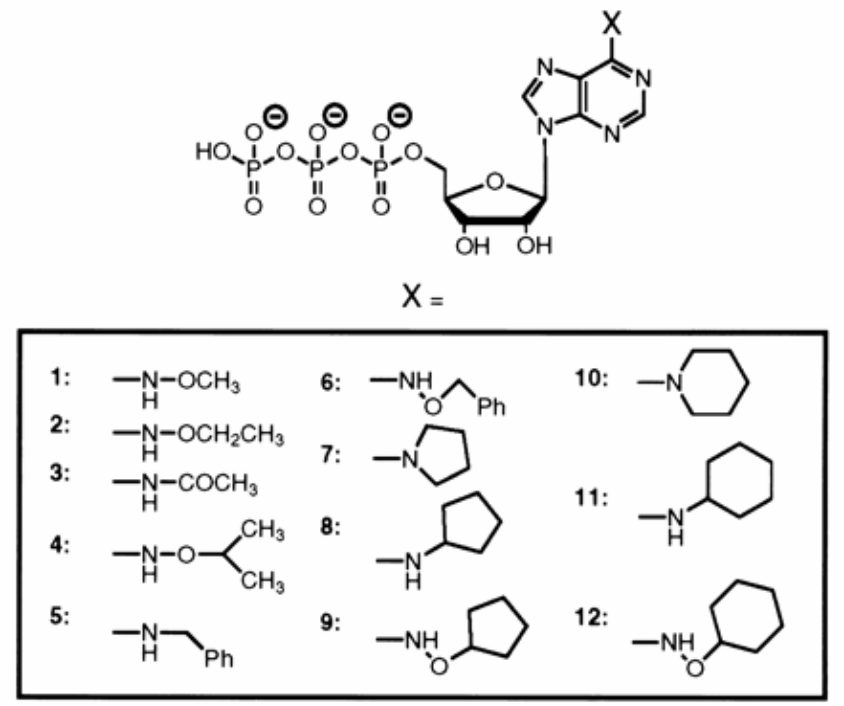

Figure 2.3: ATP analogs considered for interaction with wild type catalytic subunit and *in situ* mutated catalytic subunit. The N^6-substituted analogs that were tested are: methoxy (1), ethoxy (2), benzyl (5), benzyloxy (6), cyclopentyloxy (9), cyclohexyl (11), and phenethyl (not shown). Taken from Shah, Liu, et al. (1998).

According to the strategy adopted by the Shokat group, I used a feature called "bump" in InsightII to determine which analogs are best suited for the binding pocket. This "bump" feature measures Van der Waals steric clashes between atoms and visually displays the bumps by drawing red lines between atoms that are clashing with each other, and then prints out the list of clashes. "Bump" was used to evaluate the ATP binding pocket in PKA. A Van der Waals radii overlap of 0.1 angstroms constituted a "bump." First the number of bumps between normal adenosine and the wild type enzyme were determined. Only three bumps were found (Figure 2.4). A complete listing of the number of bumps for the optimal conformations of the groups added to the N^6 (least amount of bumps for all rotomers tested) are given in Table 2.1. Unfortunately, the bump feature does not automatically sample different conformations for the analog, so the angles must be changed manually and the bumps are then quantitated again.

The dihedral angles were modified using "Geometry" under "Modify" in the "Builder" module in Insight. The dihedral angle for the N^6-C^6 bond was adjusted initially using angles of 0°, 90°, 180°, and 270°. If significant clashes were seen in the analog molecule itself, then that rotomer was not considered a viable conformation. The dihedral angles were then changed one bond at a time from the N^6-C^6 bond. The adenosine stays locked in its position while the groups added onto the N^6 rotate around that nitrogen. Although manually modifying the dihedral angles is a rough way of sampling different rotomers, it worked well for the Hck modeling (Liu, Shah et al. 1998) and could be used quickly.

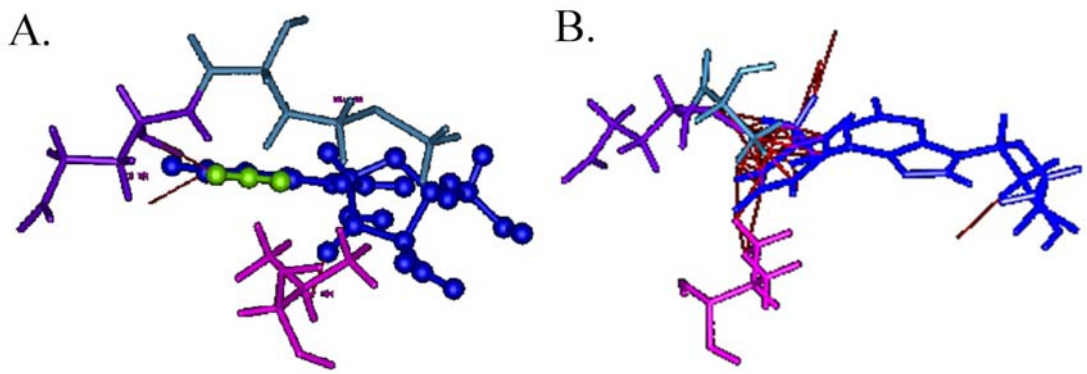

Figure 2.4: Spatial representation of adenosine and N^6(benzyl)-adenosine in the ATP binding pocket. A: Adenosine is shown as a blue ball-and-stick model with Val104 (pink), Met120 (light blue), and Glu121 (purple). The NH2 group at the 6 position on the purine ring of adenosine is highlighted in green. The red lines show Van der Waals clashes between atoms overlapping more than 0.1 Å ("bumps"). B: N^6(benzyl)-adenosine in the binding pocket of PKA where Met120 is mutated to an Ala (shown in light blue). The red lines represent bumps between the benzene ring and the residues in the pocket. These figures were created using InsightII.

Table 2.1: *In situ* interaction of adenosine analogs with wild type catalytic subunit and the M120G mutant. These numbers indicating bumps represent the best conformation found with the lowest number of bumps. The different analogs are shown in Figure 2.3: methoxy, ethoxy, benzyl, benzyloxy, cyclopentyloxy, cyclohexyl, and phenethyl.

protein	*adenosine*	*methoxy*	*ethoxy*	*benzyl*	*benzyloxy*	*cyclopentyloxy*	*cyclohexyl*	*phenethyl*
WT	3	19	32	62	52	65	48	68
M120G	3	12	18	18	20	43	43	18

Bumps were not listed in Table 2.1 for the M120A mutant because the bumps were typically twice as high as the number of bumps obtained at the optimal conformation of the analog with M120G mutant. The best analog is the one that has the most clashes with the wild type pocket, indicating that the unmutated enzyme will have difficulty accepting that analog, and yet has the least clashes with the mutant. Figure 2.4 is an example showing the bumps suffered by the N^6(benzyl)-adenosine analog in the M120A mutant.

Analysis of the smaller groups added onto the N^6 did not show striking differences between the wild type and the mutant C-subunit (see Table 2.1). However, aromatic rings added at that position showed many more clashes for the wild type C-subunit without a significant increase in clashes in the mutant. The cyclohexyl- and other non-aromatic groups appeared to clash significantly with both the wild type and the mutant catalytic subunits. Due to the additional hydrogen bond donors and acceptors on the rings compared to the simple aromatic rings, it is difficult for them to find a position where they are not markedly interfering with other atoms. Based on the number of bumps encountered for each of the analogs, N^6(phenethyl)-adenosine appeared to be the best analog for the M120G mutation in PKA, the same result as that found in v-Src (Hck). The N^6(benzyl)-adenosine also appears to be a good candidate. The dihedral angles for the best phenethyl conformation were found, starting with the angle about the N^6-C^6 bond and moving out one carbon at a time, were 160°, -160°, 180°, and -30°. The last angle is the angle of the phenyl ring rotated at the bond from the ring to the next -CH2- group. This specific rotomer in the wild type pocket has the methionine side chain going right through the aromatic ring. The best conformation for

the phenethyl group in the wild type C-subunit, however, has the phenyl ring squirming its way between the Glu121 and Val104. There were still a large number of clashes seen between the wild type and the analog compared to the mutant.

Binding energies were calculated using the University of Houston Brownian Dynamics program (UHBD). Grid sizes were set up for 55^3 units and 1.5 Å grid spacing. The wild type and the mutant enzymes were run on this program with the adenosine molecule (no analogs were used). The GRASP (Graphical Representation and Analysis of Structural Properties; Nicholls, Sharp et al. 1991) program was used to calculate the electrostatic energies and then to create the electrostatic surfaces shown in Figure 2.5. Residues 48-53, 55, 57-58, 69-71, 95, 103-106, 118-127, 170-174, 182-184, and 326-328 were isolated in a pdb file and grids were created using UHBD for the wild type and the M120G mutant. The grids were read into GRASP which calculated the surface potentials. The residues chosen were the same ones identified by Liu, Shah et al. (1998) as having interactions with the ATP in addition to any seen to have interactions with the phenethyl analog group.

Section 2.2: Mutagenesis of the Catalytic Subunit

Computer modeling and the v-Src studies suggested that mutating only Met120 was sufficient to allow the kinase to accept a bulky-substituted ATP analog. The Kunkel template method (Kunkel 1985) was then used to introduce mutations into the catalytic subunit sequence in the pRSETb vector. Constructs were engineered to

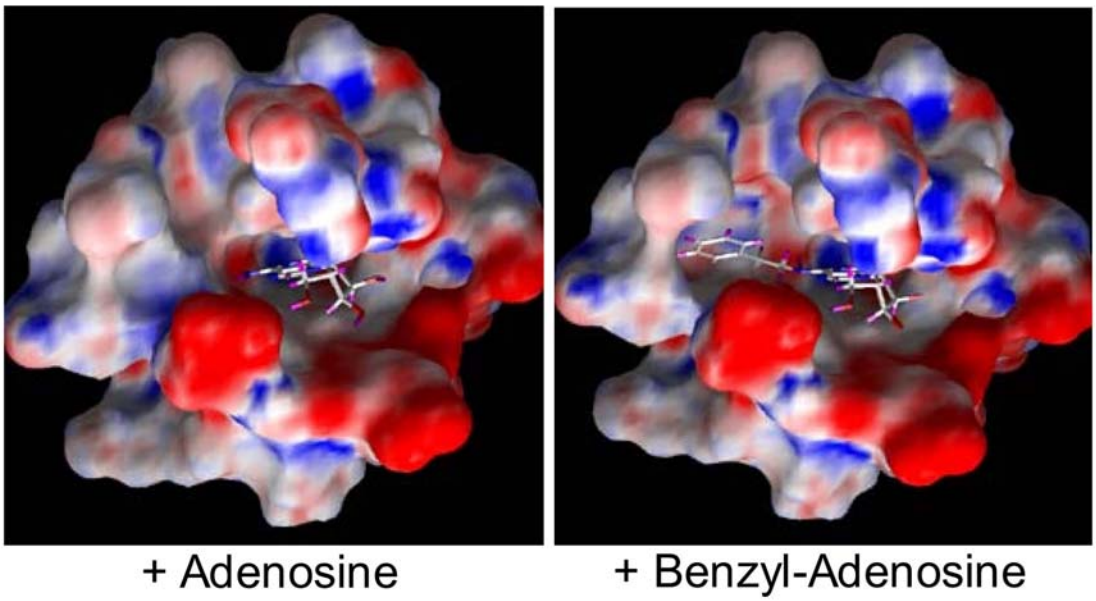

Figure 2.5: GRASP rendering of the ATP-binding pocket in the M120G C-subunit. On the left is the M120G mutant C-subunit ATP binding pocket with adenosine. On the right is M120G with N^6(benzyl)-adenosine. This an estimation of how the ATP analog would fit into the mutated pocket. The mutation of Met120 to Gly opens up a hydrophobic space that accommodates the benzyl ring. These figures were generated using GRASP (Nicholls, Sharp et al. 1991). White = hydrophobic, red = basic, blue = acidic.

convert Met120 to both Gly and Ala. In addition to these single mutants a double mutant was engineered where Val 104 was replaced with Ala. Expression was carried out as described previously (Slice and Taylor 1989). When the M120G mutant was expressed initially in *E. coli*, the protein was highly insoluble. Efforts to purify the protein via the established protocol for wild type C-subunit using P-11 resin and MonoS chromatography, also failed. Consequently, the mutation was introduced into a Histidine-tagged C-subunit construct in the pET15b vector. This allowed us to purify the protein using a nickel resin. As seen in Figure 2.6, expression improved compared to expression with the pRSETb construct; however, the protein was still mostly insoluble.

It is not uncommon for mutant PKA C-subunits to be insoluble due to defective phosphorylation of the protein. Typically when the wild type C-subunit is expressed in *E. coli* it is fully active and contains 2-4 phosphates due to autophosphorylation. Using an antibody generated against the activation loop of PKC that works well for PKA (Dutil, Toker et al. 1998), we demonstrated that the His-tagged M120G mutant is not phosphorylated on either Thr197 in the activation loop or on Ser338 in the C-terminal tail (Figure 2.7) in typical expression conditions. M120G was be found phosphorylated at Ser338 but not Thr197 if the bacterial cultures were grown more slowly and induced at a low optical density (data not shown).

To generate a soluble and active enzyme, we then tried another strategy. It is thought that that 3-phosphoinositol dependent protein kinase (PDK1), is an upstream kinase for PKA (Cheng, Ma et al, 1998). PDK1 readily phosphorylates PKA on Thr197 in the activation loop, while phosphorylation of Ser338 is due to

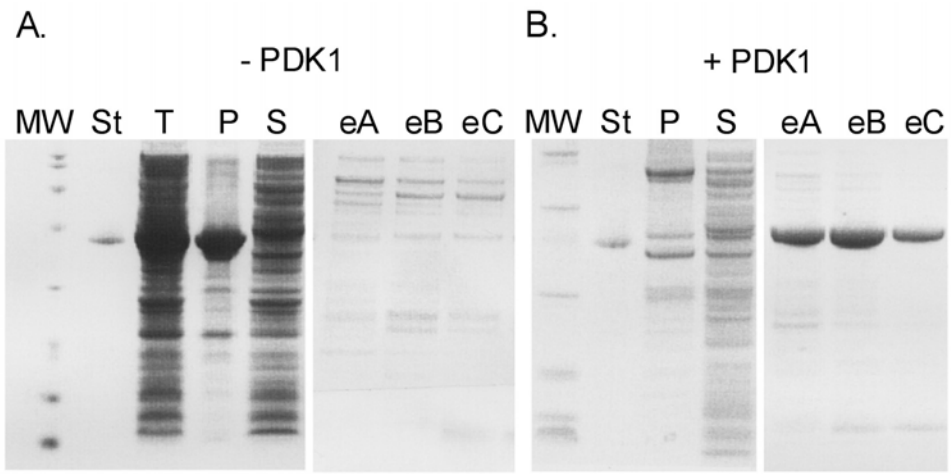

Figure 2.6: Expression and Purification of the M120G Mutant C-subunit. SDS-PAGE gels were run as described previously and stained with Coomassie blue. Figure A shows the expression and purification of his-tagged M120G C-subunit alone. Figure B shows expression and purification of his-tagged M120G C-subunit with PDK1. MW = molecular weight markers; St = WT C-subunit standard; T= total cell lysate; P = Pellet or insoluble fraction; S = Supernatant or soluble fraction; eA, eB, and eC = elutions A, B, and C from the nickel resin.

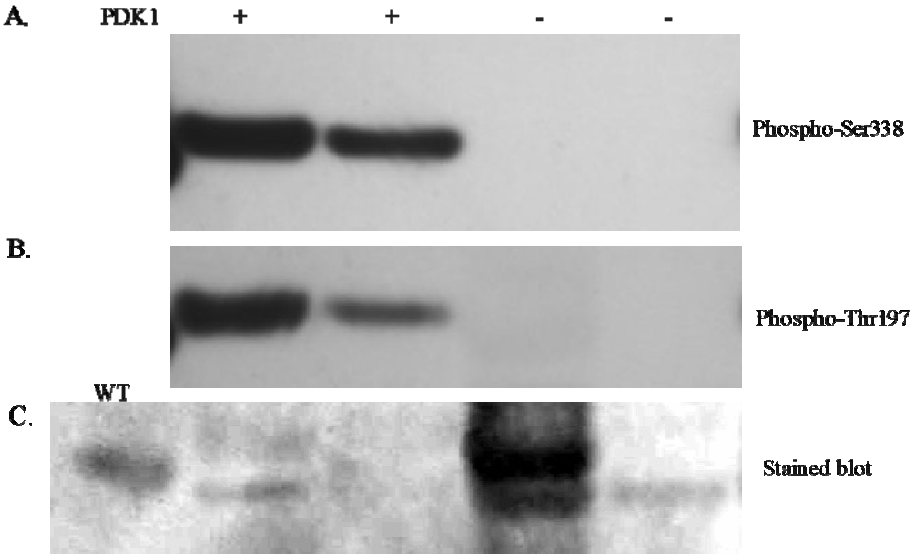

Figure 2.7: Phosphorylation state of expressed M120G catalytic subunit. The upper two panels are Western blots using antibodies that are specific for the phosphorylated sites Ser338(A) and Thr197(B) (Moore, Kanter et al. 2002). The left two lanes represent H_6-M120G expressed in the presence (+) PDK1. The right two lanes are H_6-M120G expressed in the absence of PDK1 (-). (C) Stained blot showing the levels of protein in each sample. The blot was stained with Ponceau S stain.

autophosphorylation (Moore, Iyer, et al 2005). Initially the M120G plasmid in the pRSETb construct was co-expressed with PDK1 in pGEX. The two constructs, however, were not compatible, and transformed *E. coli* expressing both proteins were difficult to obtain. In contrast, the His_6-tagged M120G in the pET15b vector co-expressed well with the PDK1. A comparison of the expression and purification of M120G with and without PDK1 is shown in Figure 2.6. As seen in the figure, the M120G mutant expressed very well on its own but was highly insoluble, and little protein eluted from the nickel resin. When the His_6-tagged M120G was co-expressed with PDK1, however, the yields of soluble pure protein were dramatically improved.

Western blots (Figure 2.7), furthermore, confirmed that both Thr197 and Ser338 were phosphorylated only when the mutant C-subunit was co-expressed with PDK1. There was still a fair amount of insoluble protein even with co-expression of PDK1, but a clear change in the phosphorylation state of the protein and in the yield of the pure protein was seen. Clearly, the mutation disrupts the ability of the mutant protein to autophosphorylate. Either the mutation leads to a conformational change that causes the protein to aggregate or the mutant has an impaired ability to accept ATP so that it is no longer capable of autophosphorylation in *E. coli*.

Section 2.3: Biochemical Characterization of the M120G mutant C-subunit.

Initially, a series of qualitative assays were performed on the mutant enzyme to determine its relative affinity for ATP and for different ATP analogs compared to wild type C subunit. As indicated in Section 2.1, computer modeling suggested that N^6(phenethyl)-ATP or N^6(Benzyl)-ATP would fit best into the newly available

hydrophobic pocket. To test this prediction, [^{32}P]- labeled ATP and ATP-analogs were used in kinetic assays. To determine qualitatively which analogs would be preferred by the mutant C-subunit and which would be worst for the wild type C-subunit, an inhibition assay was used. The inhibition assay consisted of wild type or mutant recombinant kinase, cold ATP-analog, radiolabeled ATP, and Kemptide. The radiolabeled ATP was diluted with varying concentrations of cold ATP analog. After incubation, the sample was spotted on phosphocellulose disks. After washing and drying the disks, the resultant radioactivity was counted with a scintillation counter. Phosphorylated Kemptide binds to the positively charged phosphocellulose disks while unphosphorylated Kemptide does not.

As seen in Figure 2.8, the WT C-subunit was not inhibited by the ATP analogs despite a 100+ fold excess of the analog to radiolabeled ATP. Only a slight inhibition of the wild type kinase was seen with the analog having the smallest N^6-substitutions, N^6(cyclopentyl)-ATP, suggesting that the WT C-subunit can bind to this analog to some degree. However, the mutant catalytic subunit showed a significant amount of inhibition by all of the cold analogs, with the N^6(phenethyl)ATP showing complete inhibition, and the N^6(benzyl)ATP nearly complete. The smallest N^6-substituted analog also competed least well with the radiolabeled ATP.

Following the qualitative comparison, kinetics assays were performed using ATP, N^6(phenethyl)-, and N^6(benzyl)-ATP analogs to determine the Km and *k*cat. As summarized in Table 2.2, the N^6(phenethyl)-ATP and the N^6(benzyl)-ATP had the highest affinity for the mutant C-subunit (at least 15-fold better than for ATP), but neither was turned over as quickly as the wild type C-subunit with ATP. This may be

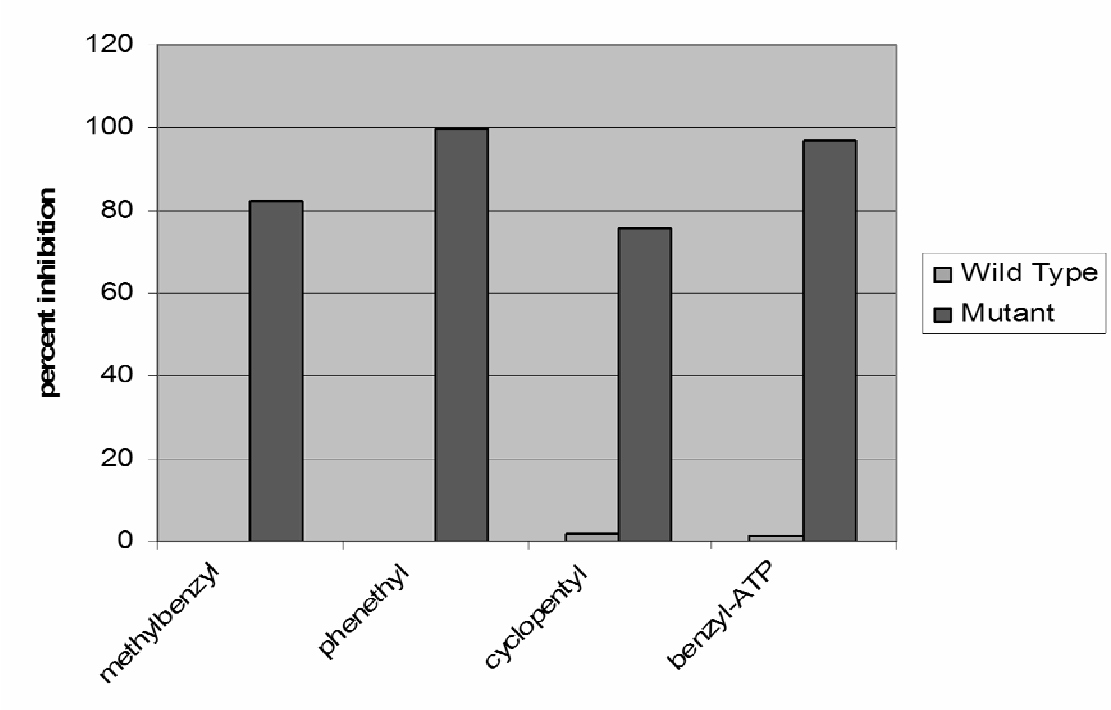

Figure 2.8: Competition of ATP analogs for [γ-^{32}P]-ATP. Each assay contained recombinant C-subunit (mutant or wild type), Kemptide, [γ-^{32}P]-ATP (<1 pM), and one of the cold analogs (100 μM). After incubating at 37°C for 30 minutes, samples were spotted on phosphocellulose disks, washed, and subsequently counted. Unlabeled phenethyl-ATP and benzyl-ATP competed best with [γ-^{32}P]-ATP when the mutant catalytic subunit was used. The wild type catalytic subunit did use the analogs well and therefore there is little or no inhibition.

Table 2.2: Kinetics properties of the native C-subunit compared to the M120G C-subunit. Assays were performed using [γ-^{32}P]-ATP or [γ-^{32}P]-benzyl-ATP and spotted on phosphocellulose disks. Km and *k*cat values were determined by plotting counts per minute vs. concentration in GraphPad Prism. *The number for the wild type catalytic subunit are from previously published results (Grant, Hemmer et al. 1998).

Protein	*Nucleotide*	*Km (μM)*	k*cat* (s^{-1})	k*cat/Km* $(s*\mu M)^{-1}$
WT	ATP	17.4	19.6	1.12
		*20	*22	*1.2
Mutant	ATP	30.5	10.6	0.34
Mutant	Phenethyl-ATP	1.5	0.12	0.24
Mutant	Benzyl-ATP	1.1	0.5	0.53
WT	Benzyl-ATP	>100mM		

due to a slower off rate for ATP. The benzyl-ATP showed a two-fold faster *k*cat/Km (0.529) than phenethyl-ATP (0.242). Other analogs, such as N^6(cyclopentyl)-ATP, did not have a significant advantage over ATP. The modified C-subunit still accepts ATP with a slightly lower affinity than wild type catalytic subunit. The pure mutant protein has a high specific activity with ATP and Kemptide of approximately 28U/mg compared to around 20-24 U/mg for wild type catalytic subunit.

To characterize other properties of the mutant enzyme, we also tested its ability to bind to the RIα subunit. Formation of holoenzyme with RIα has an absolute requirement for ATP (Herberg and Taylor, 1993). As seen in Figure 2.9, the mutant is also inhibited by RIα in a concentration dependant curve similar to the wild type catalytic subunit, demonstrating that the mutation of M120 to Gly did not disrupt regulation of the kinase. The mutant catalytic subunit was also inhibited by PKI similar to the wild type catalytic subunit (data not shown). Like RIα, high affinity binding of PKI also requires ATP.

Section 2.4: Conclusions.

Based on my model of the ATP binding pocket, mutating Met120 to Gly appeared to be the best candidate for accepting a bulky analog of ATP and for discriminating between the wild type and mutant C-subunits. When the methionine side chain is removed and replaced with a hydrogen, a hydrophobic pocket is created that appears to accommodate the bulky phenyl ring at the N^6 position. Based on our computer modeling results, as well as the previous work done on v-Src, it looked as though either benzyl- or phenethyl-ATP would be good candidates to fit into the

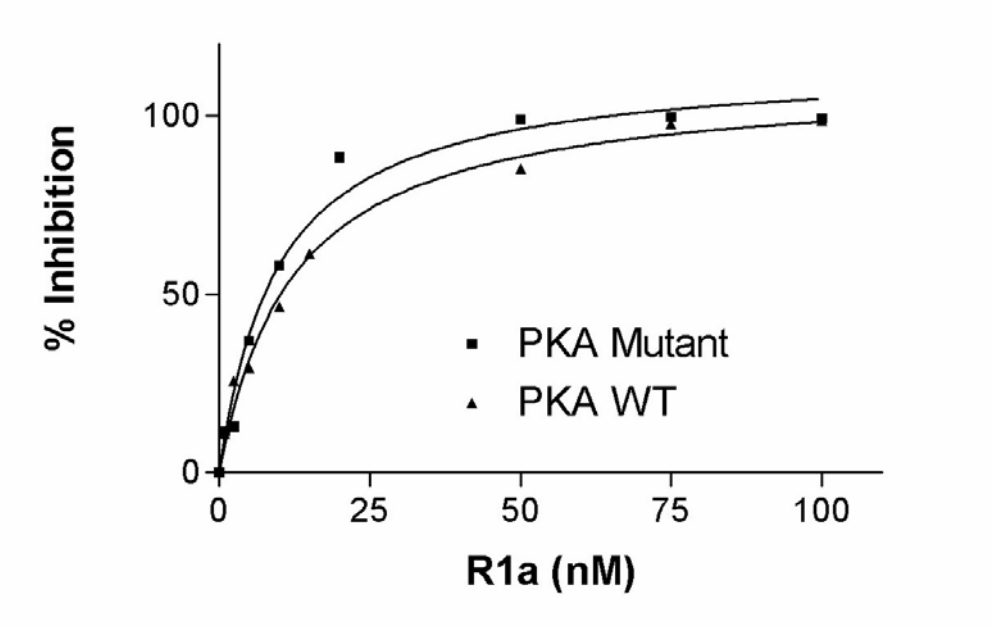

Figure 2.9: Inhibition of catalytic subunits by the regulatory subunit R1α. To test whether the mutant catalytic subunit could be inhibited by the regulatory subunit we used a mutant form of RIα that has a low affinity for cAMP. Increasing amounts of RIα (R209K) was added to each catalytic subunit. Using the standard PKA activity assay, activity of the mutant and wild type was measured.

engineered ATP binding pocket. A bulkier substituted group will also prevent the wild type kinase from using the analogs, whereas some of the smaller substituents, such as of N^6(cyclopentyl)-ATP, could be used to a slight degree by the wild type enzyme. The additional methylene group between the nitrogen and the benzene ring confers the flexibility needed for the benzene ring on the phenethyl group to work its way into the available cove in the mutant. A space filling CPK model in Figure 2.4 demonstrates best the occupation of the pocket by the benzene ring of the N^6(phenethyl)-adenosine analog in the M120G mutant. The residues surrounding the benzene ring in a plane coming out of the page would not normally see any part of the ATP molecule in the wild type enzyme. The methionine residue acts as a "molecular gate," as described by Shokat of the isoleucine 338 in v-Src (Liu, Shah et al. 1998).

In searching for reasons why the mutant kinase would actually prefer the analog over ATP, as found in v-Src, the electrostatic surfaces in the wild type and the mutant PKA were compared using GRASP in Figure 2.5. The opened pocket accommodating the N^6(phenethyl)-adenosine in the M120G mutant is revealed as a fairly hydrophobic surface. The hydrophobic phenethyl group could easily dock into that pocket, possibly resulting in a faster "on" rate of the analog into the site. Certainly the complementarity would be good for the analog, while there would be a "hole" for the wild type C-subunit. However, the rate limiting step for ATP turnover is its "off" rate - meaning it takes the ADP longer to leave the pocket than it does to bind ATP or to transfer the phosphate from ATP to the substrate (Lew, Taylor et al. 1997).

Based on the modeling, the M120G mutation was engineered into the Cα subunit of PKA. Expressing the M120G mutant in *E. coli* proved to be challenging.

The protein initially was completely insoluble and unphosphorylated. This was surprising because the wild type C subunit is completely phosphorylated when expressed in *E. coli,* and this mutant uses ATP fairly well compared to wild type C subunit. The mutation may disrupt folding or may disrupt the stability between the two lobes. The methionine side chain projects out into the ATP-binding pocket between the small and the large lobes (see Figure 2.1). It certainly disrupts the initial autophosphorylation event on Thr197 that leads to secondary phosphorylations in the C-subunit when the enzyme expressed in *E. coli*. Phosphorylation of Serine 338 is thought to be intramolecular (Moore, Iyer, et al 2005).

To overcome this problem, we decided to attempt to co-express M120G PKA with 3-phosphoinositide-dependent kinase (PDK1). PDK1 is an upstream kinase for many AGC kinases including PKA (Cheng, Ma et al. 1998). This protein is constitutively active, but it appears to be regulated by its proximity to substrates through its plextrin homology (PH) domain (Peterson and Schreiber 1999). This PH domain binds to PI-(3,4,5)-P3. PDK1 binds to an F-X-X-F motif on the C-terminal tail of PKA (Biondi, Cheung et al. 2000) and its other substrates. PDK1 then phosphorylates PKA at Thr197. When co-expressed with the unphosphorylated M120G mutant, the mutant became phosphorylated on both Thr197 and Ser338 and was consequently soluble. This technique proved to be highly useful for purification of other insoluble C-subunit mutants in the laboratory.

N^6(Benzyl)-ATP was the best choice for specificity based on the kinetic analysis. The Km was similar to N^6(phenethyl)-ATP but the turnover was faster. This is advantageous because the kinase will still be active. In other work done with this

mutant, published after this work was completed, it was found that this mutation of the catalytic subunit (M120G or M120A) also conferred specificity to a class of pyrazolo[3,4-d]pyrimidine-based inhibitors (Niswender, Ishihara et al. 2002). The inhibitors are similar to the PP1 inhibitor found to be specific for Src family kinases (Hanke, Gardner et al. 1996). The derivative inhibitors 2-NM and 1-NOM were found to be specific for the M120G mutation (Niswender, Ishihara et al. 2002). When the wild type C-subunit is replaced with the M120G mutant in mice or tissue culture cells, the kinase could then be inhibited by the cell-permeable PP1 derivatives and the phenotype or gene expression changes could be monitored. I also found that the PP1 inhibitor used for Src family kinases effectively inhibited the M120G mutant (data not shown).

As described in Chapter 3, this engineered protein was used to find direct PKA substrates by adding it to cell lysates with radiolabeled N^6(benzyl)-ATP. The [^{32}P]-labeled proteins were detected by first separating on two-dimensional SDS-PAGE, and then exposing the resulting gels to autoradiography film or a phosphoimager. Ideally, this mutant protein also could be expressed in tissue culture cells to probe for direct substrates; however, currently there is not a good way of getting the ATP analogs into the cells.

There are many different protein kinases in the cell. Nearly 2% of the human genome codes for protein kinases (Manning, Whyte et al. 2002) and each typically has multiple splice variants. This makes finding actual substrates, not just "biochemically feasible" substrates, of a specific kinase difficult. The molecular modeling results demonstrate how similar the ATP binding pockets are between Src family kinases and PKA. This demonstrates why efforts to create specific ATP-like inhibitors for kinases

are challenging. Using ATP analogs that are labeled at the γ-phosphate with [^{32}P], one can identify substrates specific to that kinase that are labeled (referring back to Figure 1.1 from Chapter 1). The direct substrates can then become specific targets for drug design, in addition to the kinase. This is important because many kinases can be mutated and thereby converted into oncogenes that lead to cancer. Genetic defects in protein kinases and protein kinase associated proteins are causative factors in many diseases, not just cancer.

Section 2.5: Materials and Methods.

Computer Modeling - Used InsightII (Molecular Simulations, Inc; San Diego, CA) to examine modified PDB file structures. PDB files of the structure 1BKX (Protein Data Bank Code) were modified to simulate mutations in the ATP binding pocket of ATP.

Mutagenesis and Expression – The oligo used for the mutation for Met 120 to Gly is: 5'-CAGCTACATACTCCCCGACCATGTA-3' (Genbase). Mutations in the C subunit in the pRSETb vector were made using the Kunkel template method. His_6-tagged C subunit in pET15b was made by cloning out of pRSETb (Invitrogen) at the NdeI and HindIII sites. Mutations introduced in the His-tagged C subunit pET15b construct were done using Quikchange by Stratagene. Constructs were transformed into *E. coli* BL21 (DE3) bacteria. In the case of the co-expression, both the M120G in pET15b and GST-PDK1 in pGEX were added during transformation.

Colonies tested for expression of the proteins in question were grown up to an optical density at 600nm of 0.6-1.0 and then induced with 0.5 mM isopropyl-β-D-thiogalactopyranoside for 4-6 hours. Cells were collected by centrifugation and

resuspended in Laemmli sample buffer. Samples then were run on SDS-PAGE (10%). To test for solubility, the harvested cell pellets were resuspended in lysis buffer (50 mM $NaHPO_4$, 20 mM Tris-HCl, 100 mM NaCl, pH 8.0) and subjected to 3 freeze/thaw cycles. The samples were then centrifuged for 30 min. at 4°C and 16,000 rpm in a microfuge to separate the soluble (supernatant) and insoluble (pellet) fractions. The proteins were then separated on an SDS-PAGE (10%) gel.

Purification of the M120G PKA Catalytic Subunit - Cultures were harvested after the induction period as described above, spun down, resuspended in lysis buffer (50 mM $NaHPO_4$, 20 mM Tris-HCl, 100 mM NaCl, pH 8.0) and lysed by one pass in a French pressure cell at 1,000 p.s.i. The resulting lysate was then spun down for 40 minutes at 15,000 rpm in a Beckman JA20 rotor at 4°C. The His_6-tagged C-subunit protein was then purified using the procedure for Talon Nickel resin (Clontech). Supernatant was batch-bound to 1.0 ml resin/1 L culture for 1 hr at 4°C. The resin was washed twice with lysis buffer and once with wash buffer (same as lysis buffer but at pH 7.0). The His-tagged protein was then eluted off with 4 increasing imidazole elutions starting from 50 mM to 500 mM.

Western Blot Analysis – Lysates from transformed *E. coli* were run on a SDS-PAGE gel and then transferred to PVDF (polyvinylidene fluoride) membrane at 30 V for 60 min. The blots were probed with an anti-phospho-threonine 197 antibody (kindly provided by A. Newton, UCSD) and anti-phospho-Serine 338 antibody (SynPep Corp.), a custom antibody described previously (Moore, Kanter et al. 2002). The secondary antibody was an anti-rabbit horseradish-peroxidase (HRP) conjugate (Pharmacia Biotech). The membranes were blocked in 5% milk in TBST (Tris-Buffered Saline Tween-20)

overnight. The blocking solution was removed and the membranes were rinsed twice with TBST. The primary antibody was incubated with the blot at room temperature for 1 hour with gentle shaking. After the primary antibody was poured off, the membranes were rinsed 4 times with TBST. The second antibody, anti-rabbit-HRP, was added at a dilution of 1:2000 and the blots were incubated for 30 min. at r.t. with gentle shaking. The blots were rinsed with TBST twice and then incubated with SuperSignal West Pico chemiluminescent substrate detection kit (Pierce) for one minute. Bands were detected with ECL Hyperfilm (Pharmacia Biotech).

Inhibition Assays – The assay mixture consisted of MOPS, $MgCl_2$, 100 μM cold ATP or ATP analog (kindly provided by K. Shah), [γ-^{32}P]-ATP (1 pM), 200 μM Kemptide and 100 nM WT or mutant enzyme in a 30μL volume. The samples were incubated at 37°C and quenched with 20μL of 50% acetic acid. Fifty μL of the mixture was spotted on phosphocellulose disks. The disks were washed for 10 min. in 0.5% phosphoric acid four times, followed by one brief rinse with acetone. They were counted in a scintillation counter. Assays were done in duplicate.

Kinetic Assays – Two assays were used to evaluate the catalytic efficiency of the mutant enzymes. Radioactive assays were performed in triplicate using [γ-^{32}P]-ATP. The assay mixture was comprised of 50 mM MOPS, 5 mM $MgCl_2$, 0.5 mM DTT, 100 μM Kemptide, cold ATP or cold N^6(benzyl)ATP or N^6(phenethyl)ATP analogs, and purified recombinant WT and mutant enzyme (0.25-0.5nM). The samples were incubated at 30° C for 5 min. Thirty microliters of each of the samples were spotted on phosphocellulose disks, washed, and radioactivity was counted in a scintillation counter as described

above. The computer program Prism (GraphPad Software, Inc.) was used to calculate Km and *k*cat values.

Activity Assay – Activity was also monitored using a coupled assay as described by Cook, Neville et al. (1982). In this assay, 200 μM Kemptide, 100 mM MOPS, 10 mM $MgCl_2$, 1 mM PEP (phosphoenolpyruvate-dependent enzyme), 1 mM ATP, 15U/ml LDH (lactate dehydrogenase), 7U/ml PK (pyruvate kinase), and 0.2 mM NADH, were incubated with 0.3 mg/ml C-subunit. All components except Kemptide and PKA were mixed. The reaction was initiated by adding 990 μL of assay mix was added to a cuvette, and then 10 μL of PKA C-subunit. The mixture was blanked in spectrophotometer and 10 μL of Kemptide was added to start the reaction.

CHAPTER III

Identification of a Novel Mitochondrial PKA Substrate

To identify direct substrates of PKA, we engineered a mutant of the PKA catalytic subunit that will preferentially accept a bulky analog of ATP. As described in Chapter 2, this mutant has a preference for N^6(benzyl)-ATP which is not utilized at all by the wild type PKA C-subunit.

We chose to focus specifically on mitochondria to identify PKA substrates since two dual specific A kinase anchoring proteins, D-AKAP1 and D-AKAP2, are shown to localize to mitochondria. Mitochondria were purified from mouse brain and then incubated with the recombinant mutant C-subunit. In this chapter we describe the identification of a novel PKA substrate using two-dimensional gel electrophoresis followed by mass spectrometry. In Chapter 4 we characterize the endogenous protein and demonstrate that it is localized to the mitochondria. We also expressed the protein in *E. coli* and showed that it is phosphorylated by PKA.

Section 3.1: Identification of PKA Substrates.

Originally, the method of engineering a kinase to accept an ATP-analog was going to be applied *in vivo* by expressing the mutant kinase in tissue culture cells. The cells would then be incubated with [γ-^{32}P]-labeled ATP analog. The negative charges on the ATP molecule, however, make it inherently difficult for the cells to take up the ATP analogs. In addition to this, a cumbersome amount of radiolabeled ATP analog would be needed. In place of the *in vivo* assay, an *in vitro* assay was thus developed to identify phosphorylated substrates of the mutant kinase. Crude mitochondria were isolated from mouse brain as described in the Experimental Procedures. After sacrificing the mice, the brains were removed and immediately homogenized. After

homogenization, the samples were subjected to a series of centrifugations in order to separate the different cellular fractions. The mitochondria were thus crudely purified, meaning that there may be some endoplasmic reticulum and golgi present in the samples. This was not of concern because PKA may also have substrates in these organelles. The samples were initially tested via a Western blot with an antibody to lipoic acid, a mitochondrial-specific marker, to demonstrate that mitochondria were enriched in this fraction.

Assays consisted of purified recombinant mutant C subunit, cold ATP, [γ-^{32}P]-benzyl-ATP, and brain mitochondrial fractions. The amount of cold ATP used in the assays had to be optimized in order to reduce background, but not too much as the mutant kinase still uses ATP quite well. As a control, parallel incubations were carried out in the presence of an inhibitor peptide (IP20) derived from PKI, which is a highly specific inhibitor of PKA. Figure 3.1 (left) shows a representative autoradiograph of a 1-D gel used to optimize the amount of cold ATP added. The ratio of 100 μM cold ATP to 1 μM recombinant mutant kinase appeared to be optimal.

After the amount of cold ATP was optimized, the samples were subjected to two-dimensional gel electrophoresis. In the first dimension, the samples were run on immobilized pH gradient strips. The first samples were run on strips of pH 3-10. Then the IPG strips were laid lengthwise across the top of a pre-cast gel. After the strips were sealed in with agarose, the gels were run in normal SDS-PAGE buffer. The proteins previously separated by their isoelectric point (pI) were then separated on the basis of their molecular weight in the second dimension. The gels were either stained and exposed directly to autoradiography film or the proteins were transferred from the gel to

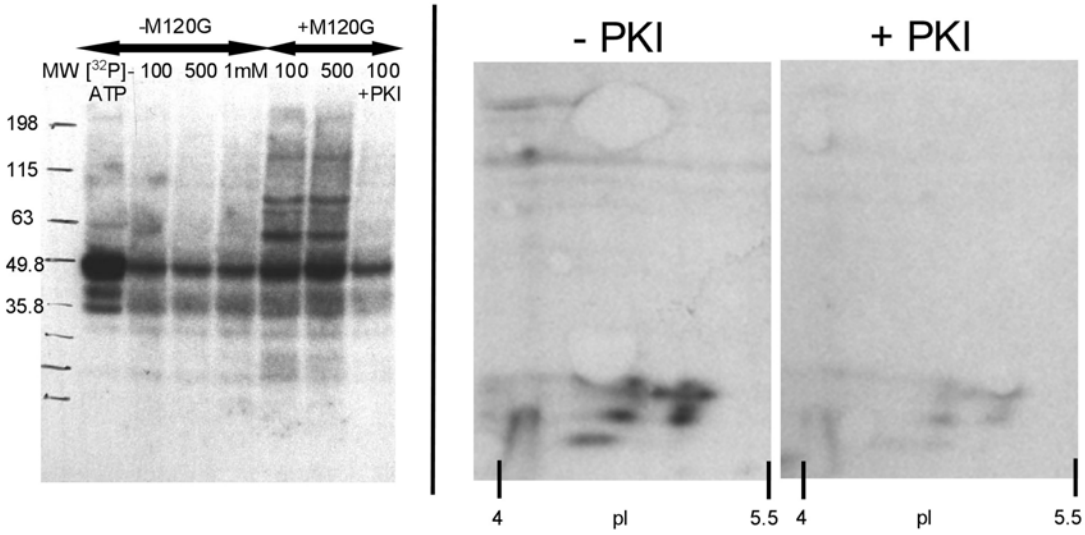

Figure 3.1: Phosphorylation of mitochondrial proteins by the M120G subunit. In both cases proteins from SDS-PAGE gels were transferred to nitrocellulose membrane prior to exposure to film. The samples contain [γ-^{32}P]-N^6(benzyl)-ATP, cold ATP, crude mouse mitochondria, and recombinant mutant C-subunit, with and without PKI. The left lane shows optimization of labeling conditions. MW = molecular weight marker. Lanes under "-M120G" (no M120G C-subunit present): [^{32}P]-ATP = [γ-^{32}P]-ATP alone; 100, 500, and 1mM corresponds to 100 μM, 500 μM, and 1mM cold ATP. Lanes under "+M120G" all contain 1μM M120G C-subunit. 100 and 500 = 100μM and 500μM cold ATP. 100 +PKI = 100μM cold ATP, 6μM PKI. Samples were incubated for 10 minutes. On the right are 2-D gels run in the presence and absence of PKI. These gels correspond to samples 2 and 4 on the left lane. The two membranes were exposed to the same piece of film for the same length of time.

nitrocellulose membrane and then exposed to film. Transferring the proteins to nitrocellulose may have resulted in some loss of protein but the spots on the autoradiographs were much sharper. Figure 3.1 (right) shows a representative autoradiograph from a nitrocellulose membrane.

A group of phosphorylated spots of low molecular weight always showed up on the 2-D gels around pH 5, so this is where I focused initially. To better isolate these proteins, samples were run in two different pI ranges, 4-7 and 6-10. Also, because these were low molecular weight proteins, the IPG strips were overloaded with protein in order to obtain enough protein to visualize. Overloading the gels resulted in streaking of higher molecular weight proteins horizontally across the gel, but the small molecular weight proteins resolved nicely.

The autoradiograph shown in Figure 3.2 demonstrates the resolution of the low-molecular weight proteins. Several of the [^{32}P]-labeled spots were excised from the nitrocellulose membrane by overlaying the autoradiograph with the membrane as described in the Experimental Procedures. As shown in Figure 3.2, labeling of most of the proteins was abolished in the presence of PKI. Both of the PKA mutant and PKA mutant plus PKI membranes were exposed to the same piece of film for the same amount of time. However, if the PKI-inhibited sample was exposed for a greater length of time, the spots eventually showed up on the autoradiograph due to a low level of residual PKA activity. Thus the spots were excised from both membranes and combined in order to get enough protein for identification by mass spectrometry.

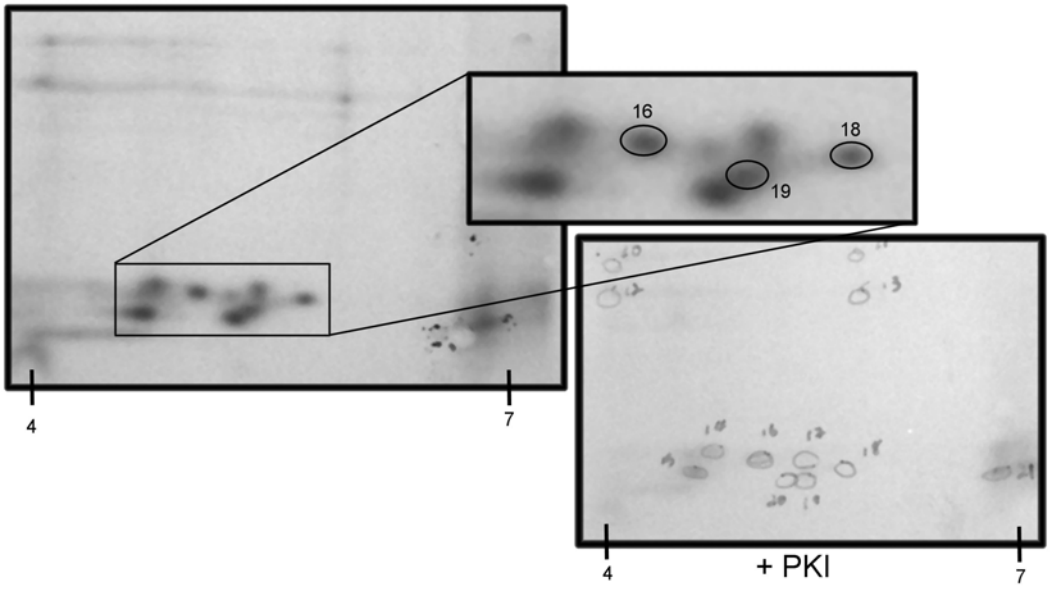

Figure 3.2: Autoradiograph of the phosphorylated proteins in a mouse brain mitochondrial sample. The pI range for this autoradiograph is 4-7 as indicated. The region containing the most phosphorylated spots, corresponding to proteins in the lower molecular range is enlarged; the spots are circled and numbered. The numbers correspond to the spot numbers in Table 3.1. The smaller autoradiograph is the PKI inhibited sample. Both membranes were exposed to the same piece of film for the same amount of time. Some spots listed in Table 3.1 are not shown on the above autoradiograph. They were taken from other 2-D gels and pI ranges.

Section 3.2: Identification of Phosphorylated Proteins by Mass Spectrometry.

The samples were prepared for analysis by MALDI-TOF mass spectrometry as described in the Experimental Procedures. After elution from the nitrocellulose membrane, the proteins were trypsinized. The resulting peptides were mixed with a matrix and then spotted on the MALDI-TOF sample plate. The peptides that were identified based on their mass over charge peaks were then entered into the Protein Prospector (UCSF) database. The program then provides a list of probable matches to the mass-over-charge peaks, with a probability score that helps one determine how likely the match actually is to the identified protein.

Initially, many of the spots turned out to be subunits of ATP synthase. This was good because it confirmed that the sample contained mitochondrial proteins. A sample of ATP synthase was obtained (kindly provided by W. Allison, UCSD) and recombinant PKA catalytic subunit was added to it to see if ATP synthase was indeed a substrate. It was not a substrate for PKA, but this major protein in the mitochondria was very abundant and contaminated a large portion of the gel. In the spots shown in Figure 3.2, no ATP synthase was found. The radiolabeled spots are numbered in the figure and the Table indicates the most probable identification of each spot. In general, values of greater than 100 represent reasonably good matches. Only a few of the spots had good enough hits to qualify. Table 3.1 lists the accession number of the protein that were the most probable match for the peptides.

The most promising hit was spot 19, as shown in Figure 3.2. The actual peptides identified that correlated with spot 19 are underlined in Fig. 3.2. Three mass over charge peaks 973.6101, 997.4132, and 1707.8722 matched the peptides shown

Table 3.1: Best match proteins identified for spots 5, 16, 18, and 19. Also indicated are the peptides sequences and the mass over charge numbers for the three peptides that were used to identify ChChd3. The peptides identified by MALDI-TOF that matched ChChd3 were as follows: AAANEQLTR (mass=973.5067); VTTEEYQK (mass=997.4842); and VTFEADENENITVVK (mass=1707.8441).

Spot	Match	Score	PKA phos. site	Description
5	X97571	111	Yes	GRIP1, a rasGEF AAH17687
16	AK003989	88.4	No	Similar to smoothelin large isoform L2
18	12849144	88.3	Yes	Homolog to protein disulfide isomerase A5 precursor
19	ChChd3	163	Yes	Coiled coil-helix coiled coil-helix containing protein; unknown

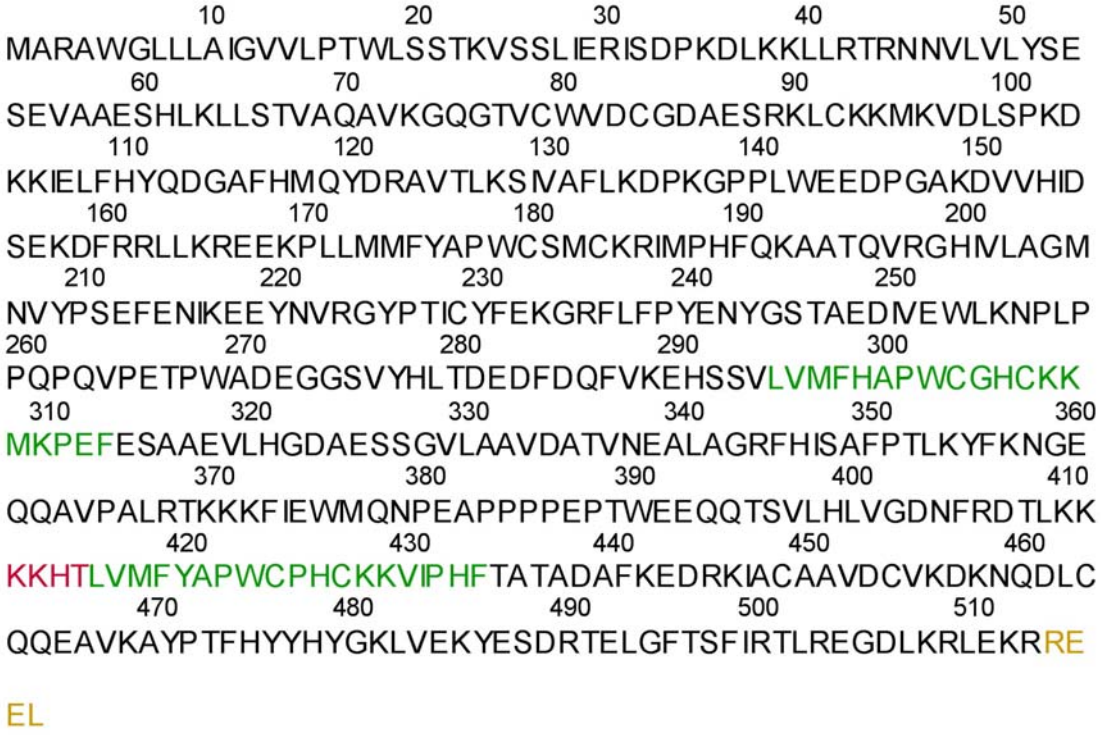

Figure 3.3: Protein sequence of protein disulfide isomerase A5. A fragment of this protein was identified in spot 18 from the table above. Highlighted in green are the thioredoxin family active sites. The proposed PKA phosphorylation site is in red. An endoplasmic reticulum targeting sequence is at the C-terminus and it is highlighted in yellow.

in Table 3.1 under the description of spot 19. The match came up as an unknown protein, accession number 12839842, which encodes for a homolog to FLJ20420, a human protein (now known as ChChd3). The original match was not the full length protein match to human ChChd3. In mouse, the full homolog to the human FLJ20420 is clone Rik 0610041L09, which is the clone number from the RIKEN cDNA sequencing project which identifies all the proteins encoded for by the mouse genome. This protein was identified to contain two coiled-coil helices at its C-terminus and was later named ChChd3. The rest of the protein has homology to a DUF737 domain, but there is no known information about the function or structure of this domain. I shall subsequently refer to this protein as ChChd3. Previously, two other groups identified this protein from their 2-D gel proteomic experiments. The first group found this protein in the inner membrane from mouse liver mitochondria (Da Cruz, Xenarios et al. 2003). The other group identified this protein while attempting to identify all of the proteins in mouse mitochondria (Mootha, Bunkenborg et al. 2003). They associate 0610041L09 Rik with oxidative phosphorylation by using a pairwise correlation matrix of gene expression and functionally related sets of genes.

Two other promising hits that are listed in Table 3.1, GRIP1, a rasGEF, and the homolog to protein disulfide isomerase A5, had decent scores and putative PKA phosphorylation site. The homolog to protein disulfide isomerase A5 is actually a fragment of protein disulfide isomerase associated 5 (PDIA5), found by entering the protein sequence into BLAST (Basic Local Alignment Search Tool; Altschul, Gish et al. 1990). Proteins in the PDI family are typically found in the endoplasmic reticulum, but recently they have been found in other cellular locations such as the nucleus, cell

surface, and cytoplasm (Turano, Coppari et al. 2002). The proposed PKA phosphorylation site in this protein is at residues 412-416 (KKHTL), and immediately following the phosphorylation site is a thioredoxin family active site (see Figure 3.3). Clones were obtained for the GRIP1 and PDIA5 constructs but they have not been followed up as of yet.

Section 3.3: Characterization of ChChd3.

The sequence of ChChd3, as well as the peptides that were identified by mass spectrometry, is shown in Figure 3.4. The presence of a C-terminal domain that contains two coiled-coil helices, which is found in other known mitochondrial proteins such as Cox19p in *S. cerevisiae* (Nobrega, Bandeira et al. 2002), is a promising motif for an unknown protein thought to be in the mitochondria. ChChd3 also has a nearly identical human homolog (see Chapter 4). It has an ideal conserved PKA phosphorylation site at Thr10 (RRVTF), and another possible site at Ser78 which is also conserved in the human form. Since the N-terminus also has a myristylation motif, the N-terminal PKA phosphorylation site may be involved in the regulation of targeting, and may even serve a similar function to the Ser10 phosphorylation site in PKA, which is known to be myristylated (this is discussed more fully later). Src also has a PKA phosphorylation site near the myristylated N-terminus. The domains are described more comprehensively in Chapter 4.

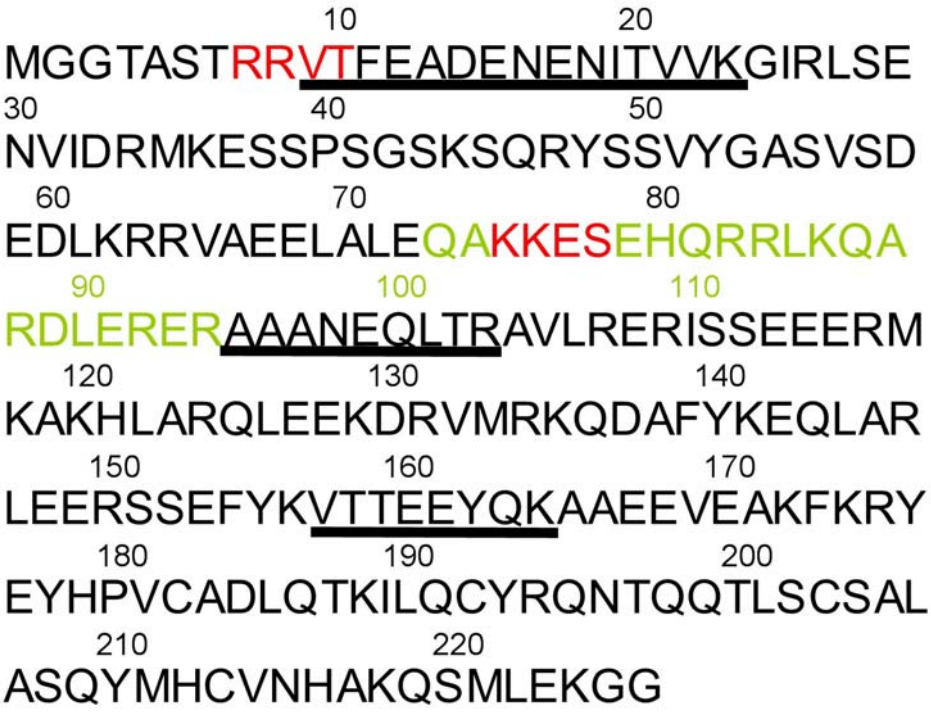

Figure 3.4: Amino acid sequence of the unknown protein identified as ChChd3. The putative phosphorylation sites are indicated in red. The peptide that was used subsequently for generating antibodies is in green. The peptides that were identified by mass spectrometry are underlined.

Section 3.4: Expression of ChChd3 in *E. coli* and phosphorylation by PKA.

The DNA clone corresponding to mouse ChChd3 was ordered from Invitrogen (catalog 5125404), and subsequently cloned from the pCMV-Sport6 vector and transferred into a pGEX vector for bacterial expression. The protein was GST-tagged in order to help solubilize the protein and for purification purposes. Although the protein expressed well in *E. coli* and had the correct molecular weight of approximately 55 kDa, most of the protein was insoluble (Figure 3.5). This made purification of the protein difficult. Purification of the protein was attempted using glutathione Sepharose beads. A very small amount of protein was eluted from the resin, however, there also appeared to be a large amount of breakdown products, as seen in the Coomassie stained gel of two of the glutathione elutions on the left in Figure 3.6A. The band at 55kDa is the GST-ChChd3 construct.

The resulting GST-ChChd3 elutions were incubated with PKA wild type C subunit and [γ-^{32}P]-ATP to look at *in vitro* phosphorylation of the novel protein. Figure 3.6A shows the comparison between the Coomassie stained protein elutions and the autoradiograph of the PKA phosphorylated bands. The band at 55kDa is phosphorylated but so is a band at 35 kDa. This band is much stronger on the autoradiogram because there is considerably more of this apparent breakdown product. It is unknown where the protein is breaking down, but it could possibly be ChChd3 protein without the GST tag. Alternatively the C-terminal CHCH domain could be cleaved off.

Another experiment was carried out to see if PKA does indeed recognize and phosphorylate the N-terminus of ChChd3. Using an automated peptide synthesizer,

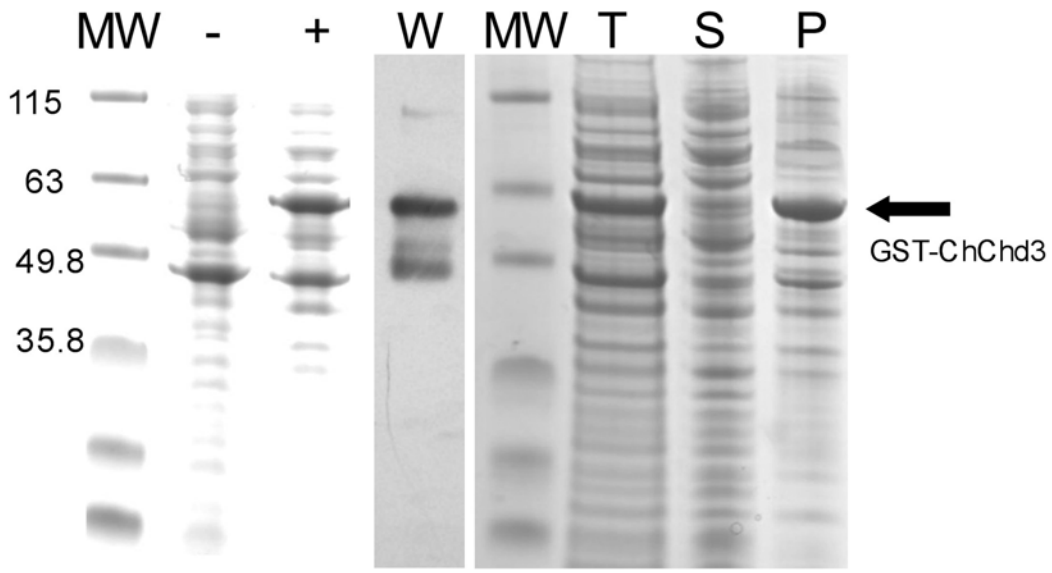

Figure 3.5: Expression and solubility of GST-ChChd3 in *E. coli*. The left lanes show a representative expression experiment. Gels were stained with Coomassie blue. Induction was carried out for 4 hours. The minus indicates samples that were not induced, the plus lane is the induced *E. coli* sample. Following lysis and centrifugation (right panel), the protein is mostly in the pellet fraction. The lane in the middle is a Western blot of the total cell lysate, where the antibody to ChChd3 was used. (T = total cell lysate, S = supernatant or soluble fraction, P = pellet, or insoluble fraction, MW = molecular weight markers, W = Western).

A.

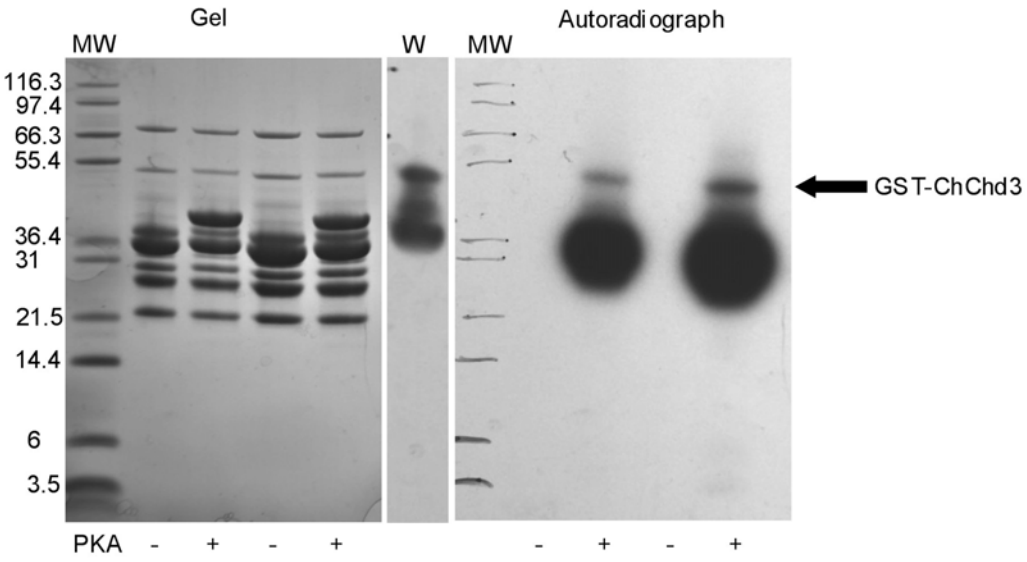

B.

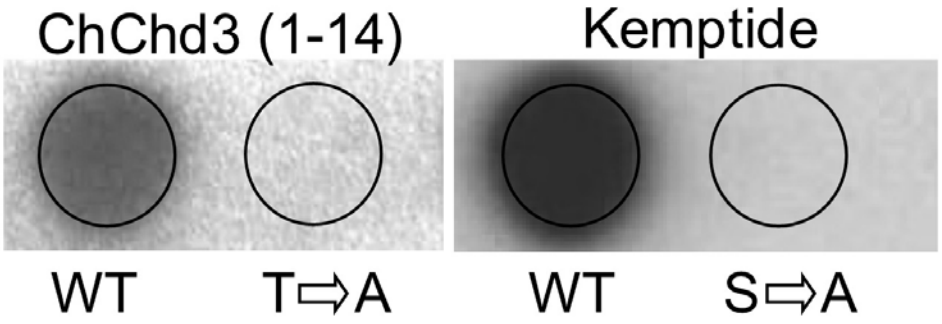

Figure 3.6: Phosphorylation of ChChd3 constructs by PKA. A. On the left is a Coomassie stained gel, the middle lane is a Western blot, and on the right is the autoradiograph of the gel. In both the gel and autoradiograph, the first lane is the molecular weight marker, the second and third lanes contain Elution A, and the fourth and fifth lanes contain Elution B. The Western blot (W) is of Elution A. Assays consisted of glutathione-resin purified GST-ChChd3, [γ-^{32}P]-ATP, with or without wild type PKA C-subunit. B. Peptides synthesized and spotted on a membrane were incubated with wild type C-subunit and [γ-^{32}P]-ATP. The ChChd3 peptides are: WT = MGGTASTRRVTFEA, T→A = MGGTASTRRVAFEA. The Kemptide peptides are: WT = LRRASLG, S→A = LLRAALG.

a peptide corresponding to the first fourteen residues from the N-terminus of ChChd3 was synthesized on a derivatized cellulose membrane. A control peptide with a mutation at Thr10 to Ala was also made. Kemptide and Ala-Kemptide peptides were made for a positive control. The membrane was incubated with purified recombinant wild type C-subunit and [γ-^{32}P]-ATP. The results are shown in Figure 3.6B. PKA does indeed phosphorylated the peptide at Thr10, as there is no [^{32}P] incorporation in the Thr10Ala peptide.

Section 3.5: Conclusions.

The C-subunit of PKA was engineered to accept N^6(benzyl)-ATP and characterized, as described in Chapter 2. This mutant was then applied to find direct, phosphorylated substrates of the kinase. Ideally, this would be done *in vivo* but this is not possible due to the difficulty of getting the ATP analogs across the cellular membrane. Thus, an *in vitro* assay was created, where mitochondria is crudely isolated from fresh mouse brain cells. Recombinantly expressed mutant C-subunit, cold ATP, and [γ-^{32}P]-benzyl-ATP is added to the mitochondria. The PKA inhibitor protein, PKI, was used as a control.

The samples were then subjected to 2-D gel electrophoresis in order to separate the proteins by their pI and molecular weight. The conditions for the 2-D gel analysis had to be optimized. The resulting gels were either exposed directly to autoradiography film or transferred first to nitrocellulose membrane before exposure. In the 4-7 pI range, a group of phosphorylated proteins always appeared in the low molecular weight range. These phosphorylated proteins were not seen in the PKI-treated control sample. The

spots were excised from the membrane and prepared for mass spectrometry analysis via MALDI-TOF. Using the mass over charge peak data generated from the MALDI-TOF, a search for the best possible matches was undertaken. The data from spot number 19 yielded the best match to ChChd3, an unknown protein. Two other spots yielded promising matches, protein disulfide isomerase A5 and GRIP1.

Initial analysis of ChChd3 revealed that it contains a CHCH domain that is found in other mitochondrial proteins, and an uncharacterized DUF737 (domain of unknown function). The N-terminus contains a well-conserved PKA phosphorylation site and a myristylation site. The clone was obtained from Invitrogen and subsequently cloned into a bacterial expression vector. The protein expressed well in *E. coli* at approximately 55kDa, but was very insoluble despite the GST-tag. Purification attempts resulted in very little full length GST-ChChd3, and a considerable amount of either breakdown products or contaminants. This could be due to the CHCH domain not forming the proper disulfide bonds when expressed in *E. coli*, leading to instability of the protein.

An *in vitro* assay utilizing wild type PKA C-subunit, [γ-^{32}P]-ATP and glutathione-purified recombinant ChChd3 resulted in the phosphorylation of ChChd3. Whether PKA phosphorylated ChChd3 at Thr10, Ser78 or both is not known. PKA does recognize and phosphorylate at Thr10 on a peptide, but this cannot be directly translated to what occurs *in vivo*. Either site may not be accessible to PKA if they are bound to other proteins or buried within the protein.

Section 3.6: Materials and Methods.

Cell fractionation - Live mice were sacrificed and brains immediately removed and homogenized on ice. Homogenization buffer was added to the brains before homogenization in the ratio of 5ml per gram of brain tissue. The homogenization buffer consisted of 250 mM sucrose, 10 mM MOPS, pH 7.2, 10 mM Tris, 5 mM EDTA, 1 mM EGTA. The resulting homogenized solution was centrifuged at 500 G for 5 minutes in a microfuge centrifuge and the pellet was discarded. This procedure was repeated twice to remove tissue that was not homogenized well. A fourth spin at 5000 rpm for 5 min. was carried out to remove the nuclei from the samples. The final spin at 11,500 rpm for 10 min. pelleted the mitochondria. The mitochondria were resuspended in buffer and centrifuged again at 11,500 rpm for 10 min.

Assay for PKA substrates - To identify PKA substrates, 100-600 μg of crude mitochondrial fraction protein was incubated with 1μM mutant or wild type kinase, 100 μM cold ATP, and [γ-^{32}P]-Benzyl-ATP. The control samples were incubated with 6 μM IP20. The reactions were started by addition of either the kinase or the radiolabeled analog. Samples were incubated at 30° C for 10-30 min. They were then prepared for 2-D gel electrophoresis.

Regular gel electrophoresis and transfer – To optimize for [^{32}P] incorporation samples were run directly on SDS gels in MES buffer. The gels were then transferred to nitrocellulose membrane at 30 V for 60 minutes. The resulting membranes were exposed to autoradiograph film.

Two-dimensional gel electrophoresis - IPG buffer containing 20 mM DTT, 8 M urea, and ampholytes corresponding to various pI ranges were added to the samples as

prepared under the assay conditions described above Then 160ml of the resultant mixture was pipetted into a chamber where an dried IPG strip was placed. The sample was allowed to sit overnight at room temperature in order to allow the IPG strip to re-swell and adsorb the proteins in the sample. The first-dimension separation which resolves the proteins on the basis of their pI, was run according to the protocol developed by Invitrogen for the IPG Runner system. This separation was run for approximately 1200 volt-hours. After the run, the strips were removed and placed along the top of a pre-cast SDS-PAGE gel. The strips were then sealed in with agarose and the gels were run for 35-45 min. at 200 V to separate the proteins on the basis of their molecular weights.

Autoradiography. After the 2-D gels were run, the proteins in the gels were either transferred to nitrocellulose or the gels were silver stained using a silver stain safe for mass spectrometry (Invitrogen). The membranes or gels were then exposed to Kodak MS film for 24 hours to one week at -80° C. The boundaries of the gels or membranes were marked on the film so that they could be lined up later.

Preparation of samples for Mass Spectrometry. In order to extract the specific spots that corresponded to the radiolabeled proteins, the autoradiography film was overlaid onto the membranes using the markings previously made. The phosphorylated spots could be visualized through the membrane when placed on a light box and the corresponding areas were excised from the membrane with a scalpel blade. The proteins were reduced with 10 mM dithiothreitol (DTT) in 0.1 M NH_4HCO_3 (ammonium bicarbonate) at 56°C for 1 hr. Next the cysteines in the proteins were carboxymethylated for 30 min. at r.t. in the dark using 100 mM iodoacetic acid. After rinsing with 50% 0.1 M NH_4HCO_3 and

50% acetonitrile (ACN) the samples are dried down in a speed vac. The proteins were digested overnight at 37°C with 0.10 mg/ml modified trypsin (Promega) in 50 mM NH_4HCO_3 + 5% ACN. Peptides were extracted by treating with 50ml 5% ACN + 0.1% acetic acid (HOAc) for 45 min. with shaking. For the desalting and purification of the peptides, they were passed through an equilibrated C18 ZipTip (Millipore), washed with 5% ACN + 0.1% HOAc, and eluted with the matrix. The resulting elution was spotted directly onto the MALDI-TOF plate.

Mass Spectrometry and Identification - C.C. King aided in the analysis of the peaks via MALDI-TOF. Mass over charge numbers of the peaks were compiled and entered into the University of California, San Francisco (UCSF) Protein Prospecter MS-search tool (http://prospector.ucsf.edu). Hits were generated based on a database of theoretically trypsin-digested proteins, with the mass over charge peak numbers matching each mass over charge peak number with specific sequences of the theoretically digested proteins.

Cloning - The cDNA clone in the pCMV-Sport6 vector was obtained from Invitrogen. The DNA sequence of interest was excised from the vector with NcoI and HindIII and cloned into a pGEX vector for GST-tagged bacterial expression.

Expression and Purification - The GST-tagged ChChd3 expression was carried out in *E. Coli* strain BL21(DE3) cells. Cells were grown in YT medium containing 50 μg/ml kanamycin at 37°C. After reaching an optical density at 600nm of about 0.6-0.8, 0.5 mM isopropyl-β-D-thiogalactopyranoside was added to the cell cultures to induce expression of the protein. Induction was allowed to continue for 4-6 hours before collecting the cells via centrifugation. For the expression tests, the cell pellets were resuspended in Laemmli buffer and run on an SDS-PAGE gel. For the solubility tests,

the harvested cell pellets were resuspended in lysis buffer (50 mM $NaHPO_4$, 20 mM Tris-HCl, 100 mM NaCl, pH 8.0) and subjected to 3 freeze/thaw cycles. The samples were then centrifuged for 30 min. at 4°C and 16,000 rpm in a centrifuge to separate the soluble (supernatant) and insoluble (pellet) fractions. The proteins were then separated on an SDS-PAGE (10%) gel.

Purification – GST-ChChd3 was expressed as described above and cells were harvested by centrifugation. Cells were resuspended in 10ml lysis buffer (PBS plus 1% Triton X-100) per 1 gram of cells and lysed by one pass in a French pressure cell at 1,000 p.s.i. Insoluble material was removed by centrifugation at 15,000 rpm in a Beckman JA20 rotor at 4°C for 40 min. Purification from Glutathione Sepharose® 4B (Pharmacia Biotech) was performed following the procedure given. In short, the supernatant was batch-bound to 1.0ml resin per 2L culture volume for 30 min. at r.t. The resin was batch-washed three times with PBS, then the GST-fusion protein was eluted from the resin with three glutathione elutions (10 mM glutathione in 50 mM Tris-HCl, pH 8.0).

Peptide Synthesizer – Peptides were synthesized on an automated Intavis AG Multipep (Bioanalytical Instruments) with help from C.J. Allison (Susan Taylor's laboratory), using the SPOT method for peptide synthesis (Frank 1992). Peptides were created on an Amino-PEG derivatized cellulose membrane (Intavis AG). The basic automated procedure involves seven steps: Fmoc (9-fluorenyl-methoxycarbonyl) deprotection, DMF (dimethyl fluorine) wash, ethanol wash, air drying of the membrane, spotting of activated amino acids and reaction time, capping, and finally a wash with DMF. After the peptides are synthesized, the final Fmoc deprotection and side chain deprotection must be done manually. The membranes are dried thoroughly and then incubated in a

solution of 47.6% trifluoroacetic acid (TFA), 47.6% dichloromethane (DCM), and 2.9% Triisopropylsilane for two hours. After incubation, the membrane is washed with 20 ml DCM four times, then washed with DMF four times for 2 min. each wash. The final wash is twice for two min. with ethanol. The membrane is then dried and stored at -20°C.

For the radioactive phosphorylation assay, a solution of 10 μg/ml purified recombinant C-subunit was prepared in 50 mM MOPS/5 mM $MgCl_2$. To this solution, [γ-^{32}P]-ATP diluted in 100 μM unlabeled ATP was added. The membrane was incubated for 10 min. at 30°C. The first wash was 10% acetic acid for 30 min. to stop the reaction. The membrane was then rinsed with 0.5% phosphoric acid four times (5 min. each). Final quick washes were in acetone and the membrane was allowed to dry. The membrane was exposed to Kodak MS autoradiograph film.

CHAPTER IV

Characterization of ChChd3

The unknown protein ChChd3 was identified as a putative PKA substrate through the use of a modified C-subunit that preferentially uses N^6(benzyl)-ATP as a substrate as described in Chapter 2. The protein was subsequently identified by 2-D gel electrophoresis followed by mass spectrometry as described in Chapter 3. In this chapter I profile this protein, showing its sequence homology to other organisms and describing its conserved motifs and domains. In addition, subcellular distribution to mitochondria of the endogenous protein was demonstrated by immunofluorescence and cell fractionation. Within the mitochondria ChChd3 was shown to be enriched in the inner mitochondrial membrane. Section 4.1 describes the domain organization of ChChd3 while section 4.2 describes the localization of ChChd3. Expression of GFP-tagged ChChd3 constructs are described in Section 4.3.

Section 4.1: Domain Organization and Homology.

ChChd3 has two conserved domains, the DUF737 domain and the coiled coil-helix coiled coil-helix (CHCH) domain. In Figure 4.1, the domain organization is laid out, along with the protein sequence of the mouse and human homologs. The protein is highly conserved between mouse and human. The colored bars underneath correspond to the exons indicated in Figure 4.2. The DUF737 domain is shown in black letters and the CHCH domain is shown in blue. At the N-terminus is a myristylation motif, shown in red.

The exons associated with ChChd3 are shown in Figure 4.2 and correlated with the domain organization. Exon 6 encodes for a stop codon at the end of the DUF737 domain, indicating a possible splice variant that does not have the CHCH domain.

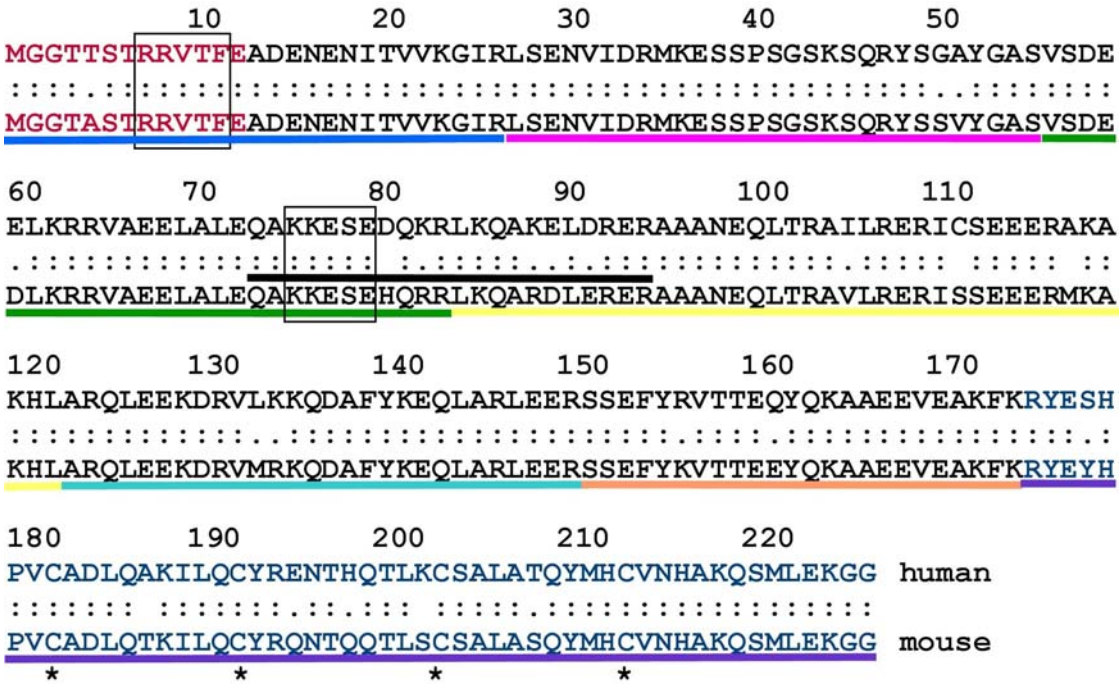

Figure 4.1: Protein sequence comparison of mouse and human ChChd3. Mouse exons are highlighted by bars underneath the sequence. Bar colors correspond to exon colors in Figure 4.2. The N-terminal 14 residues colored in red are not part of the DUF737 domain (sequence colored in black). The CHCH domain sequence is colored in blue at the C-terminus. The two putative PKA phosphorylation sites have boxes drawn around them. Dots between the mouse and human sequences indicate homology. Two dots represent a conserved residue; one dot represents a conserved similar residue. The four cysteines in the CHCH domain are starred. The ChChd3 antibody recognition sequence is highlighted with a black bar above it. This sequence was determined to be the most antigenic.

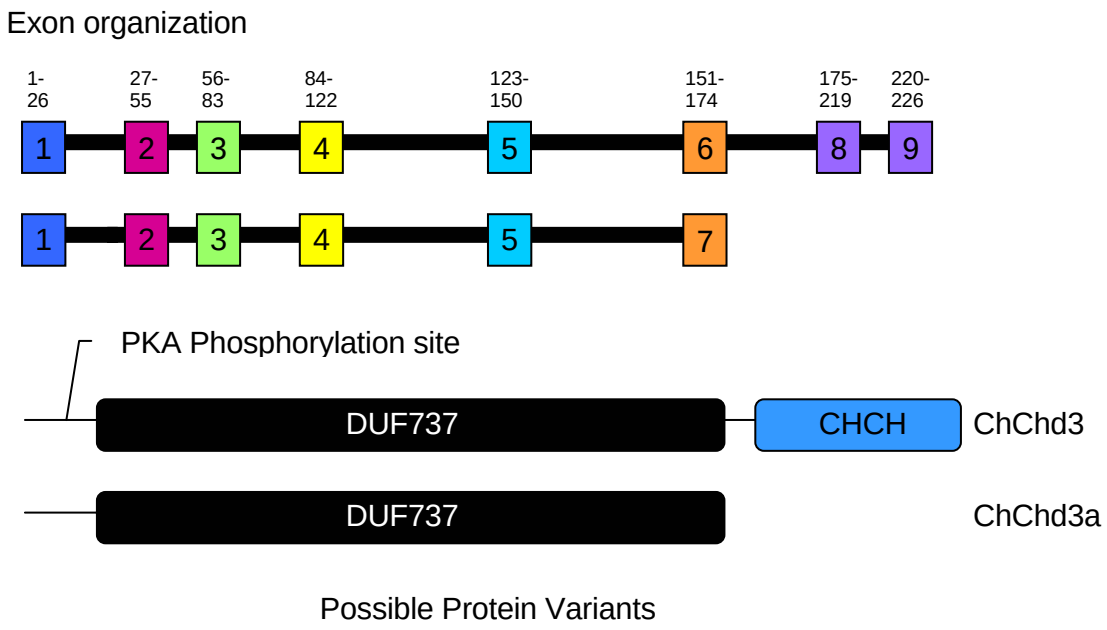

Figure 4.2: Domains and exon organization of two possible ChChd3 variants. The top figure shows the two possible exon sequences, with exons 8 and 9 encoding for the coiled coil-helix coiled coil-helix domain at the C-terminus. Exon 1 contains the N-terminal sequence with the conserved PKA phosphorylation site. Numbers correspond to the amino acid residues in each exon.

4.1a: Myristylation motif. At the N-terminus of each protein (highlighted in red in the protein sequence in Fig. 4.1), there is a well-conserved PKA phosphorylation site at Thr10 (RRVTF) and a myristylation site at Gly1. The myristylation site may be involved in targeting and/or anchoring the protein to the mitochondria. This PKA phosphorylation site is also conserved as a Thr10 or a Ser10 in other species such as bovine, frog, and rat (Figure 4.4). Rat is predicted to have a longer N-terminal sequence. This site is interesting because the C-subunit of PKA is also myristylated at its N-terminal Gly and has an autophosphorylation site at Ser10 (Toner-Webb, van Patten et al. 1992). A crystal structure of the unphosphorylated unmyristylated Ser10 C-subunit shows the A-helix ordered and projecting the myristylation site out into solution (Breitenlechner, Engh et al. 2004). The unphosphorylated C-subunit with Asn2 shows the myristylation motif folded into a hydrophobic acyl binding pocket (Zheng, Knighton et al. 1993). In structures of the Ser10 phosphorylated C-subunit lacking the myristyl group the N-terminus is disordered (Knighton, Zheng et al. 1991). These results suggest a myristylation switch mechanism. The phosphorylation of PKA at Ser10 may be involved in regulating localization of the myristylated protein. The negative charge on the phosphate would counter-act the positive charges of the basic residues found on the N-terminus, which are also important for targeting to membranes. Src is another example of a myristylated protein that has a PKA phosphorylation site at its N-terminus (Obara, Labudda et al. 2004).

4.1b: DUF737 domain. The DUF737 domain is conserved amongst a family of unknown proteins. Based on my analysis of this domain, these proteins are probably

Figure 4.3: Secondary structure prediction of ChChd3. Analysis performed with PredictProtein (Rost, Yachdav et al. 2004). Green L = loop; Blue E = beta strand; Red H = helical. In the sequence, acidic residues are colored red and basic residues blue.

mitochondrial in location. There is no published information about this domain, so its function and structure are completely unknown. Using the online secondary structure prediction program PredictProtein (Rost, Yachdav et al. 2004), ChChd3 is predicted to be mostly alpha-helical (see Figure 4.3). The sequence of this domain is also well conserved between homologs in different organisms, as can be seen in the alignment shown in Figure 4.4. Alignments were done using ClustalW (Network Protein Sequence Analysis; Thompson, Higgins et al. 1994). ChChd3 appears to be related to another protein found in mouse and human, ChChd6.

There may be a second possible PKA phosphorylation site at Ser78 (KKESE), however, it is not as plausible a site because the consensus sequence contains two glutamates that flank the serine. Other possible features are a tyrosine phosphorylation site at Tyr140 and an N-glycosylation site at Asn19 (19-22 NITV). A protein BLAST (Altschul, Gish et al. 1990) search reveals that only proteins named “ChChd3” or

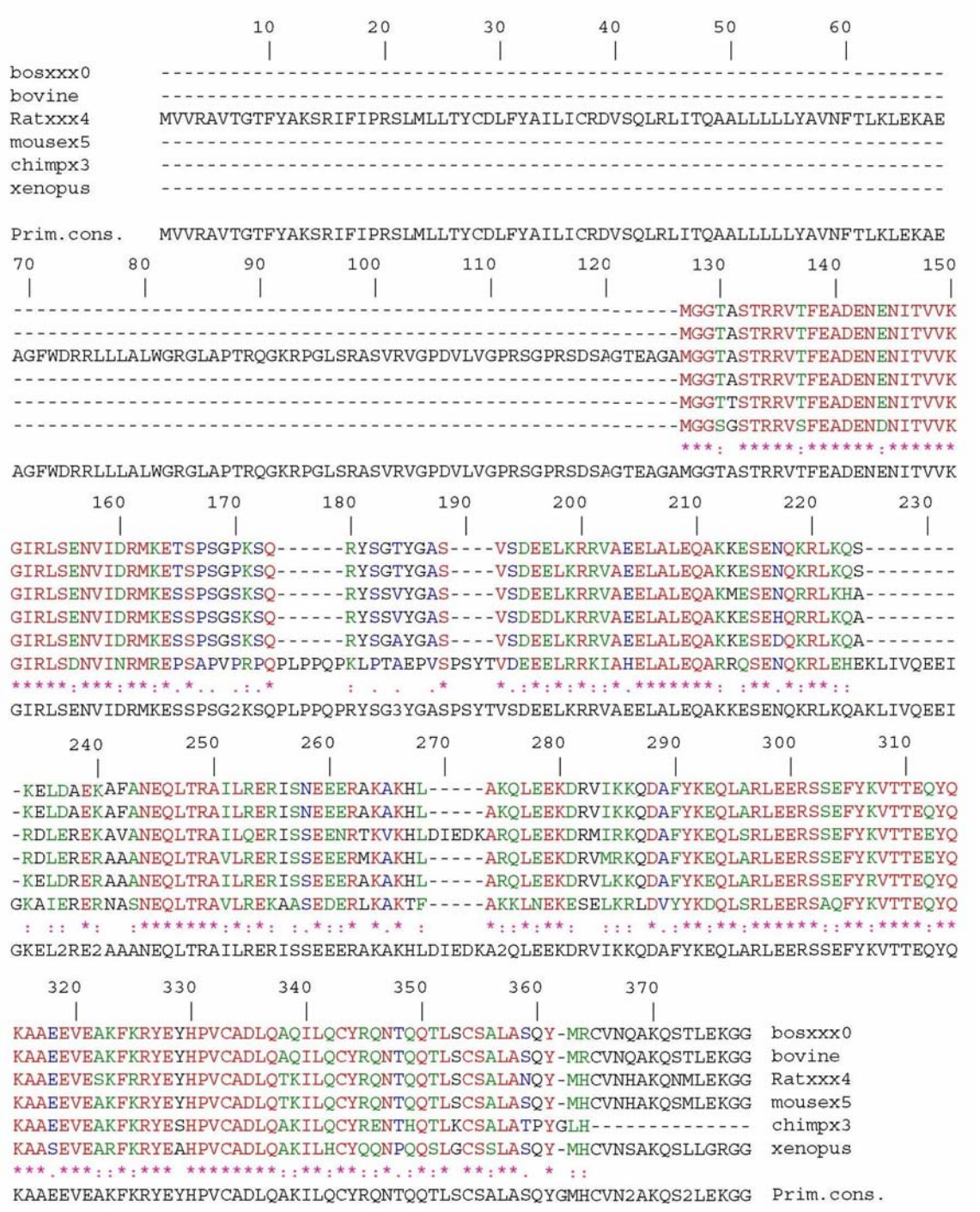

Figure 4.4: Conservation of ChChd3 in vertebrates. Protein sequence alignment of species *Bos taurus* (bosxxx0), bovine, *Pan troglodytes* (chimpx4), *Mus musculus* (mousex5), *Xenopus laevis* (xenopus), and *Rattus Norvegicus* (Ratxxx4). Alignment done with ClustalW at PBIL (Pôle Bioinformatique Lyonnais). The sequence is highly conserved. Red, * = identity, green, : = strongly similar, blue, . = weakly similar, Prim. cons. = Primary consensus sequence.

"ChChd6" appear to have this domain. Furthermore, this domain appears to be highly conserved in vertebrates. According to BLAST analysis, there is no homolog in fungi, plants, or arthropoda, although a possible distant variant is found in blood fluke.

4.1c: CHCH domain. The CHCH domain is found in many other proteins, most notably cytochrome c oxidase subunits such as Cox19 and Cox17 (Glerum, Shtanko et al. 1996; Nobrega, Bandeira, et al. 2002; Punter, Adams et al. 2000). Figure 4.5 contains an alignment of CHCH domains from ChChd3 and other known proteins. Although the amino acid sequence has considerable variation, all have a repeating Cys-X_9-Cys motif. Cox19 is essential for cytochrome c oxidase expression in mitochondria (Nobrega, Bandeira et al. 2002). The CHCH domain appears to be a novel domain for proteins that are located in the intermembrane space of the mitochondria (Arnesano, Balatri et al. 2005). The structure of Cox17 has been solved and is shown in Figure 4.5, giving us a representative CHCH domain structure. In the structure one can see that the four cysteines that define this motif are disulfide-bonded together such that the two coiled coil-helices are linked to one another in an antiparallel arrangement. Ivano Bertini (University of Florence) and Dennis Winge (University of Utah Health Sciences Center) used NMR to compare the structures of the CHCH domain in its reduced and oxidized states (Arnesano, Balatri et al. 2005). It was also found previously that the CHCH domain is a copper-binding domain (Glerum, Shtanko et al. 1996). The cysteines in the domain bind copper depending on their oxidation state (Palumaa, Kangur et al., 2004), and the Bertini and Winge groups propose that the oxidized and copper bound states are important steps in the transport of Cox17 into the mitochondria and to the IMS. They have constructed a model of how Cox17 is transported into the

```
                    10        20        30        40        50        60
                     |         |         |         |         |         |
ChChd3      ----------------RYEYHP-------------VCADLQTKILQCYRQNTQQTL--
ChChd6      ----------------PRRVEP-------------VCSGLQAQILRCYRDHLHEVL--
Cox19x1     ---------MSTAMNFGTKSFQPRPPDKGSFPLDHLGECKSFKEKFMKCLHNNNFENA--
Cox17p      -MPGLAAASPAPPEAQEKKPLKP------------CCACPETKKARDACIIEKGEE----
NADHxx5     HYGAQCDKTNKEFMLCRWEEKDP-------------RRCLKEGKLVNGCALNFFRQIK-S
Mia40x3     -------------PCLGGMAHGP---------------CGEEFKSAFSCFVYSEAEPKGI
                                 *               *         *      :

                    70        80        90       100
                     |         |         |         |
ChChd3      SCSALASQYMHCVNHAKQSMLE-----------KGG--------
ChChd6      LCSDLVKAYQHCVSTAR----------------KG---------
Cox19x1     LCRKESKEYLECRMERKLMLQEPLEKLGFGDLTSGKSEAKK---
Cox17p      HCGHLIEAHKECMRALGFKI------------------------
NADHxx5     HCAEPFTEYWTCLDYSNMQLFRHCRQ------QQAKFDQCVLDK
Mia40x3     DCVEKFQHMQDCFRKYPEHYAE----------------------
             *         *
```

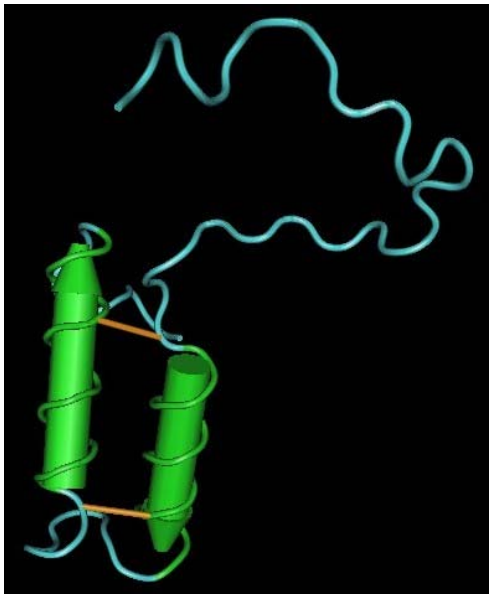

Figure 4.5: Sequence alignment of CHCH domains and a representative structure of the CHCH domain in Cox17. Protein sequence alignment of CHCH domains in several different proteins: ChChd3 (mouse), ChChd6 (mouse), Cox19 (human), Cox17p (mouse), NADH-ubiquinone oxidoreductase 19kDa subunit (mouse), and Mia40 (*S. cerevisiae*). The only absolute conservation between the domains is the Cys-X_9-Cys repeat. In the structure, the CHCH domain contains two alpha-helices in green with intrachain disulfide bonds linking the two helices. Red, * = identity, green, : = strongly similar.

inner membrane space through a transport protein (TOM). The CHCH domain either becomes disulfide-bonded in the IMS or binds 4 copper atoms (one per cysteine) (Heaton, George et. al, 2001), which leads to multimerization in the IMS (Figure 4.12).

Section 4.2: Localization of Endogenous ChChd3.

Although ChChd3 has been reported in the mitochondria (Mootha, Bunkenborg et al. 2003), and more specifically, in the mitochondrial inner membrane in proteomics screens (Da Cruz, Xenarios et al. 2003), the endogenous protein has not been examined *in vivo*. In this next section, we describe the localization of the endogenous protein in tissue culture cells and its presence in rat and mouse tissues.

4.2a: Immunofluorescence. In order to characterize the endogenous protein, we employed immunofluorescence to determine where the protein was located in mammalian cells. An antibody to the protein was generated using a peptide corresponding to residues 73-94. Four different cell lines were used: 10T1/2 (mouse embryo), Cos (African Green Monkey kidney), 293A (human embryonic kidney) and HeLa (human cervical cancer) cells. Figure 4.6A and B shows confocal pictures of endogenous ChChd3 in 10T1/2 and Cos cells. MitoTracker (Molecular Probes) was added to the live cells as a marker for mitochondria. The mitochondria take up the dye that is visible at the red wavelength (598nm) when subjected to fluorescence. The cells were then fixed one hour later, and probed with the antibody to ChChd3. The secondary antibody was a fluorescein conjugate and is visible at the green wavelength (516nm). In Figure 4.6, the stained mitochondria appear on the left, the endogenous ChChd3 fluorescence is in the middle, and the merge of the two colors is on the right. In both

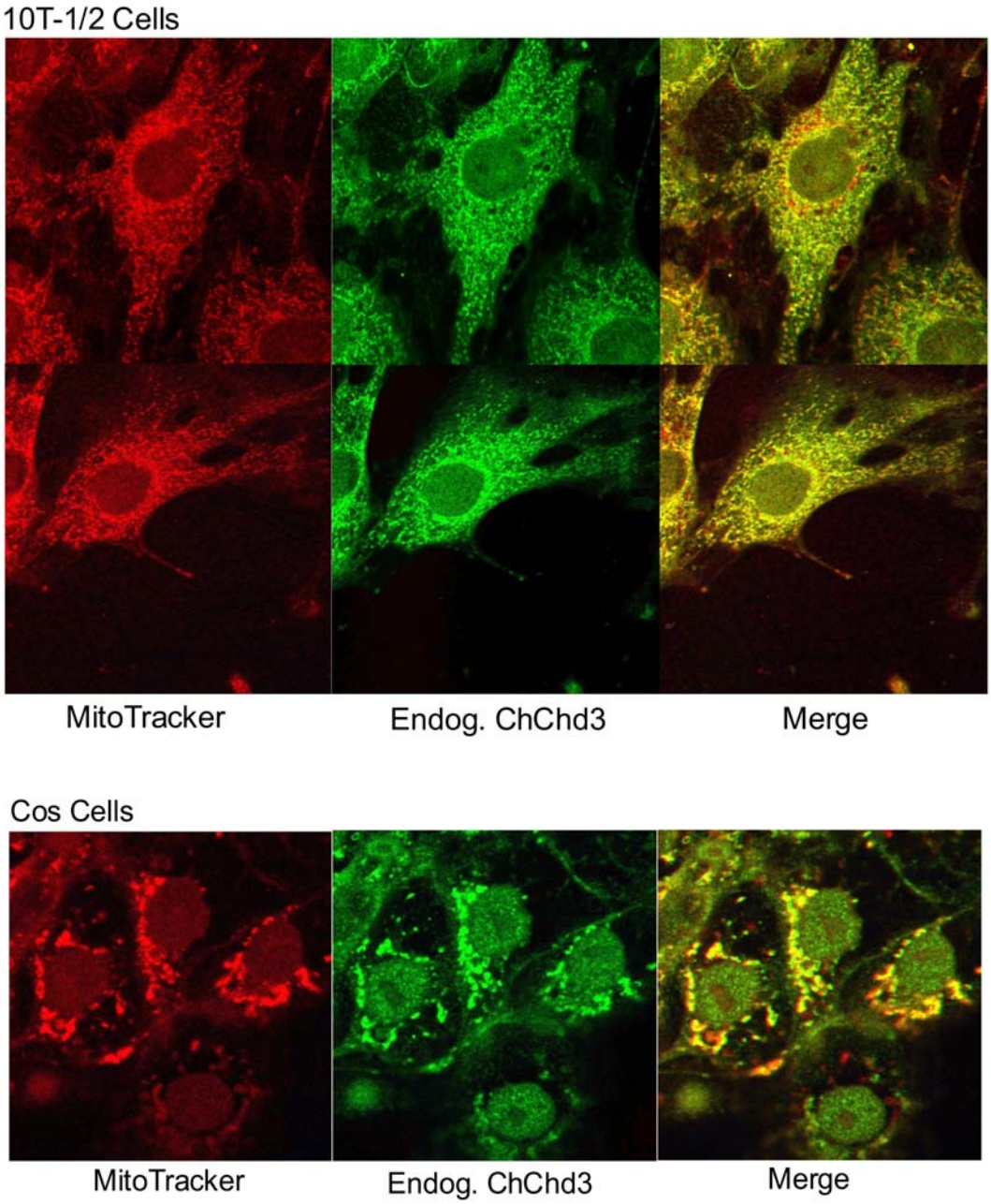

Figure 4.6: Confocal images of endogenous ChChd3 in fixed cells. Used the Antibody to ChChd3 for immunocytochemistry. On the left in red is the fluorescence from MitoTracker red, a mitochondrial dye (Molecular Probes). In green (center) is the stain for ChChd3. On the right are the merges of the red and green. These show that the endogenous ChChd3 overlays mostly with the mitochondrial pattern. Cells were incubated with MitoTracker one hour before fixing and imaged on a Bio-Rad MRC1024 confocal microscope. The top two panels are 10T-1/2 cells while the bottom panel is a representative sample from Cos cells.

10T1/2 and Cos cells, the ChChd3 showed a mitochondrial localization pattern. The 10T1/2 cells showed the nicest pattern, most likely because the cell line is derived from mouse embryos. HeLa and 293A cells did not image as well. There is not a distinct pattern in either cell line and this may be because the antibody is to the mouse ChChd3 protein and there are slight differences between the proteins. The immunofluorescence studies in 10T-1/2 and Cos cells, however, confirm that ChChd3 is a mitochondrial protein.

4.2b: Tissue Distribution. Although the ChChd3 protein was initially discovered as a PKA substrate in mouse brain mitochondria, its expression in other tissues was not known. When the SymAtlas (Genomics Institute of the Novartis Research Foundation, http://symatlas.gnf.org) database was searched for the mRNA expression levels of this protein, the resulting expression profile shown in Figure 4.7 was obtained. ChChd3 mRNA appears to be most highly expressed in brown fat, heart, and skeletal muscle. Both brown fat and heart tissue have high amounts of mitochondria, which would be consistent with this protein being a mitochondrial protein.

Several tissue and organism types were probed for ChChd3. Figure 4.8 shows the resulting Western blot. Mouse brain, rat heart and liver, HeLa (human) mitochondria, and 293A (human) cells were probed for expression of the protein. The strongest band appears at around 33kDa. The calculated molecular weight for ChChd3 is approximately 27kDa but on the Western blot it runs at around 33kDa in the mouse brain nuclei, mitochondria and rat heart mitochondrial fractions. This aberrant

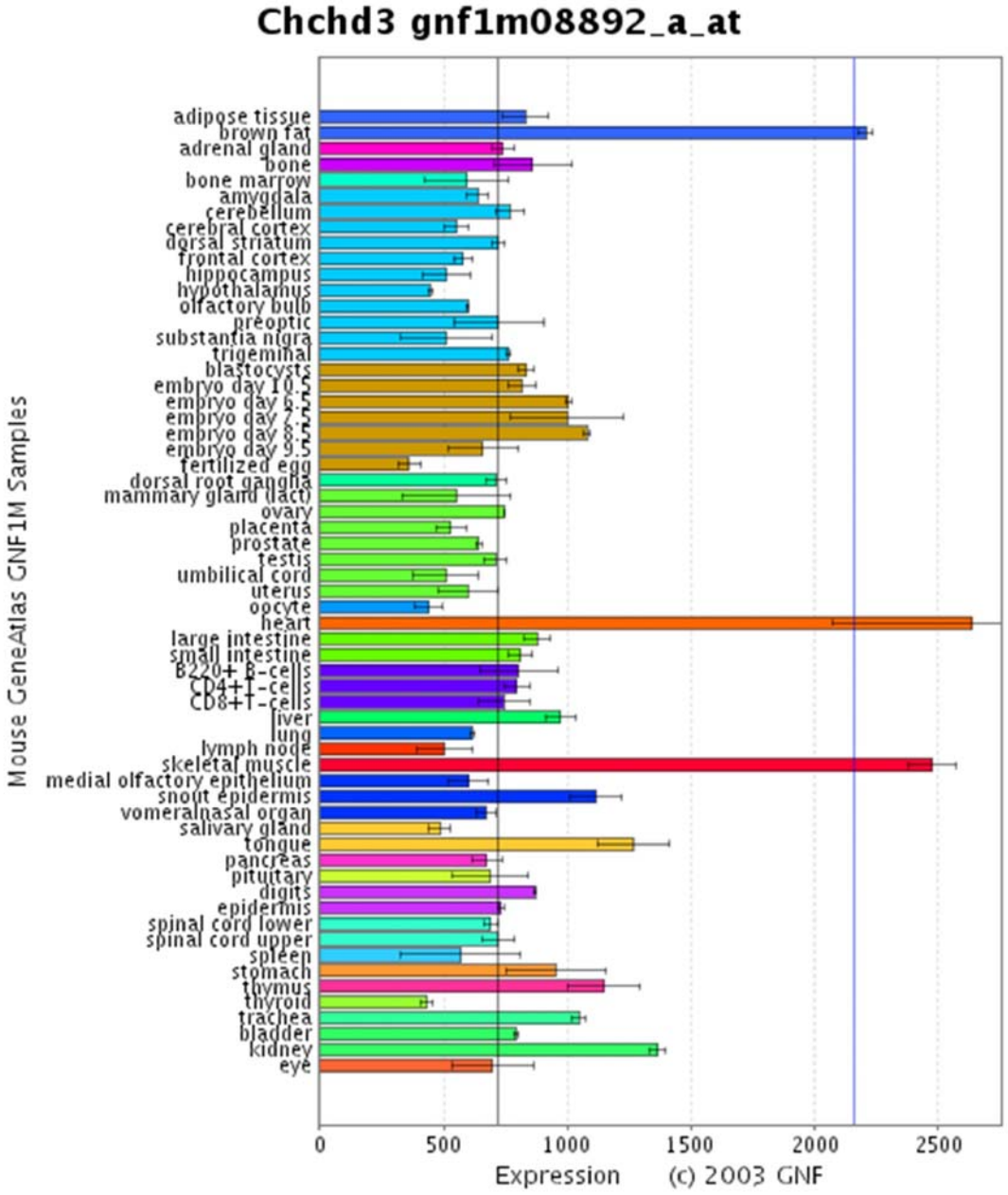

Figure 4.7: RNA expression levels of ChChd3 based on Affymetrix chip samples. Produced by using gene functionalization dataset software SymAtlas maintained by Genomics Institute of the Novartis Research Foundation. ChChd3 mRNA appears to be most highly expressed in brown fat, heart, and skeletal muscle.

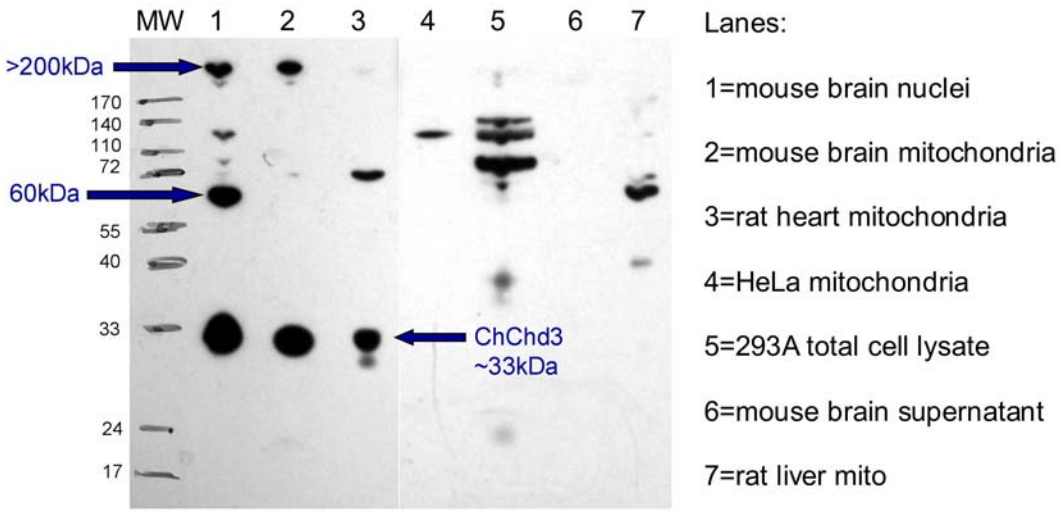

Figure 4.8: Protein expression of ChChd3 in various tissue samples. ChChd3 protein expression was followed by Western blot analysis using an antibody generated to residues 73-94 in mouse ChChd3. ChChd3 is primarily a 33kDa protein in mouse brain nuclei, mitochondria and rat heart mitochondria. Higher bands were observed in some of the tissues. .

migration is not unusual for CHCH domain containing proteins as both Cox17 and Cox19 run higher than their predicted molecular weights. Cox17p from *S. cerevisiae* ran at ~14kDa on an SDS-PAGE gel but has a predicted mass of 7.9kDa (Beers, Glerum et al. 1997). The yeast Cox 19p has a predicted molecular weight of 11kDa but was found to run at ~16kDa on an SDS-PAGE gel (Nobrega, Bandeira et al. 2002).

Higher molecular weight bands (~55kDa) are also seen in the mouse brain nuclei and rat tissues. It is not clear, however, why there is a higher band in mouse. In rat there is another splice variant with a longer N-terminus (an additional 126 residues) that would account for the higher band. ChChd3 was not found in the mouse brain supernatant (lane 6 in Figure 4.8), indicating that there are no soluble versions of this protein; it is all membrane bound. In rat liver, only a higher molecular weight band was seen; whereas in rat heart mitochondria, both the higher band and the 33kDa band were seen.

Notably, we do not see a band lower than 33kDa, indicating that the initial proposal of two possible splice variants (one with and one without the CHCH domain) of ChChd3 in mouse is incorrect, or at least we see no evidence to substantiate this prediction. If there were indeed two splice variants, then we should see a lower molecular weight band around 15kDa, indicating the existence of the splice variant without the CHCH domain.

In the tissue culture cell samples in Figure 4.8, the banding pattern is very different. Because an overlap of mitochondria and endogenous ChChd3 was not seen in the immunofluorescence studies of endogenous ChChd3 in HeLa or 293A cells, these two cell lines were probed for endogenous ChChd3 via Western blot. Crudely purified

mitochondria from HeLa cells and the total cell lysate from 293A cells were used in lanes 4 and 5. Since both cell lines are human, the antibody may or may not accurately recognize the protein as there are some slight differences in the sequence. Only a single high molecular weight band is seen in HeLa cell mitochondria, which is interesting because when these cells were subjected to immunocytochemistry the endogenous protein looked diffuse and the cells did not image well. In 293A cells, three high molecular weight bands were seen. The identity of these bands needs to be confirmed by mass spectrometry. In addition we need to generate an antibody to a more highly conserved region such as the N-terminus or the C-terminus which are both identical in mouse, rat, and human.

Westerns were also done on a 2-D gel blot of the crude mouse brain mitochondria, similar to the samples used to run the 2-D gels where ChChd3 was first identified. Two pI range 2-D gels were created, 3-10 and 6-10, and then the gels were transferred to nitrocellulose membranes. These 2-D westerns are shown in Figure 4.9. There are three spots from a pI range of 3-5 at molecular weight of 33kDa on the 3-10 blot and at a pI of around 3.5-4 at a molecular weight of 75kDa. On the pI 6-10 blot, there are two distinct spots at 33kDa at pIs of approximately 7 and 9. This may indicate different states of post-translational modifications such as phosphorylations. The spot at pI 9 may be the unmodified version of the protein because the theoretical pI of the protein without any modifications is 8.56 (Expasy Compute pI/MW tool).

4.2c: Distribution of ChChd3 in Fractionated Mitochondria. ChChd3 is clearly a mitochondrial protein but the specific location in the mitochondria is not known. It was previously reported that ChChd3 was found in the inner mitochondrial

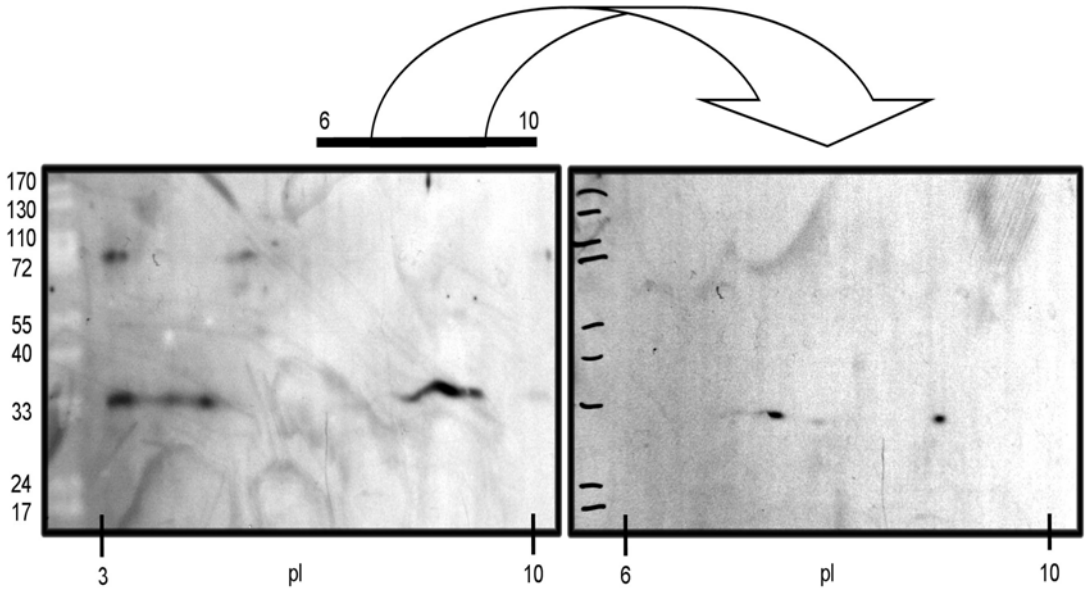

Figure 4.9: Isoelectric focusing of endogenous ChChd3. Western blot analysis was used to identify spots corresponding to ChChd3. Both pictures, representing different pH ranges, are of 2-D gels transferred to membrane and then subjected to Western blot using the antibody to ChChd3. The calculated pI for the unmodified protein is 8.56. The protein appears to run at pI's of 3-5, 7.5, and 9. At pI = 3, a higher molecular weight protein (~72kDa) also was detected.

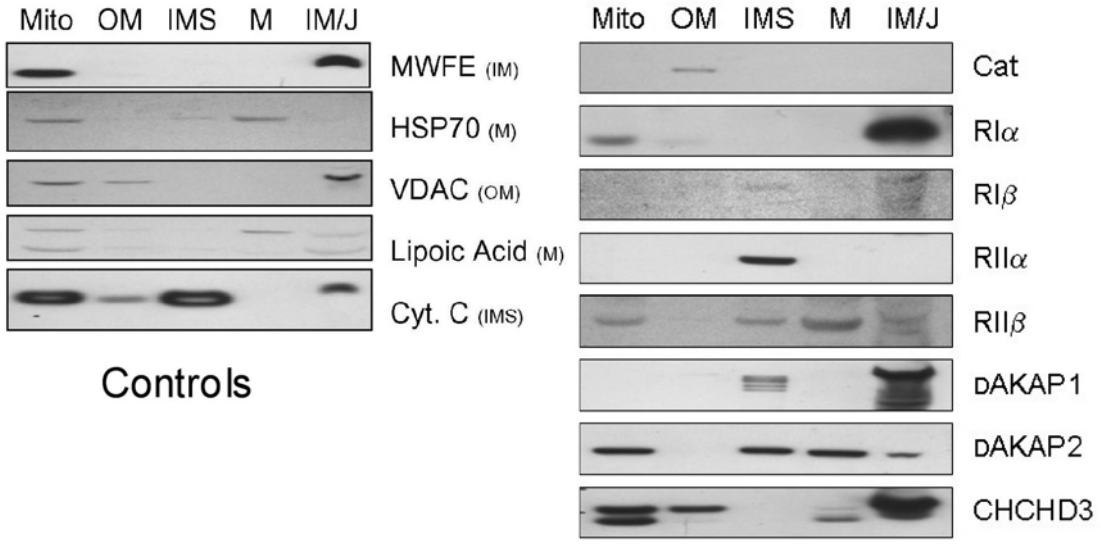

Figure 4.10: Mitochondrial location of endogenous ChChd3 and other PKA-associated proteins. On the left is Western blots of proteins known to be in specific mitochondrial fractions, and is a control for the mitochondrial fractionation. Right, a Western blot of ChChd3 and PKA associated proteins in the fractionated mouse liver mitochondria. The doublet seen may be the disulfide-bonded and reduced state ChChd3. Cyt. C = cytochrome c, Cat = catalytic subunit of PKA, Mito = whole mitochondria, OM = outer membrane, IMS = intermembrane space, M = matrix, IM/J = inner membrane/other non-specified.

membrane by another group in a proteomic analysis of proteins in the inner mitochondrial membrane (IM) (Da Cruz, Xenarios et al. 2003). Another group, also using proteomics to identify all proteins in the mitochondria and what functions they may be involved in, speculate that this protein (referred to as 061041L609Rik) is involved in oxidative phosphorylation (Mootha, Bunkenborg et al. 2003). We probed for the location of ChChd3 in rat liver and mouse liver mitochondria by further fractionating the mitochondria into the outer membrane (OM), inner membrane space (IMS), matrix (M), and inner membrane (and other unclassifiable-IM/J) fractions. The results in mouse liver mitochondria can be seen in Figure 4.10. Again the antibody to ChChd3 was used to probe a membrane with samples of each of the mitochondrial fractions as well as the whole mitochondria. ChChd3 is primarily seen in the inner membrane, with a small amount appearing in the matrix and the outer membrane. Since this protein could possibly be transported into the mitochondria, similarly to the working model of Cox17 transport through the OM via its CHCH domain, it is possible that some protein would be found at the OM, with the cysteines in the CHCH domain in a reduced state. A light lower band is seen in the matrix, and this may be a disulfide-bonded version of the protein. The inner membrane appears to have a very strong higher band and a secondary lower band.

Section 4.3: Cell imaging of transfected ChChd3-GFP constructs.

Chchd3 has a myristylation site at Gly1 on the N-terminus. Because the protein is localized to the mitochondria, and not to the plasma membrane like Src or PKA when

myristylated, we became interested in the requirements for targeting a myristylated sequence.

We developed many N-terminal constructs of PKA, Src, ChChd3, and others to determine whether this motif is necessary and/or sufficient for targeting a myristylated sequence to the plasma membrane or to the mitochondria. Marilyn Resh first reported that in Src, the myristylation motif was sufficient to target Src to membranes and that changing the lysines to arginines disrupted the ability of Src to associate with the membranes (Silverman and Resh, 1992) In looking at the N-terminal 14 residues of many known myristylated proteins, one can see that proteins known to be localized at the plasma membrane have several lysines, such as Src (Figure 4.11) (Silverman and Resh, 1990). Proteins known to be mitochondrial in location, such as ChChd3, have arginines instead of lysines. We thus examined whether the arginines or lysines play a role in membrane targeting.

Through immunocytochemistry we were able to determine that ChChd3 is localized to the mitochondria. We speculated that ChChd3 may be targeted to the mitochondria through its myristylation site on the N-terminus. The PKA phosphorylation site at Thr10 may also regulate the ability of the myristylation site to interact with membranes, and therefore influence the targeting of ChChd3. To test the importance of the N-terminus for targeting, we made two constructs to examine whether the first fourteen residues of ChChd3 are sufficient to target GFP to the mitochondria. The first fourteen residues of ChChd3 (MGGTASTRRVTFEA) were cloned into a pEGFP vector. Two more constructs were made where the Thr10 was mutated to Ala and to Glu. As a control, we engineered a similar construct for Src, a myristylated

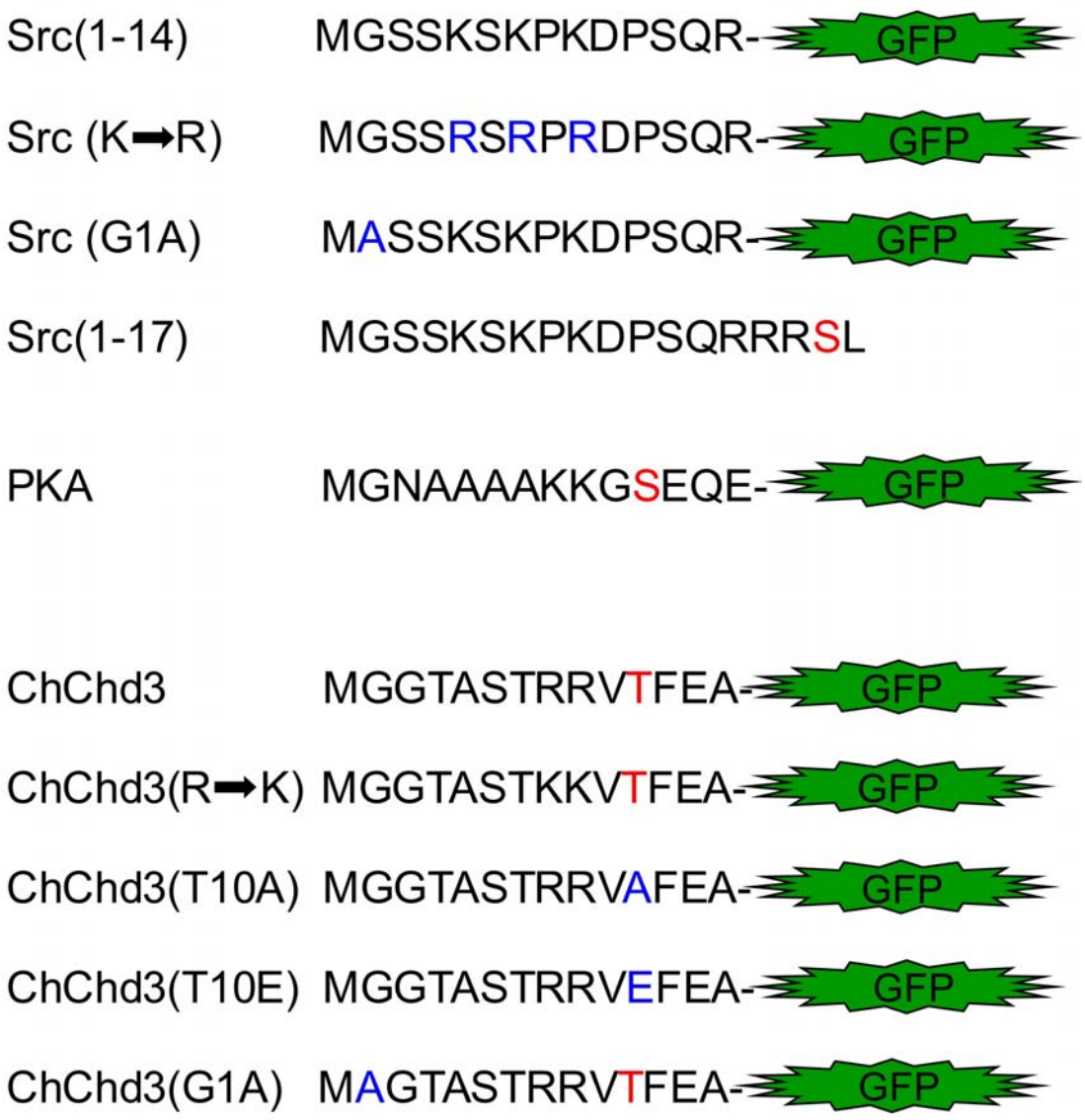

Figure 4.11: Src, PKA, and ChChd3 myristylation motifs fused to GFP. The N-terminal 14 residues of each protein were fused to GFP. Highlighted in red is a PKA phosphorylation site at Thr10 of ChChd3, the autophosphorylation site at Ser10 of PKA and the PKA phosphorylation site at Ser16 of Src. Src and ChChd3 constructs were made where the lysines and arginines were switched. Amino acid changes away from the wild type sequence are shown in blue.

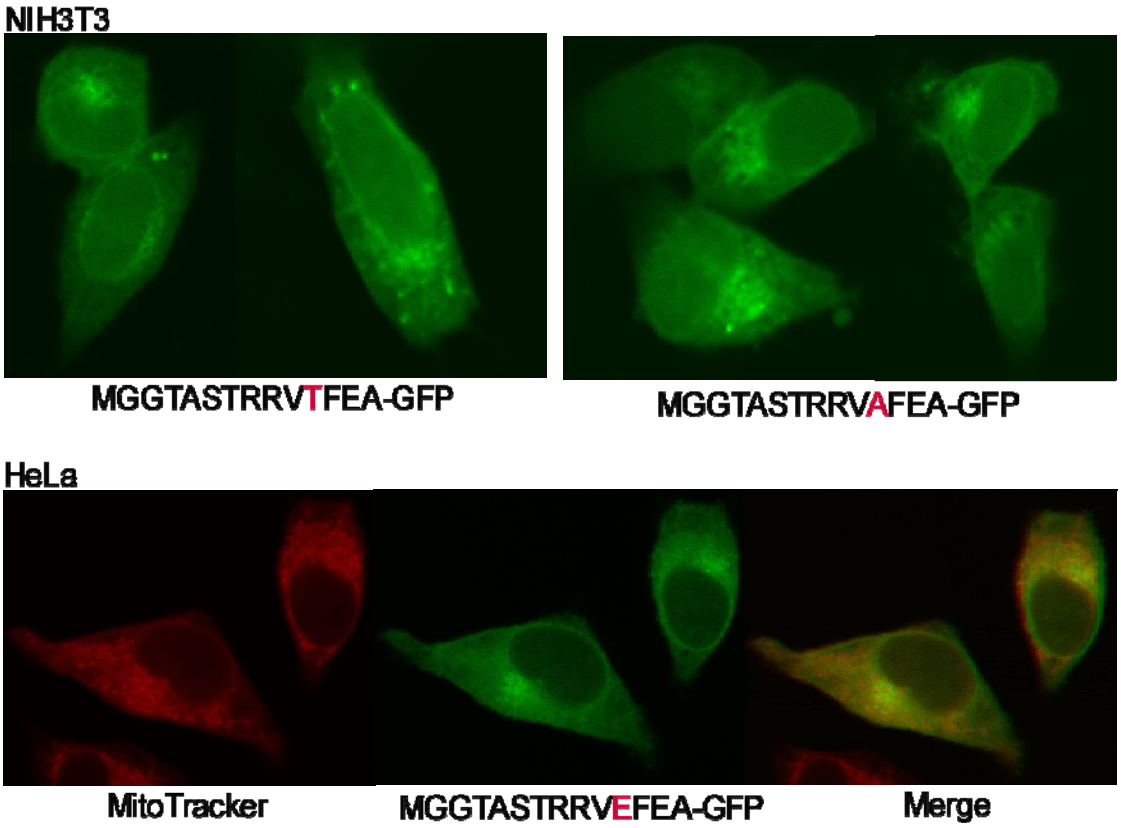

Figure 4.12: Localization of the N-terminus of ChChd3 with GFP. Top, NIH3T3 (mouse fibroblast) cells were transfected with ChChd3 constructs of the first 14 residues fused to GFP (green fluorescent protein). The cells on the left have been transfected with the PKA phosphorylation site intact, while on the right the PKA site has been mutated to prevent phosphorylation. Bottom, HeLa cells were transfected with the Thr10Glu construct. The HeLa cells were incubated with MitoTracker for one hour before fixing to look for an overlap in targeting at the mitochondria. All transfections show a similar targeting pattern.

protein that is known to target to the plasma membrane (see Figure 4.11). Mouse fibroblast (NIH3T3) tissue culture cells were transfected with the plasmids and the resulting expressed protein was tagged at the C-terminus with GFP.

As predicted, the N-terminal 14 residues in Src are sufficient to target it to the plasma membrane (Figure 4.13). However, the first 14 residues of ChChd3 when fused to GFP were not sufficient to target ChChd3 to the mitochondria or to the plasma membrane. The resulting pictures in Figure 4.12 indicate that the 14 residues target elsewhere, either perinuclear or the golgi apparatus. When the Thr10 PKA phosphorylation site was mutated to both an Ala and a Glu, the localization pattern did not change (Figure 4.12, Glu pictures not shown). Although mutation of the PKA phosphorylation site did not affect localization, mutation of Gly1 to Ala did disrupt localization (Figure 4.14). In this case, the GFP-tagged constructs were found mostly in the nucleus where GFP is found if expressed alone.

It was predicted earlier that the lysines in the N-terminus of Src were essential for targeting to the plasma membrane and that replacing the lysines with arginines would abolish targeting to the plasma membrane. Since the N-terminus of ChChd3 has arginines rather than lysines we thought that this might be a critical difference and that targeting of Src to the plasma membrane might be abolished by replacing the lysines with arginines. Since targeting of this myristylated motif had not been tested previously by immunofluorescence in cells, we made the altered Src motif shown in Figure 4.11. As shown in Figure 4.13, in transfected HeLa cells the Src sequence still targeted to the plasma membrane demonstrating that the lys to arg difference is not important. C-terminally GFP-tagged constructs were also made where the arginines were replaced

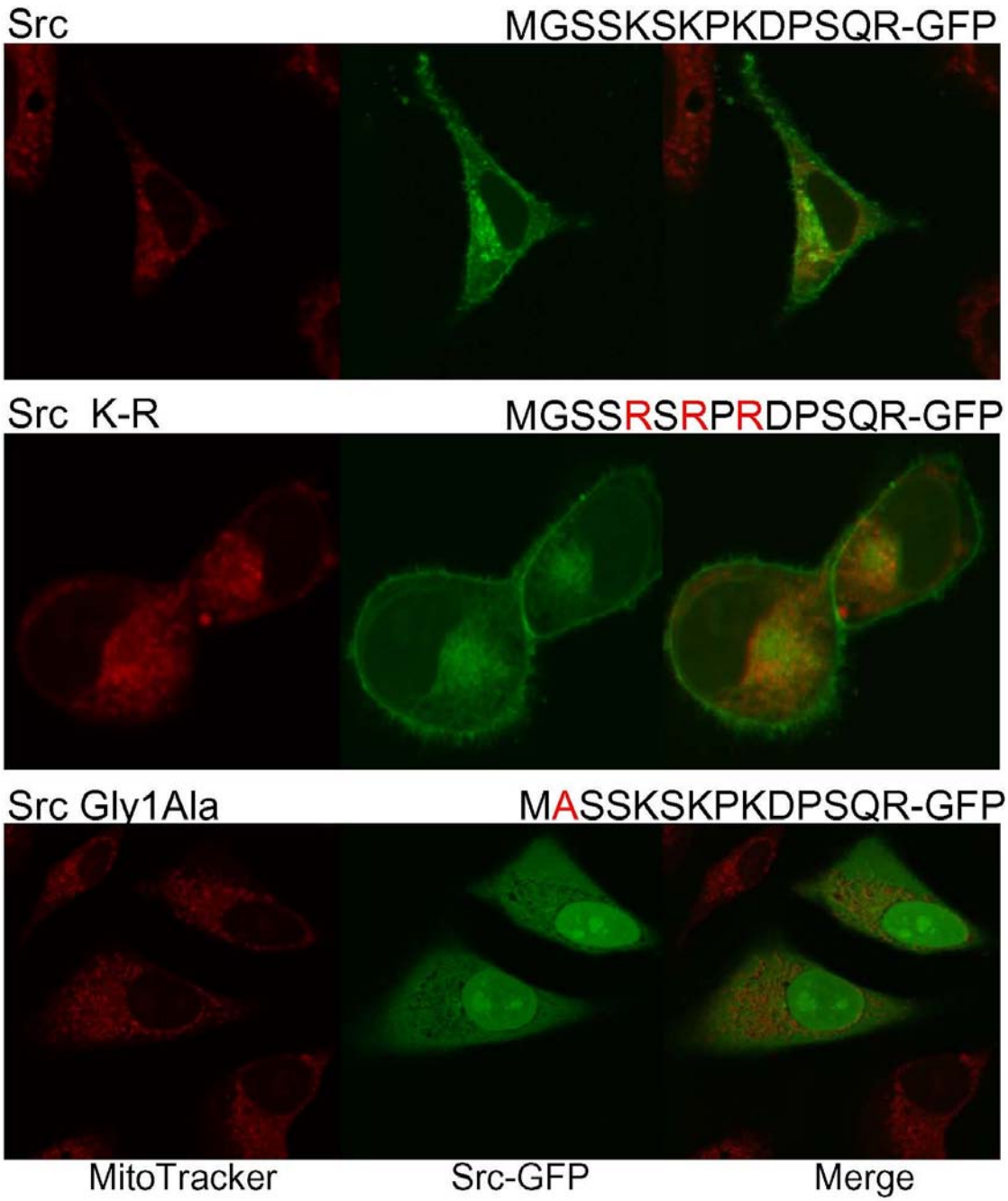

Figure 4.13: Localization of Src N-terminal constructs fused to GFP. HeLa cells were transfected with the constructs listed to the right of the cell pictures. On the very left, staining for mitochondria using MitoTracker red. Middle, images of the GFP-tagged constructs. Right, the merge of the two fluorescent signals. Imaged at NCMIR.

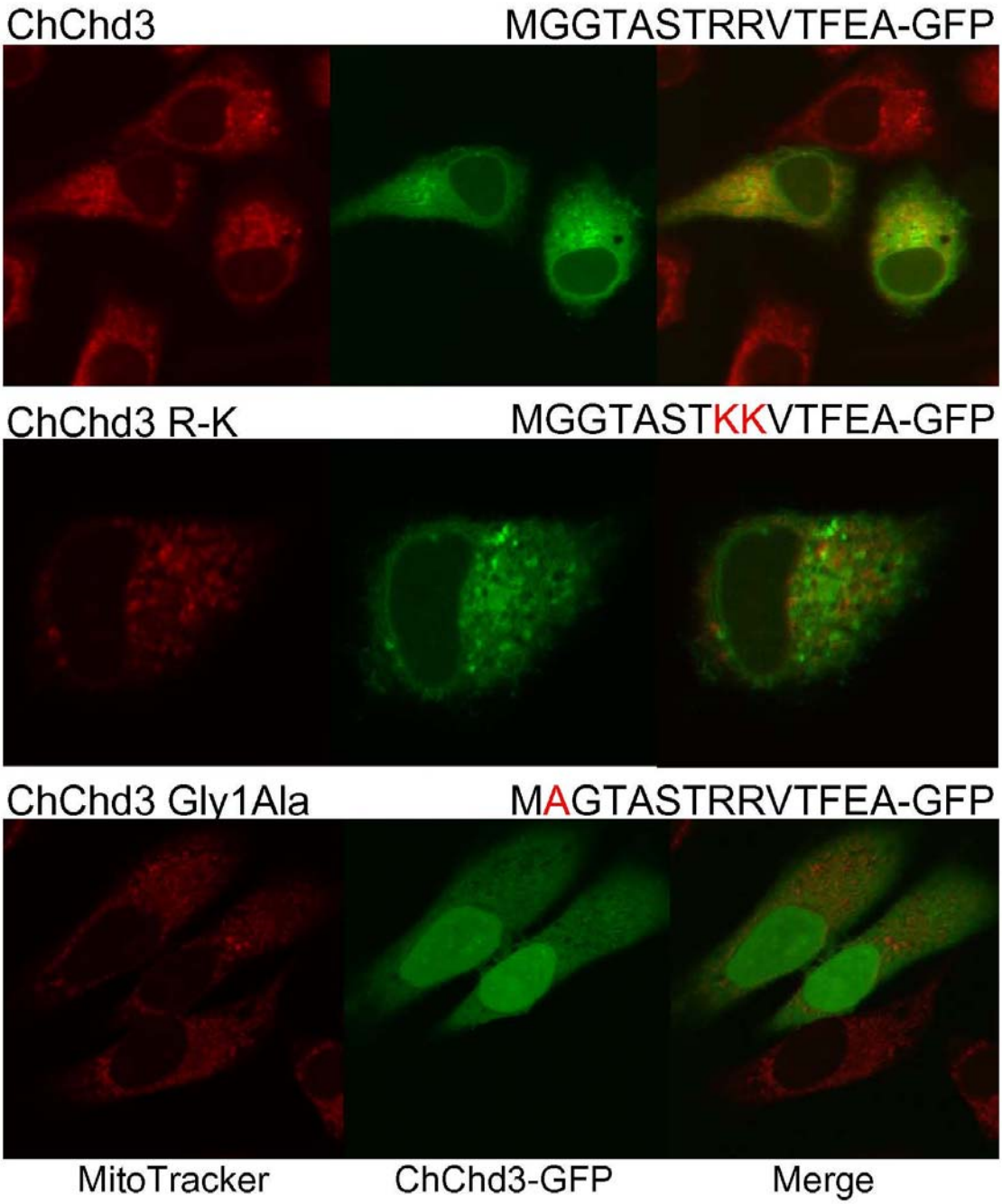

Figure 4.14: Localization of ChChd3 N-terminal constructs fused to GFP. HeLa cells were transfected with the constructs listed to the right of the cell pictures. On the very left, staining for mitochondria using MitoTracker red. Middle, images of the GFP-tagged constructs. Right, the merge of the two fluorescent signals. Imaged at NCMIR.

with lysines in the first 14 N-terminal residues of ChChd3. In Figure 4.14, the ChChd3 constructs also showed no change in localization. In the results, switching the lysines and arginines did not have an effect on the localization of GFP. Src targets GFP to the plasma membrane regardless of arginines or lysines present in the N-terminal 14 residues. Mutation of the myristylation site at Gly1 resulted in the GFP-tagged constructs accumulating in the nucleus (Figures 4.13 and 4.14).

Full length ChChd3 constructs with GFP on the C-terminus were also made to examine whether the full-length protein localizes properly (data not shown). ChChd3-GFP showed a diffuse pattern. If the CHCH domain is necessary for uptake into the mitochondria, then the GFP on the C-terminus may be interfering with this process. Therefore, we made a full length ChChd3 construct with the smaller FLAG epitope tag on the C-terminus. The FLAG tag is an eight amino acid that is visualized with monoclonal antibodies. Also, a ChChd3 truncation construct was made where the CHCH domain is removed. These constructs were transfected into 10 T-1/2 cells and the results are shown in Figure 4.15. The ChChd3 truncation shows a diffuse pattern similar to that seen when the full-length protein is fused to GFP. The ChChd3 full-length with a FLAG tag shows a beautiful mitochondrial localization pattern.

We conclude that the C-terminal CHCH domain is important for targeting to the mitochondria and that fusion of the C-terminus to GFP interferes with localization. The myristylation motif may be important for localizing ChChd3 to the inner membrane, once it gets into the inner membrane space, but it is not sufficient to target ChChd3 to the mitochondria on its own.

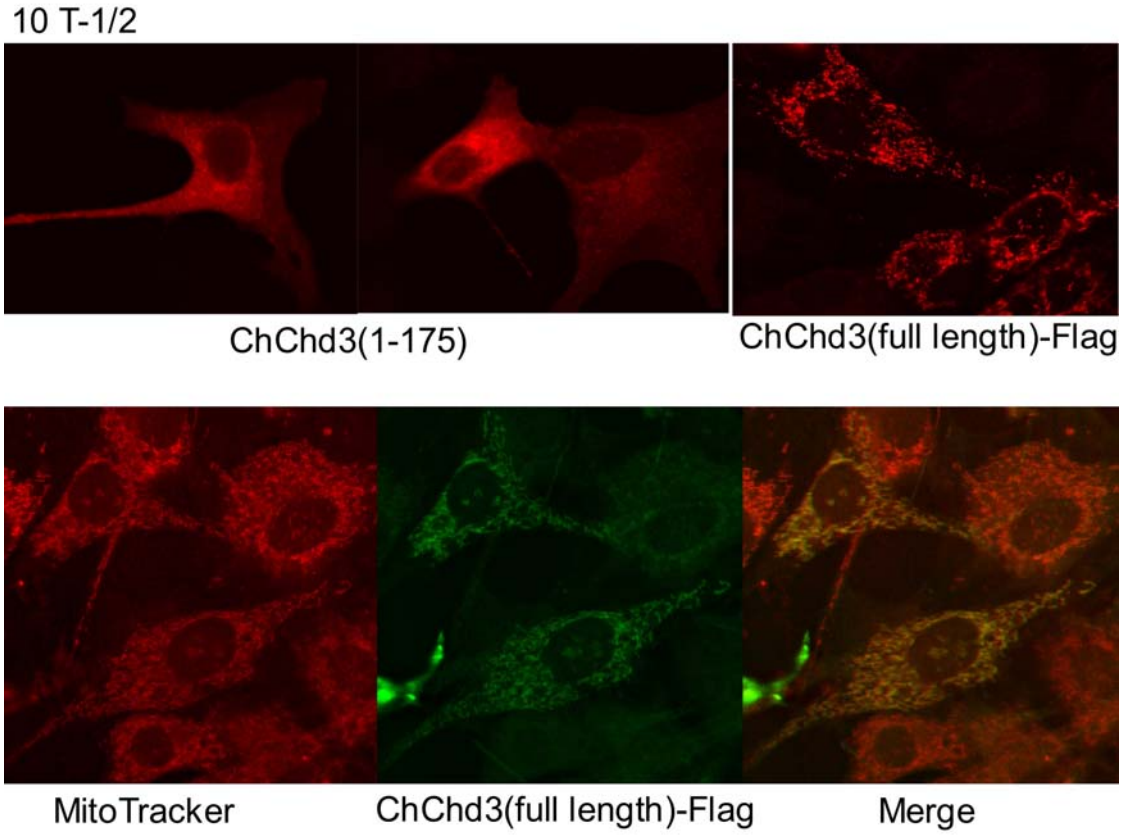

Figure 4.15: Truncated ChChd3 and full length ChChd3 transfected into 10 T-1/2 cells. Top left, truncated ChChd3 without the CHCH domain, immunostained with the antibody to ChChd3 and rhodamine labeled secondary. Top right, full length ChChd3 with a FLAG tag at the C-terminus, immunostained with the antibody to FLAG tag, rhodamine secondary. Bottom, MitoTracker labeled mitochondria on the left, ChChd3 full length with FLAG tag (Flag primary Ab, FITC-conjugated secondary), and the merge of the two pictures showing mitochondrial localization of the full length ChChd3 on the right. The sequence of the FLAG tag is Asp-Tyr-Lys-Asp-Asp-Asp-Asp-Lys.

Section 4.4: Conclusions.

ChChd3 has two distinct domains, a DUF737 domain which is completely unknown but highly conserved among vertebrates and a CHCH domain, an exclusive mitochondrial domain seen in several other known proteins. In addition, the N-terminal portion of the protein contains a distinct myristylation site and PKA phosphorylation site. The CHCH domain is characterized by the Cys-X_9-Cys repeat and appears to be important for other proteins for transport into the mitochondria as well as metal binding inside the inner mitochondrial space as suggested for Cox17 (Arnesano, Balatri et al. 2005). Murine ChChd3 is closely conserved with the human form. After analyzing the putative exons, there may be two spice variants in mouse, one with and one without the CHCH domain. However, the Western blots of mouse tissue do not show a lower band that would correspond to the protein without the CHCH domain.

This protein seems to be most highly expressed in tissues high in mitochondria according to the mRNA expression profile. In culture cells of monkey or mouse origin ChChd3 showed a distinct mitochondrial localization pattern. Tissue analysis shows two possible versions of the protein in mouse brain nuclei and rat heart mitochondria. The majority of the protein runs at molecular weight of 33kDa, slightly higher than its predicted molecular weight of 26.5kDa, which is typical of other CHCH domain containing proteins. Further fractionation of mouse liver mitochondria reveals that the protein is primarily in the inner membrane, consistent with previous reports of its location and possible function.

Although ChChd3 is very closely conserved in mammals, it is interesting to note that this protein does not have a homolog in yeast, plants, or arthropoda. This indicates

that ChChd3 is found only in higher evolved organisms. Due to the location of ChChd3 in the inner membrane of mitochondria and the presence of CHCH domain, this protein is most likely involved in oxidative phosphorylation and may be involved in metal transport. Other CHCH containing proteins, such as Cox17 and Cox19, are subunits of the cytochrome c oxidase and appear to function in metal transport. They may play a role in the delivery of metal ions to the large cytochrome c oxidase complex although the precise mechanism for such a function is unknown. However, ChChd3 is much larger than both Cox17 or Cox19. This protein may also form complexes once bound to metal, much like Cox17 was shown to do. In the case of Cox17 the aggregation state and the metal binding properties appear to depend critically on the oxidation state of the cysteines (Arnesano, Balatri et al. 2005).

Another CHCH domain containing protein is human Mia40, which is also located in the inner mitochondrial space (Hofmann, Rothbauer et al. 2005). The CHCH domain in this protein was shown to be essential for import of Mia40 into the mitochondria and for stabilization of the protein. Mutation of some of the cysteines resulted in destabilization of the protein in the IMS and mutation of all of the cysteines prevented the import of Mia40 into the mitochondria (Hofmann, Rothbauer et al. 2005). Similarly, mutation of a single Cys in Cox17 caused the accumulation of the protein in the cytosol (Heaton, Nittis et al. 2000). Another group described the role of Mia40 in the transport system for proteins containing the Cys-X_9-Cys motif, where CHCH domain-containing proteins are transported into the mitochondria via the translocase of the outer membrane (TOM) channel. Mia40 then forms disulfide bridges with the CHCH domain-containing proteins in order to keep them sequestered in the IMS

(Mesecke, Terziyska et al. 2005). Erv1, a conserved sulfhydryl oxidase located in the IMS, assists Mia40 by oxidizing the cysteines in the CHCH domain of Mia40 (Lee, Hofhaus et al. 2000). This allows Mia40 to be ready to form intermolecular disulfide bridges with newly transported proteins (Mesecke, Terziyka et al. 2005).

From the targeting studies we demonstrated that the N-terminus of Src is sufficient to target to the plasma membrane whether there are lysines or arginines. In contrast, the similar N-terminal sequence of ChChd3 does not target to the plasma membrane or to the mitochondria. The N-terminal 14 residues of ChChd3 does not appear to be the determining factor for localization of ChChd3 to the mitochondria. The ChChd3 N-terminus did target GFP to another undetermined cellular location, possibly golgi, and mutation of the PKA phosphorylation site did not change the location. Removal of the myristylation site, however, by converting the N-terminal Gly to Ala did abolish the golgi-like targeting.

When the full-length protein is expressed fused to GFP, the expressed protein shows no distinct pattern. Dennis Winge at the University of Utah also saw that GFP blocked the uptake of the CHCH domain into the mitochondria, although a flag tag at the C-terminus could be tolerated (personal communication). We then expressed the full-length ChChd3 with a flag tag at the C-terminus. This protein does localize to the mitochondria. This indicates that ChChd3 may need the C-terminus to be free in order to localize to the mitochondria; tethering to GFP could obstruct its targeting properties. When the CHCH domain is removed from the protein, the transfected protein no longer localizes to the mitochondria. These results support the hypothesis that ChChd3 may be

transported via the TOM channel and trapped in the mitochondria by Mia40 and Erv1. The CHCH domain of ChChd3 would be essential for these functions.

Section 4.5: Materials and Methods.

Western blot – Samples were ran on an SDS-PAGE gel and then transferred to nitrocellulose membrane (30V for 60min.). The membranes were blocked in 5% milk in TBST overnight. The blocking solution was removed and the membranes were rinsed twice with TBST. The primary antibody, the antibody to ChChd3, was added at a 1:5000 dilution and incubated at room temperature for 1 hour with gentle shaking. After the primary antibody was poured off, the membranes were rinsed 4 times with TBST. The second antibody, anti-rabbit-horseradish peroxidase (HRP), was added at a dilution of 1:2000 and the blots were incubated for 30 min. at r.t. with gentle shaking. The blots were rinsed after with TBST twice times and then incubated with SuperSignal West Pico chemiluminescent substrate detection kit (Pierce) for one min. Blots were then exposed to ECL Hyperfilm.

2-D gel electrophoresis - IPG buffer containing 20 mM DTT, 8 M urea, and ampholytes corresponding to various pI ranges were added to the mouse brain crude mitochondrial fraction (prepared as described in Chapter 3). Then 160mL of the resultant mixture was pipetted into a chamber where an dried IPG strip was placed. The sample was allowed to sit overnight at room temperature in order to allow the IPG strip to re-swell and adsorb the proteins in the sample. The first-dimension separation which resolves the proteins on the basis of their pI, was run according to the protocol developed by Invitrogen for the IPG Runner system. This separation was run for approximately 1200

volt-hours. After the run, the strips were removed and placed along the top of a pre-cast SDS-PAGE gel. The strips were sealed in with agarose and the gels were run for 35-45 min. at 200 V to separate the proteins on the basis of their molecular weights.

Immunocytochemistry – The cell lines 10T-1/2, 293a, Cos, and HeLa were used to probe for the location of endogenous ChChd3 protein. Cells were grown to 60-70% confluence. Medium was removed and replaced with serum-free medium containing MitoTracker red (Molecular Probes) at a concentration of 500 nM one hour before fixing. Cells were fixed in 4% paraformaldehyde in PBS for 15 min. at r.t. The cells were rinsed 3 times with PBS on ice before the ChChd3 antibody (1:1000 dilution in PBS) was added to the culture dishes. Cells were incubated with the primary antibody for 1 hour on ice. After rinsing again with PBS, the cells were incubated for 2 hours one ice with anti-rabbit fluorescein conjugated secondary antibody. After the incubation, the cells were rinsed and stored in PBS. Cells were imaged on a Bio-Rad MRC1024 fluorescent confocal microscope at NCMIR (National Center for Microscopy and Imaging Research).

Transfection of N-terminal-GFP constructs – The N-terminal 14 residues of ChChd3 were ordered as separate DNA oligos, annealed and then cloned into pEGFP. NIH3T3 cells were transfected with 1-2 mg DNA and Fugene (Roche Diagnostics) transfection agent. Cells were fixed 12-24 hours later and imaged as described above.

Mitochondrial subcellular fractionation – Protocol from Dave Pagliarini (Dixon Lab) adapted by David Barraclough (Taylor lab). Eight-ten g of mouse liver tissue were minced immediately after isolation from live mouse using surgical scissors. Any connective or fatty tissue was discarded. The tissue was rinsed with MSHE (210mM

mannitol, 70mM Sucrose, 5mM HEPES (pH to 7.4 using KOH) 1mM EGTA, with and without 0.5% BSA, plus protease inhibitor cocktail). Five volumes of MSHE was added to the tissue and the whole amount was homogenized until smooth. MSHE was added to about 8 volumes of starting material before centrifugation at 2500 rpm for 10 min. at 4°C. The supernatant (which contain the mitochondria) was poured through cheesecloth into centrifuge tubes. The pellet, which may still have some mitochondria, is resuspended in 20 ml MSHE and re-centrifuged at the previous centrifugation conditions. The supernatants from both spins are combined and centrifuged at 11,000 rpm for 10 min. and 4°C to pellet the mitochondria. The mitochondria pellet is resuspended with very small amounts of MSHE. The pellet is washed by resuspending in 20 ml with MSHE without BSA and re-centrifuged at 11,000 rpm to repellet the mitochondria. The mitochondria are resuspended with 500 µl to 1ml of MSHE. A small volume of mitochondria is added on top of a discontinuous gradient of 2 mL 35% Histodenz, 3mL 17% Histodenz, 5mL 6% Percoll. Recentrifuged in a Beckman ultracentrifuge with swinging bucket rotor SW40Ti for 45 min. at 4°C and 19,000 rpm. The mitochondrial layer at the interface of the 17 and 35% histodenz layers is removed, resuspended in 20 ml of MSHE and then centrifuged at 15,000 for 10 min.

For the mitochondrial fractionation, 5 ml swelling buffer (10 mM KH_2PO_4, pH 7.5 with protease inhibitors) is added to the mitochondrial pellet. The mixture is incubated with rotation at 4°C for 20 min. Then 5 ml of shrinking buffer (10 mM KH_2PO_4 pH 7.4, 32% Sucrose, 30% Glycerol, 10 mM $MgCl_2$ with protease inhibitors) is added and the mixture is incubated again for 20 min. The mixture is centrifuged at 8500 rpm (10,000g) for 10 min. The supernatant contains the OM and IMS which is saved as

mixture 1. The pellet is the mitoplast and is saved and washed 3 times using a 1:1 mixture of swelling to shrinking buffer followed by centrifugation at 8500 rpm. The final mitoplast pellet is resuspended in about 500 μL of Swelling buffer. The mitoplasts are sonicated in the swelling buffer twice for 15 seconds with 1 minute interval in between. This is now mixture 2 and contains the IM and M.

Mixture 1 and Mixture 2 are centrifuged for 1 hour at 50,000 rpm (150,000g) in the Beckman MLA130 rotor. Mixture 1 pellet is the OM (outer mitochondrial membrane) and the mixture 2 pellet is the matrix (M). The supernatants contain the inner mitochondrial space (IMS) and the inner membrane (IM). The proteins in the supernatants are precipitated by adding 1/5 volume of 50% TCA in water to each supernatant and incubated on ice for 30 min. The samples are then centrifuged at max speed in a tabletop centrifuge for 10 minutes. The resulting pellets are the IMS (mixture 1) and IM (mixture 2).

CHAPTER V

Conclusions

Cyclic-AMP dependent protein kinase proved to be a good candidate for engineering using the chemical genetics approach. Chapter 2 described the modeling, mutation, expression, and characterization of the engineered PKA C-subunit. Computer modeling of the ATP-binding pocket using the available protein structures gave insight to the dimensions of the mutated pocket and how a bulky N^6-substituted ATP analog could fit. Modeling also helped determine that only a single mutation was needed at methionine 120. Initially, the recombinantly-expressed protein was difficult to work with, it was insoluble and unphosphorylated. Wild type C-subunit autophosphorylates and is soluble when expressed in *E. coli*. Using a new approach, the mutant was co-expressed with PDK1 and the resulting protein was more soluble, phosphorylated, and active.

The purified recombinant M120G C-subunit was stable for long periods so it was ideal for qualitative and quantitative analyses. Kinetic assays revealed that the mutant preferred N^6(benzyl)-ATP and N^6(phenethyl)-ATP over wild type ATP. M120G C-subunit still used ATP with a slightly lower affinity than WT C-subunit for ATP. It is intriguing that the mutant is not phosphorylated when expressed alone in *E. coli*, even though it can use ATP. Perhaps removal of the methionine side chain disrupts the flexibility of the hinge region between the two lobes, or disrupts the ATP binding affinity just enough so that the initial autophosphorylation event does not occur.

The chemical genetics approach was originally designed to be used *in vivo*. However, the ATP analogs do not cross the cell membrane well. In addition to this, a large amount of radioactively labeled ATP analogs would be needed for *in vivo* assays involving tissue culture cells. An *in vitro* assay was developed using recombinant

engineered kinase and specific cell fractions. We were most interested in PKA substrates at the mitochondria, so mitochondria were isolated from mouse brain in order to be probed for novel PKA substrates using the engineered mutant C-subunit.

Two-dimensional gel electrophoresis was used to separate the mouse brain proteins, as described in Chapter 3. Phosphorylated proteins were detected by gel exposure to autoradiography film. Many phosphorylated spots were excised and subjected to mass spectrometry, however it was difficult to obtain enough protein from the gels to get respectable mass spectrometry data. A few spots had decent matches. The most interesting substrate identified from the *in vitro* assays was ChChd3.

ChChd3 is a novel mitochondrial protein with no currently known function. Characterization of this protein is detailed in Chapter 4. The protein is abundant in mouse brain mitochondria according to Western blots. It also appears to be limited to higher animals, as there appears to be no homolog in fungi, plants, and arthropoda. The protein has two domains and an N-terminal myristylation motif. The myristylation motif contains a well-conserved PKA phosphorylation site at Thr10. A second PKA phosphorylation site is possible at Ser78 in the DUF737 domain, a domain of unknown function that appears to have nothing in common with any other known domain.

The CHCH domain at the C-terminus is characterized by the Cys-X_9-Cys motif. Several other mitochondrially located proteins contain this domain as discussed in Chapter 4. The CHCH domain is necessary for ChChd3 localization to the mitochondria; ChChd3 constructs expressed in HeLa cells without the CHCH domain do not target to the mitochondria. The cysteines in this domain may also bind metal ions and transport them to other proteins in the mitochondria.

ChChd3 is predicted to utilize a transport system previously described for other CHCH domain containing proteins. A proposed model for ChChd3 import into the mitochondria and the proteins that may interact with ChChd3 is shown in Figure 5.1. Possibly, ChChd3 enters the mitochondria through a TOM transport channel, and once in the IMS an oxidized Mia40 forms disulfide bridges with the cysteines in the CHCH domain of ChChd3. Mia40 may then release ChChd3 with the cysteines trapped in intramolecular disulfide bridges possibly with the help of another protein, Hot13, or "Helper of Tim" (Curran, Leuenberger et al. 2004). Hot13 is a protein that oxidizes Tim proteins in the IMS and keeps them in their active conformations. This may put the protein in its proper folding conformation, and, according to the folding trap hypothesis, proteins are locked into the IMS once they are folded correctly and stable (Lu, Allen et al. 2004; Lutz, et al. 2003). Once in the IMS, the myristylation motif may then come into play by localizing the protein to the inner membrane, where it can take part in the electron transport chain. No other CHCH domain-containing proteins have been found to have a myristylation motif at the N-terminus. Most CHCH domain-containing proteins have been found to be soluble in the IMS, except Mia40, which was reported to be anchored to the IM through a N-terminal hydrophobic region (Mesecke, Terzyska et al. 2005). However, another group reported that the fungal Mia40 is anchored at the IM but is soluble in the IMS in humans (Hofmann, Rothbauer et al. 2005). Further studies are needed to confirm if the CHCH domain alone is sufficient to target ChChd3 to the mitochondria or whether the myristylation motif is also important for targeting to the mitochondria outer membrane or the inner membrane.

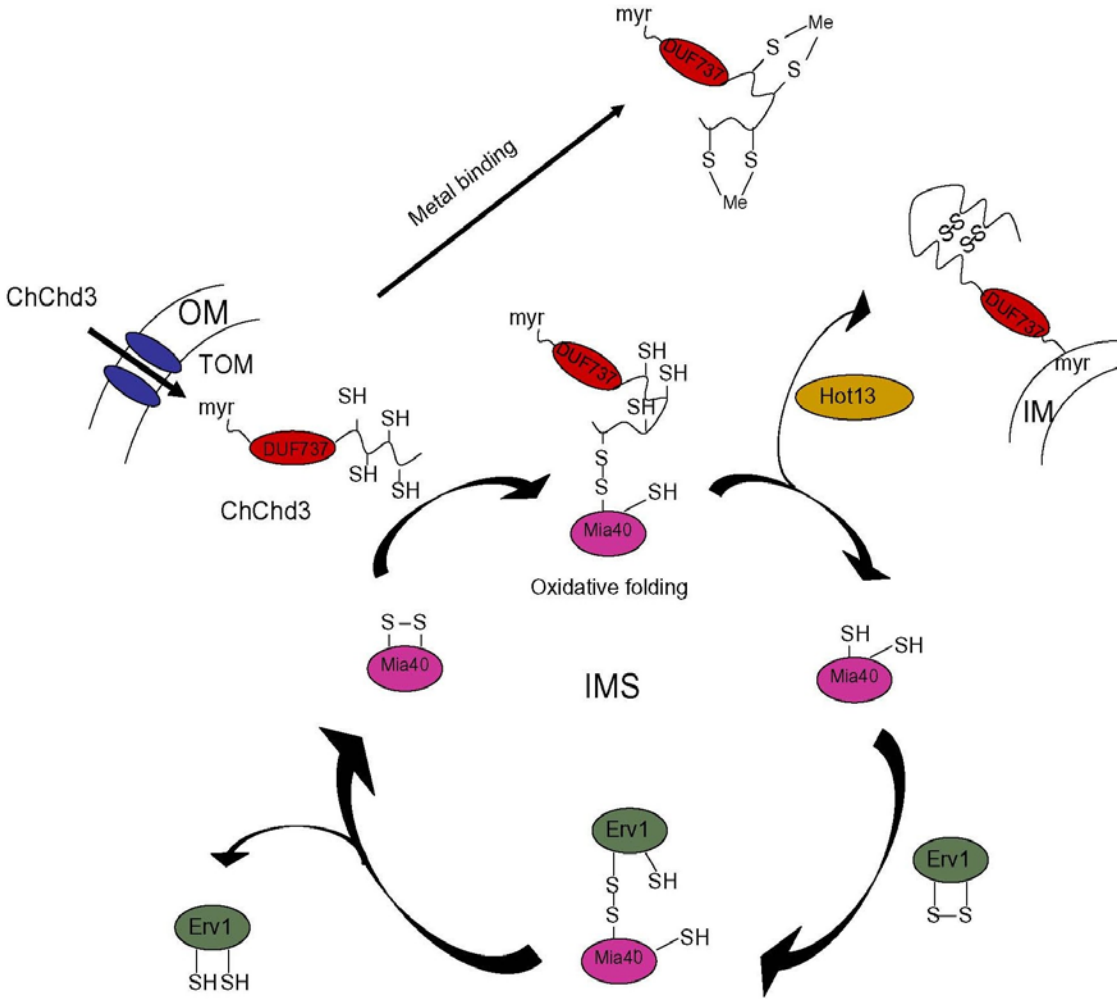

Figure 5.1: Proposed model for ChChd3 entry into the mitochondria. The non-disulfide bonded ChChd3 passes through the outer membrane (OM) of the mitochondria via TOM (translocase of the outer membrane). Once in the IMS (inner mitochondrial space), ChChd3 may bind metal ions, or form disulfide bonds with the oxidized Mia40 to undergo oxidative folding. Mia40 releases an intra-disulfide-bonded ChChd3 possibly with the help of Hot13 ("Helper of Tim"). ChChd3 then targets to the inner membrane (IM) through its myristylation motif. The cysteines in the CHCH domain of Mia40 are regenerated to the oxidized state with the help of Erv1. This figure was modeled on figures from Mesecke, Terziyska et al. 2005 and Arnesano, Balatri et al. 2005.

In Figure 4.10 it is important to note that both D-AKAP1, RIα, and to a lesser degree D-AKAP2 are found in the same mitochondrial location as ChChd3. A possible scenario has the RIα holoenzyme complex localized to the inner membrane via D-AKAP1 so that PKA can phosphorylate ChChd3 when the C-subunit is activated. The phosphorylation of ChChd3 by PKA may regulate the myristylation motif of ChChd3, and therefore the localization of the protein. We still do not know the role of PKA phosphorylation at the N-terminus of proteins with myristylation motifs. Both Src and PKA have PKA phosphorylation sites on the N-terminus. The positive charges present in the myristylation motifs along with the myristyl group are necessary for targeting to membranes (Silverman and Resh 1992). The negative charge of the phosphate may reduce the overall charge of the arginine or lysine-rich N-terminus, similar to the electrostatic switch seen in MARCKS, a Protein Kinase C (PKC) substrate (McLaughlin, Aderem 1995). PKC phosphorylates MARCKS in the basic myristylation motif, and the introduction of the negative charges releases MARCKS from the plasma membrane (Thelen, Rosen et al. 1991). PKA may regulate the ability of ChChd3 to localize to either the outer mitochondrial membrane or the inner mitochondrial membrane.

ChChd3 is an interesting link to PKA because of its transport into the mitochondria, which may give us clues to the transport of RIα into the mitochondria as well. RIα also forms disulfide bonds that link alpha-helices in an anti-parallel fashion in its dimerization/docking domain. Perhaps RIα uses the same transport mechanism as CHCH domain containing proteins. ChChd3 may also provide a link for PKA to oxidative metabolism. Recently, an Italian group linked the interaction of D-AKAP1

(AKAP121), PTPD1, Src, and cAMP levels to oxidative metabolism (Livigni, Scorziello et al. 2006). D-AKAP1 would localize either the RI:C or RII:C complex to the inner mitochondrial membrane, possibly putting the catalytic subunit in close proximity to ChChd3. A role for ChChd3 must be elucidated. Future directions for research on this protein will focus on its role in the mitochondria and the cell.

REFERENCES

Adams JA, McGlone ML, Gibson R, Taylor SS. Phosphorylation modulates catalytic function and regulation in the cAMP-dependent protein kinase. *Biochemistry.* 1995 Feb 28;34(8):2447-54.

Altschul, S.F., Gish, W., Miller, W., Myers, E.W. & Lipman, D.J. (1990) "Basic local alignment search tool." *J. Mol. Biol.* 215:403-410.

Arnesano F, Balatri E, Banci L, Bertini I, Winge DR.Folding studies of Cox17 reveal an important interplay of cysteine oxidation and copper binding. *Structure.* 2005 May;13(5):713-22.

Beers J, Glerum DM, Tzagoloff A. Purification, characterization, and localization of yeast Cox17p, a mitochondrial copper shuttle. *J Biol Chem.* 1997 Dec 26;272(52):33191-6.

Benjamin KR, Zhang C, Shokat KM, Herskowitz I. Control of landmark events in meiosis by the CDK Cdc28 and the meiosis-specific kinase Ime2. *Genes Dev.* 2003 Jun 15;17(12):1524-39.

Biondi RM, Cheung PC, Casamayor A, Deak M, Currie RA, Alessi DR. Identification of a pocket in the PDK1 kinase domain that interacts with PIF and the C-terminal residues of PKA. *EMBO J.* 2000 Mar 1;19(5):979-88.

Breitenlechner C, Engh RA, Huber R, Kinzel V, Bossemeyer D, Gassel M. The typically disordered N-terminus of PKA can fold as a helix and project the myristoylation site into solution. *Biochemistry*. 2004 Jun 22;43(24):7743-9.

Cardone L, de Cristofaro T, Affaitati A, Garbi C, Ginsberg MD, Saviano M, Varrone S, Rubin CS, Gottesman ME, Avvedimento EV, Feliciello A. A-kinase anchor protein 84/121 are targeted to mitochondria and mitotic spindles by overlapping amino-terminal motifs. *J Mol Biol.* 2002 Jul 12;320(3):663-75.

Cardone L, Carlucci A, Affaitati A, Livigni A, DeCristofaro T, Garbi C, Varrone S, Ullrich A, Gottesman ME, Avvedimento EV, Feliciello A. Mitochondrial AKAP121 binds and targets protein tyrosine phosphatase D1, a novel positive regulator of src signaling. *Mol Cell Biol.* 2004 Jun;24(11):4613-26.

Champion A, Kreis M, Mockaitis K, Picaud A, Henry Y. Arabidopsis kinome: after the casting. *Funct Integr Genomics.* 2004 Jul;4(3):163-87.

Chen R, Fearnley IM, Peak-Chew SY, Walker JE. The phosphorylation of subunits of complex I from bovine heart mitochondria. *J Biol Chem.* 2004 Jun 18;279(25):26036-45.

Cheng X, Ma Y, Moore M, Hemmings BA, Taylor SS. Phosphorylation and activation of cAMP-dependent protein kinase by phosphoinositide-dependent protein kinase. *Proc Natl Acad Sci U S A.* 1998 Aug 18;95(17):9849-54.

Cook PF, Neville ME Jr, Vrana KE, Hartl FT, Roskoski R Jr. Adenosine cyclic 3',5'-monophosphate dependent protein kinase: kinetic mechanism for the bovine skeletal muscle catalytic subunit. *Biochemistry.* 1982 Nov 9;21(23):5794-9

Curran SP, Leuenberger D, Leverich EP, Hwang DK, Beverly KN, Koehler CM. The role of Hot13p and redox chemistry in the mitochondrial TIM22 import pathway. J Biol Chem. 2004 Oct 15;279(42):43744-51.

Da Cruz S, Xenarios I, Langridge J, Vilbois F, Parone PA, Martinou JC. Proteomic analysis of the mouse liver mitochondrial inner membrane. *J Biol Chem.* 2003 Oct 17;278(42):41566-71.

Dalton GD, Dewey WL. Protein kinase inhibitor peptide (PKI): A family of endogenous neuropeptides that modulate neuronal cAMP-dependent protein kinase function. *Neuropeptides.* 2006 Feb;40(1):23-34.

Dephoure N, Howson RW, Blethrow JD, Shokat KM, O'Shea EK. Combining chemical genetics and proteomics to identify protein kinase substrates. *Proc Natl Acad Sci U S A.* 2005 Dec 13;102(50):17940-5.

Diller TC, Madhusudan, Xuong NH, Taylor SS. Molecular basis for regulatory subunit diversity in cAMP-dependent protein kinase: crystal structure of the type II beta regulatory subunit. *Structure*. 2001 Jan 10;9(1):73-82.

Dutil EM, Toker A, Newton AC. Regulation of conventional protein kinase C isozymes by phosphoinositide-dependent kinase 1 (PDK-1). *Curr Biol.* 1998 Dec 17-31;8(25):1366-75.

Frank, R. Spot Synthesis: An easy technique for the positionally addressable, parallel chemical synthesis on a membrane support. *Tetrahedron* 1992, 48:9217-9232.

Glerum DM, Shtanko A, Tzagoloff A. Characterization of COX17, a yeast gene involved in copper metabolism and assembly of cytochrome oxidase. *J Biol Chem*. 1996 Jun 14;271(24):14504-9.

Ginsberg MD, Feliciello A, Jones JK, Avvedimento EV, Gottesman ME. PKA-dependent binding of mRNA to the mitochondrial AKAP121 protein. *J Mol Biol.* 2003 Apr 4;327(4):885-97.

Hanke JH, Gardner JP, Dow RL, Changelian PS, Brissette WH, Weringer EJ, Pollok BA, Connelly PA. Discovery of a novel, potent, and Src family-selective tyrosine with kinase inhibitor. Study of Lck- and FynT-dependent T cell activation. *J Biol Chem.* 1996 Jan 12;271(2):695-701.

Harada H, Becknell B, Wilm M, Mann M, Huang LJ, Taylor SS, Scott JD, Korsmeyer SJ. Phosphorylation and inactivation of BAD by mitochondria-anchored protein kinase A. *Mol Cell.* 1999 Apr;3(4):413-22.

Hauer JA, Taylor SS, Johnson DA. Binding-dependent disorder-order transition in PKI alpha: a fluorescence anisotropy study. *Biochemistry.* 1999 May 25;38(21):6774-80.

Heaton DN, George GN, Garrison G, Winge DR. The mitochondrial copper metallochaperone Cox17 exists as an oligomeric, polycopper complex. *Biochemistry.* 2001 Jan 23;40(3):743-51.

Heaton D, Nittis T, Srinivasan C, Winge DR. Mutational analysis of the mitochondrial copper metallochaperone Cox17. *J Biol Chem.* 2000 Dec 1;275(48):37582-7.

Herberg FW, Taylor SS. Physiological inhibitors of the catalytic subunit of cAMP-dependent protein kinase: effect of MgATP on protein-protein interactions. *Biochemistry.* 1993 Dec 21;32(50):14015-22.

Hofmann S, Rothbauer U, Muhlenbein N, Baiker K, Hell K, Bauer MF. Functional and mutational characterization of human MIA40 acting during import into the mitochondrial intermembrane space. J Mol Biol. 2005 Oct 28;353(3):517-28.

Huang LJ, Durick K, Weiner JA, Chun J, Taylor SS. Identification of a novel protein kinase A anchoring protein that binds both type I and type II regulatory subunits. *J Biol Chem*. 1997 Mar 21;272(12):8057-64.

Huang LJ, Durick K, Weiner JA, Chun J, Taylor SS. D-AKAP2, a novel protein kinase A anchoring protein with a putative RGS domain. *Proc Natl Acad Sci U S A*. 1997 Oct 14;94(21):11184-9.

Huang LJ, Wang L, Ma Y, Durick K, Perkins G, Deerinck TJ, Ellisman MH, Taylor SS NH2-Terminal targeting motifs direct dual specificity A-kinase-anchoring protein 1 (D-AKAP1) to either mitochondria or endoplasmic reticulum. *J Cell Biol.* 1999 May 31;145(5):951-9.

Iyer GH, Moore MJ, Taylor SS. Consequences of lysine 72 mutation on the phosphorylation and activation state of cAMP-dependent kinase. *J Biol Chem.* 2005 Mar 11;280(10):8800-7.

Järv, J and Ragnarsson, U. Linear free energy relationships in cAMP-dependent protein kinase reactions with synthetic substrates. *Bioorg. Chem.* 19:77-87.

Juris SJ, Shah K, Shokat K, Dixon JE, Vacratsis PO. Identification of otubain 1 as a novel substrate for the Yersinia protein kinase using chemical genetics and mass spectrometry. *FEBS Lett.* 2006 Jan 9;580(1):179-83.

Kandel ER, Squire LR. Neuroscience: breaking down scientific barriers to the study of brain and mind. *Science.* 2000 Nov 10;290(5494):1113-20.

Kemp BE. Phosphorylation of synthetic peptide analogs of rabbit cardiac troponin inhibitory subunit by the cyclic AMP-dependent protein kinase. *J Biol Chem.* 1979 Apr 25;254(8):2638-42.

Kemp BE, Graves DJ, Benjamini E, Krebs EG. Role of multiple basic residues in determining the substrate specificity of cyclic AMP-dependent protein kinase. *J Biol Chem.* 1977 Jul 25;252(14):4888-94.

Kim C, Xuong NH, Taylor SS. Crystal structure of a complex between the catalytic and regulatory (RIalpha) subunits of PKA. *Science.* 2005 Feb 4;307(5710):690-6.

Kim KH, Lopez-Casillas F, Bai DH, Luo X, Pape ME. Role of reversible phosphorylation of acetyl-CoA carboxylase in long-chain fatty acid synthesis. *FASEB J.* 1989 Sep;3(11):2250-6.

Knighton DR, Zheng JH, Ten Eyck LF, Ashford VA, Xuong NH, Taylor SS, Sowadski JM. Crystal structure of the catalytic subunit of cyclic adenosine monophosphate-dependent protein kinase. *Science.* 1991 Jul 26;253(5018):407-14.

Kunkel TA. Rapid and efficient site-specific mutagenesis without phenotypic selection. *Proc Natl Acad Sci U S A.* 1985 Jan;82(2):488-92.

Lee I, Salomon AR, Ficarro S, Mathes I, Lottspeich F, Grossman LI, Huttemann M. cAMP-dependent tyrosine phosphorylation of subunit I inhibits cytochrome c oxidase activity. *J Biol Chem.* 2005 Feb 18;280(7):6094-100.

Lee J, Hofhaus G, Lisowsky T. Erv1p from Saccharomyces cerevisiae is a FAD-linked sulfhydryl oxidase. *FEBS Lett.* 2000 Jul 14;477(1-2):62-6.

Lew J, Taylor SS, Adams JA. Identification of a partially rate-determining step in the catalytic mechanism of cAMP-dependent protein kinase: a transient kinetic study using stopped-flow fluorescence spectroscopy. *Biochemistry.* 1997 Jun 3;36(22):6717-24.

Liu Y, Shah K, Yang F, Witucki L, Shokat KM. Engineering Src family protein kinases with unnatural nucleotide specificity. *Chem Biol.* 1998 Feb;5(2):91-101.

Liu Y, Shah K, Yang F, Witucki L, Shokat KM. A molecular gate which controls unnatural ATP analogue recognition by the tyrosine kinase v-Src. *Bioorg Med Chem.* 1998 Aug;6(8):1219-26.

Livigni A, Scorziello A, Agnese S, Adornetto A, Carlucci A, Garbi C, Castaldo I, Annunziato L, Avvedimento EV, Feliciello A. Mitochondrial AKAP121 Links cAMP and src Signaling to Oxidative Metabolism. *Mol Biol Cell.* 2006 Jan;17(1):263-71.

Lizcano JM, Morrice N, Cohen P. Regulation of BAD by cAMP-dependent protein kinase is mediated via phosphorylation of a novel site, Ser155. *Biochem J.* 2000 Jul 15;349(Pt 2):547-57.

Lu H, Allen S, Wardleworth L, Savory P, Tokatlidis K. Functional TIM10 chaperone assembly is redox-regulated in vivo. J Biol Chem. 2004 Apr 30;279(18):18952-8.

Lutz T, Neupert W, Herrmann JM. Import of small Tim proteins into the mitochondrial intermembrane space. EMBO J. 2003 Sep 1;22(17):4400-8.

Manning G, Whyte DB, Martinez R, Hunter T, Sudarsanam S. The protein kinase complement of the human genome. *Science.* 2002 Dec 6;298(5600):1912-34.

McLaughlin S, Aderem A. The myristoyl-electrostatic switch: a modulator of reversible protein-membrane interactions. *Trends Biochem Sci.* 1995 Jul;20(7):272-6.

McPherson JM, Whitehouse S, Walsh DA. Possibility of shape conformers of the protein inhibitor of the cyclic adenosine monophosphate dependent protein kinase. *Biochemistry.* 1979 Oct 30;18(22):4835-45.

Mesecke N, Terziyska N, Kozany C, Baumann F, Neupert W, Hell K, Herrmann JM. A disulfide relay system in the intermembrane space of mitochondria that mediates protein import. *Cell.* 2005 Jul 1;121(7):1059-69.

Moore MJ, Kanter JR, Jones KC, Taylor SS.Phosphorylation of the catalytic subunit of protein kinase A. Autophosphorylation versus phosphorylation by phosphoinositide-dependent kinase-1. *J Biol Chem.* 2002 Dec 6;277(49):47878-84.

Mootha VK, Bunkenborg J, Olsen JV, Hjerrild M, Wisniewski JR, Stahl E, Bolouri MS, Ray HN, Sihag S, Kamal M, Patterson N, Lander ES, Mann M. Integrated analysis of protein composition, tissue diversity, and gene regulation in mouse mitochondria. *Cell.* 2003 Nov 26;115(5):629-40.

Narayana N, Cox S, Nguyen-huu X, Ten Eyck LF, Taylor SS. A binary complex of the catalytic subunit of cAMP-dependent protein kinase and adenosine further defines conformational flexibility. *Structure.* 1997 Jul 15;5(7):921-35.

Nicholls, A; Sharp, K; and Honig, B, PROTEINS, *Structure, Function and Genetics*, Vol. 11, No.4, 1991, pg. 281ff

Niswender CM, Ishihara RW, Judge LM, Zhang C, Shokat KM, McKnight GS. Protein engineering of protein kinase A catalytic subunits results in the acquisition of novel inhibitor sensitivity. *J Biol Chem.* 2002 Aug 9;277(32):28916-22.

Nobrega MP, Bandeira SC, Beers J, Tzagoloff A. Characterization of COX19, a widely distributed gene required for expression of mitochondrial cytochrome oxidase. *J Biol Chem.* 2002 Oct 25;277(43):40206-11.

Obara Y, Labudda K, Dillon TJ, Stork PJ. PKA phosphorylation of Src mediates Rap1 activation in NGF and cAMP signaling in PC12 cells. *J Cell Sci.* 2004 Dec 1;117(Pt 25):6085-94.

Palumaa P, Kangur L, Voronova A, Sillard R. Metal-binding mechanism of Cox17, a copper chaperone for cytochrome c oxidase. *Biochem J.* 2004 Aug 15;382(Pt 1):307-14.

Papa S, Sardanelli AM, Cocco T, Speranza F, Scacco SC, Technikova-Dobrova Z.The nuclear-encoded 18 kDa (IP) AQDQ subunit of bovine heart complex I is phosphorylated by the mitochondrial cAMP-dependent protein kinase. *FEBS Lett.* 1996 Feb 5;379(3):299-301.

Peterson RT, Schreiber SL. Kinase phosphorylation: Keeping it all in the family. *Curr Biol.* 1999 Jul 15;9(14):R521-4.

Punter FA, Adams DL, Glerum DM.Characterization and localization of human COX17, a gene involved in mitochondrial copper transport. *Hum Genet.* 2000 Jul;107(1):69-74.

Ranganathan G, Phan D, Pokrovskaya ID, McEwen JE, Li C, Kern PA. The translational regulation of lipoprotein lipase by epinephrine involves an RNA binding complex including the catalytic subunit of protein kinase A. *J Biol Chem.* 2002 Nov 8;277(45):43281-7.

Rost, B (2004) Meth. Mol. Biol., submitted PROFsec predicts secondary structure from multiple sequence alignments.

Rost, B; Yachdav, G; and Liu, J. (2004) The PredictProtein Server. Nucleic Acids Research 32(Web Server issue):W321-W326

Scott JD, McCartney S. Localization of A-kinase through anchoring proteins. *Mol Endocrinol.* 1994 Jan;8(1):5-11.

Shah K, Liu Y, Deirmengian C, Shokat KM. Engineering unnatural nucleotide specificity for Rous sarcoma virus tyrosine kinase to uniquely label its direct substrates. *Proc Natl Acad Sci U S A.* 1997 Apr 15;94(8):3565-70.

Shah K, Shokat KM. A chemical genetic screen for direct v-Src substrates reveals ordered assembly of a retrograde signaling pathway. *Chem Biol.* 2002 Jan;9(1):35-47.

Shoji S, Titani K, Demaille JG, Fischer EH. Sequence of two phosphorylated sites in the catalytic subunit of bovine cardiac muscle adenosine 3':5'-monophosphate-dependent protein kinase. *J Biol Chem.* 1979 Jul 25;254(14):6211-4.

Slice LW, Taylor SS. Expression of the catalytic subunit of cAMP-dependent protein kinase in Escherichia coli. *J Biol Chem.* 1989 Dec 15;264(35):20940-6.

Silverman L, Resh MD. Lysine residues form an integral component of a novel NH2-terminal membrane targeting motif for myristylated pp60v-src. J Cell Biol. 1992 Oct;119(2):415-25.

Steen RL, Martins SB, Tasken K, Collas P. Recruitment of protein phosphatase 1 to the nuclear envelope by A-kinase anchoring protein AKAP149 is a prerequisite for nuclear lamina assembly. *J Cell Biol.* 2000 Sep 18;150(6):1251-62.

Stratakis CA, Cho-Chung YS. Protein kinase A and human disease. *Trends Endocrinol Metab.* 2002 Mar;13(2):50-2.

Su Y, Dostmann WR, Herberg FW, Durick K, Xuong NH, Ten Eyck L, Taylor SS, Varughese KI. Regulatory subunit of protein kinase A: structure of deletion mutant with cAMP binding domains. *Science.* 1995 Aug 11;269(5225):807-13.

Taylor SS, Buechler JA, Yonemoto W. cAMP-dependent protein kinase: framework for a diverse family of regulatory enzymes. *Annu Rev Biochem*. 1990;59:971-1005.

Thelen M, Rosen A, Nairn AC, Aderem A. Regulation by phosphorylation of reversible association of a myristoylated protein kinase C substrate with the plasma membrane. *Nature*. 1991 May 23;351(6324):320-2.

Thomas J, Van Patten SM, Howard P, Day KH, Mitchell RD, Sosnick T, Trewhella J, Walsh DA, Maurer RA. Expression in Escherichia coli and characterization of the heat-stable inhibitor of the cAMP-dependent protein kinase. *J Biol Chem.* 1991 Jun 15;266(17):10906-11.

Thompson JD, Higgins DG, Gibson TJ. CLUSTAL W: improving the sensitivity of progressive multiple sequence alignment through sequence weighting, position-specific gap penalties and weight matrix choice. *Nucleic Acids Res.* 1994 Nov 11;22(22):4673-4680.

Toner-Webb J, van Patten SM, Walsh DA, Taylor SS. Autophosphorylation of the catalytic subunit of cAMP-dependent protein kinase. *J Biol Chem.* 1992 Dec 15;267(35):25174-80.

Trendelenburg G, Hummel M, Riecken EO, Hanski C. Molecular characterization of AKAP149, a novel A kinase anchor protein with a KH domain. *Biochem Biophys Res Commun.* 1996 Aug 5;225(1):313-9.

Turano C, Coppari S, Altieri F, Ferraro A. Proteins of the PDI family: unpredicted non-ER locations and functions. *J Cell Physiol.* 2002 Nov;193(2):154-63.

Wang L, Sunahara RK, Krumins A, Perkins G, Crochiere ML, Mackey M, Bell S, Ellisman MH, Taylor SS. Cloning and mitochondrial localization of full-length D-AKAP2, a protein kinase A anchoring protein. *Proc Natl Acad Sci U S A.* 2001 Mar 13;98(6):3220-5.

Wehrens XH, Lehnart SE, Reiken S, Vest JA, Wronska A, Marks AR. Ryanodine receptor/calcium release channel PKA phosphorylation: a critical mediator of heart failure progression. *Proc Natl Acad Sci U S A.* 2006 Jan 17;103(3):511-8.

Weiss EL, Bishop AC, Shokat KM, Drubin DG. Chemical genetic analysis of the budding-yeast p21-activated kinase Cla4p. *Nat Cell Biol.* 2000 Oct;2(10):677-85.

Wen W, Meinkoth JL, Tsien RY, Taylor SS. Identification of a signal for rapid export of proteins from the nucleus. *Cell.* 1995 Aug 11;82(3):463-73.

Whitehouse S, Walsh DA. Purification of a physiological form of the inhibitor protein of the cAMP-dependent protein kinase. *J Biol Chem.* 1982 Jun 10;257(11):6028-32.

Winder WW, Wilson HA, Hardie DG, Rasmussen BB, Hutber CA, Call GB, Clayton RD, Conley LM, Yoon S, Zhou B. Phosphorylation of rat muscle acetyl-CoA carboxylase by AMP-activated protein kinase and protein kinase A. *J Appl Physiol.* 1997 Jan;82(1):219-25.

Yang WL, Iacono L, Tang WM, Chin KV. Novel function of the regulatory subunit of protein kinase A: regulation of cytochrome c oxidase activity and cytochrome c release. *Biochemistry.* 1998 Oct 6;37(40):14175-80.

Yukitake H, Furusawa M, Taira T, Iguchi-Ariga SM, Ariga H. AAT-1, a novel testis-specific AMY-1-binding protein, forms a quaternary complex with AMY-1, A-kinase anchor protein 84, and a regulatory subunit of cAMP-dependent protein kinase and is phosphorylated by its kinase. *J Biol Chem.* 2002 Nov 22;277(47):45480-92.

Zheng J, Knighton DR, Xuong NH, Taylor SS, Sowadski JM, Ten Eyck LF. Crystal structures of the myristylated catalytic subunit of cAMP-dependent protein kinase reveal open and closed conformations. *Protein Sci*. 1993 Oct;2(10):1559-73.